STRUCTURE, ACCESSIBILITY AND 'REACTIVITY' OF CELLULOSE I AS REVEALED BY CP/MAS ^{13}C-NMR SPECTROSCOPY AND ATOMIC FORCE MICROSCOPY

by

VIREN CHUNILALL

Submitted in fulfilment of the academic
requirements for the degree of
PhD in the
Faculty of Science and Agriculture,
University of KwaZulu-Natal
Durban

December 2009

As the candidate's supervisor I have approved this thesis/dissertation for submission.

Signed: _____ Name: _____ Date: _____

Abstract

The dissolving pulps used in this thesis are high-grade cellulose pulps, with low amounts of hemicellulose, degraded cellulose and lignin, produced by acid bi-sulphite pulping of a fast growing South African hardwood Eucalypt clone. Microcrystalline cellulose (MCC) grade, viscose grade and cellulose acetate grade dissolving pulp were produced using a 4 stage bleaching process. MCC, viscose and cellulose acetate are the cellulose derivatives of 91% α-cellulose, 92% α-cellulose and 96% α-cellulose respectively.

The key properties of the dissolving pulp considered for cellulose derivatisation are: (1) Structure (2) Accessibility and (3) 'Reactivity'. The 'reactivity' depends to a large extent on the supra-molecular structure of cellulose I. Supra-molecular structure deals with the arrangement of cellulose I molecules into cellulose fibrils which then make up the cellulose fibril aggregate. The accessibility of cellulose I depends on the surface area, as determined by the size of the cellulose fibril aggregates, that are accessible; the structure of the cellulose molecules, which will determine which hydroxyl groups are accessible; and the size and type of reagent used during derivatisation. Supra-molecular changes in cellulose fibril aggregation of cellulose I, in hardwood acid bi-sulphite pulp, during bleaching and drying were studied using Atomic Force Microscopy (AFM) and Cross-polarization/Magic Angle Spinning Carbon-13 Nuclear Magnetic Resonance Spectroscopy (CP/MAS ^{13}C-NMR – Solid state NMR) in combination with spectral fitting.

There was a marked increase in cellulose fibril aggregation (i.e. supra-molecular structure) during bleaching of hardwood acid bi-sulphite pulp using 96% α-cellulose conditions. In contrast there was no increase in cellulose fibril aggregation pulp bleached using 91% α-cellulose and 92% α-cellulose bleaching conditions. An increase in hemicellulose and degraded cellulose / short chain glucan was shown to correlate with a decrease in cellulose fibril aggregation recorded using solid state NMR. Further changes in supra-molecular structure were noticed when each of the dissolving pulp samples were dried. First time drying of hardwood acid bi-sulphite pulp samples induces a significantly different degree of irreversible cellulose fibril

aggregation in the 92% α-cellulose and the 96% α-cellulose pulp samples. The irreversible increase in cellulose fibril aggregation correlates with the estimated amount of hemicellulose and degraded cellulose / short chain glucan present in the pulp. The percentage increase in cellulose fibril aggregation upon drying is as follows: 96% α-cellulose > 92% α-cellulose > 91% α-cellulose. Hemicellulose and degraded cellulose / short chain glucan are among the wet chemical properties that influence cellulose fibril aggregation and the presence in dissolving pulp samples could provide steric hindrance preventing the aggregation of fibrils.

Reactivity studies were carried out on the 91% α-cellulose, 92% α-cellulose and 96% α-cellulose grades of dissolving pulp. During 91% α-cellulose reactivity studies, there was no relationship between cellulose fibril aggregation, acid hydrolysis or MCC preparation. Other possible techniques for 91% α-cellulose reactivity evaluation such as the degree of polymerization (DP) determination using AFM have been discussed. Size exclusion chromatography with multi-angle laser light scattering detection was shown as a more suitable method of estimating the reactivity of 92% α-cellulose pulp samples. 96% α-cellulose reactivity studies were carried with the aid of a model system consisting of the acetylation of high purity pulp samples viz. cotton linters cellulose and 96% α-cellulose. Results indicate that the initial reaction rate constant is proportional to the specific surface area for the two cellulose pulp samples showing that specific surface area is directly related to initial reactivity of the performed acetylation. This work has shown that it is possible to control the cellulose fibril aggregation and hence specific surface area in laboratory produced 91% α-cellulose, 92% α-cellulose and 96% α-cellulose by the method in which the pulp is dried. Thus controlling cellulose fibril aggregation can probably be one viable route for controlling the initial reactivity of dissolving pulp towards acetylation.

DECLARATION 1 – PLAGIARISM

I, **Viren Chunilall**, declare that

1. The research reported in this thesis, except where otherwise indicated, is my original research.

2. This thesis has not been submitted for any degree or examination at any other university.

3. This thesis does not contain other persons' data, pictures, graphs or other information, unless specifically acknowledged as being sourced from other persons.

4. This thesis does not contain other persons' writing, unless specifically acknowledged as being sourced from other researchers. Where other written sources have been quoted, then:
   a. Their words have been re-written but the general information attributed to them has been referenced
   b. Where their exact words have been used, then their writing has been placed in italics and inside quotation marks, and referenced.

5. This thesis does not contain text, graphics or tables copied and pasted from the Internet, unless specifically acknowledged, and the source being detailed in the thesis and in the References sections.

Signed:

DECLARATION 2 – PUBLICATIONS

Publication 1**:** Chunilall, V., Wesley-Smith, J. and Bush, T., **Cellulose fibril aggregation studies of *eucalyptus* dissolving pulps using atomic force microscopy** Proc. Microsc. Soc. South Afr., 36, 45, 2006.

Publication 2: Chunilall, V., Wesley-Smith, J. and Bush, T., **Cellulose Fibril aggregation studies of *Eucalyptus* dissolving pulps during drying using Atomic force microscopy,** Proc. Microsc. Soc. South Afr., 38, 46, 2008.

Publication 3: *in press* – Journal '***Holzforschung'***
Controlling cellulose fibril aggregation of *Eucalyptus* dissolving pulp samples
Viren Chunilall, Tamara Bush, Per Tomas Larsson, Tommy Iversen, Andrew Kindness.

Publications 1 and 2 were written by Chunilall, Bush and Wesley-Smith.

Publication 3 was written by Chunilall, Bush and Larsson. The last two co-authors edited the paper in their capacity as supervisors.

Signed:

Acknowledgements

Firstly, I am thankful to the CSIR for giving me the opportunity to pursue my PhD.

I am grateful for the financial support provided for the study by CSIR, Sappi Saiccor and the South African – Swedish Research Links programme.

I would like to express my extreme gratitude to the following people for their guidance and assistance during my study:

Dr. Tammy Bush, Prof. P. T. Larsson and Prof. A. Kindness, my supervisors.

Staff and colleagues at the CSIR Forestry and Forest Products Research Centre, in particular Mr. N. Gounden, Miss. S. Gounden, Mr. M. Isiah Dhlamini, for their assistance with the experimental work.

Staff and colleagues at the Department of Chemistry, University of Kwa-Zulu Natal.

Staff and colleagues at the Electron Microscopy Unit, University of Kwa-Zulu Natal.

I am grateful for the warmth and generosity shown by the staff, in particular Prof. T. Iversen and Prof. L. Salmén, at Innventia (Swedish Pulp and Paper Research Institute) in Sweden.

I am thankful for the open-heartedness shown to me by Mr. Ashok Ramsarup and family.

Lastly, it is with sincere gratitude that I wish to acknowledge my mother, brothers and sister, my wife Lee-Ann and son Anvir for their support during my studies.

DEDICATION

This thesis is dedicated to those that have played a silent yet significant part in my life:

My father	Kemlall Chunilall
My brother	Rabin Chunilall
My nephew	Roscoe Rajanah

Table of contents

Chapter 3

List of figures

List of tables

List of abbreviations

AFM – Atomic Force Microscopy

Alkcell – Alkali cellulose

AR – Analar reagent

cP – centipoises

CP/MAS ^{13}C-NMR – Cross Polarisation / Magic Angle Spinning Nuclear Magnetic Resonance

CS_2 – carbon disulphide

DP – Degree of Polymerisation

FTIR – Fourier Transform Infrared spectroscopy

^{1}H-NMR – Proton Nuclear Magnetic Resonance

L – Lumen

LFD – Lateral Fibril Dimensions

LFAD – Lateral Fibril Aggregate Dimension

$LFAD_{NMR}$ – Lateral Fibril Aggregate Dimensions Nuclear Magnetic Resonance

$LFAD_{AFM}$ – Lateral Fibril Aggregate Dimensions Atomic Force Microscopy

LODP – Level Off Degree of Polymerisation

MCC – Microcrystalline cellulose

MHz – Mega hertz

μm – micrometer

N/m – Newton/metre

nm – nanometer

m/m – mass per mass

m/v – mass per volume

OM – Official method

PPM – Parts per million

P – Primary wall

RH – relative humidity

SEC-MALLS – Size Exclusion Chromatography coupled with Multi-Angle Laser Light Scattering

S1 – The first secondary layer in the wood cell wall

S2 – The second secondary layer in the wood cell wall

S3 – The third secondary layer in the wood cell wall

S_{10}% – Total extractable hemicellulose content and degraded cellulose content

S_{18}% – Total extractable hemicellulose content

SSA – Specific Surface Area

SSS-NCLR – Super Sharp Silicon – Non Contact/Tapping mode Long cantilever Reflex coating

STFI – Swedish pulp and paper research institute

TM – Test method

TMS – Tetra methyl silane

UM – Useful method

WAXS – Wide-angle X-ray scattering

Glossary

Acid bi-sulphite process – treatment of wood chips with a mixture of sulphurous acid and bi-sulphite ions under specific conditions.

Acid hydrolysis – hydrolysis with dilute acids at elevated temperatures.

Anhydroglucose unit – Two glucose monomers polymerise to form an anhydroglucose unit.

Bleaching – Removal or modification of the coloured components in pulp with the object of increasing its brightness.

Cellulose – β-(1-4) linked homopolymer of anhydroglucose comprising 40 – 50% of the dry mass of wood.

Condition dried – pulp dried in a condition room at 50% relative humidity and 23ºC for 5 days.

Consistency – percentage solid content in wet pulp.

Cu-Number – This gives an indication of the reducing end groups in pulp.

D_1 stage – First chlorine dioxide bleaching stage.

D_2 stage – Second chlorine dioxide bleaching stage.

Degree of Polymerisation (DP) – average number of glucose units in the cellulose chain.

Dissolving pulp – It is a high grade cellulose pulp, with low amounts of hemicellulose, degraded cellulose and lignin, produced by pulping.

E stage – Alkaline extraction stage.

Hemicellulose – group of heterogeneous polymers that play a supporting role in the fibre wall.

Holocellulose – wood that has been subjected to successive chlorite delignification.

H stage – Hypochlorite bleaching stage.

Klason lignin – Acid insoluble lignin content in wood and pulp samples determined by gravimetric analysis.

Kraft process – treatment of wood chips with a mixture of sodium hydroxide and sodium sulphide under specific conditions.

Lignin – Branched heterogeneous aromatic polymer former of phenylpropane units linked together mainly by β-O-4 arylether linkages.

Liquor – pulping liquor made up of a mixture of sulphurous acid and bi-sulphite ions for the acid bi-sulphite process or a mixture of sodium hydroxide and sodium sulphide for the Kraft process.

Never dried – pulp that has not been dried and has a moisture content of approximately 70%.

Oven dried – pulp that has been dried in an oven at 104ºC for 12 hours.

O stage – Oxygen delignification stage.

Permanganate number (k-number) – This test is used to assess the lignin content after each stage of processing.

Pulping – Treatment of wood chips in a pressurised vessel at elevated temperature in a solution containing pulping chemicals until a certain degree of delignification is reached.

P stage – Peroxide bleaching stage.

Solubility – Provides information on the degradation of cellulose and loss or retention of hemicellulose during the pulping and bleaching process.

Viscosity – Provides an estimate of the degree of polymerisation of a cellulose chain.

χ^2 – value (Chi squared – value) – statistic measure used to characterise how well an experimentally observed distribution matches an expected distribution.

Chapter 1

1. Introduction

Dissolving pulp is a high-grade cellulose pulp, with low amounts of hemicellulose, lignin and resin (Christoffersson, 2005) and is the raw material used in the manufacture of various cellulose derivatives such as cellulose acetate, viscose, microcrystalline cellulose etc. The important criteria of the dissolving pulp, needed to produce cellulose derivatives, are the supra-molecular structure of cellulose I, accessibility to chemicals and consequently 'reactivity' (Christoffersson, 2005). The 'reactivity' of dissolving pulp is often viewed as a significant quality parameter; Krässig stated that the structure of the fibre determines the 'reactivity' and accessibility of the cellulose to chemicals (Krässig, 1996). Cellulose I is one of the major components of dissolving pulp and constitutes the cell wall of plants and woods. It is the β-1,4-homopolymer of anhydroglucose (Krässig, 1996) (Sarko, 1987). Maximising the commercial use of cellulose I dissolving pulp is dependant on developing a clear understanding of its chemical properties as a function of the structural characteristics (Larsson *et al.*, 1999).

The popularity of hardwoods for dissolving pulp production has increased gradually over the last two decades due to the lower cost and better availability of the hardwood raw material (Sixta *et al*., 2004). Acid bi-sulphite pulping and the pre-hydrolysis kraft process are of major importance for dissolving pulp production (Sixta *et al.*, 2004; Christoffersson, 2005). In South Africa, Sappi Saiccor, a major manufacturer of dissolving pulp from *Eucalyptus* clones, produces approximately 600 thousand tons per year of dissolving pulp (68 % of total world production) using acid bi-sulphite pulping.

In the present study, a single Eucalyptus clone *E. grandis* x *E. urophylla* (GU A380) sampled from a single site* was selected.

* Site Quality Classification based on Forest Land Types for Sappi Landholdings. (Pallett, 2001)

Genetic and environment differences between the clones have been shown to influence the pulp properties (Clarke, 2001) hence the single clone was selected for this study in order to minimize the effects of genetics and the environment on dissolving pulp quality. The GU clone was processed in the laboratory using acid bi-sulphite pulping and a four stage bleaching sequence to produce different purity grades of 'final' dissolving pulp i.e. 91%, 92% and 96% α-cellulose. The α-cellulose classification is based on the amount of total hemicellulose and degraded cellulose removed during bleaching. A 96% α-cellulose sample will have low amounts of hemicellulose and degraded cellulose.

The properties of dissolving pulp depend on the supra-molecular structure of the cellulose. It is thus essential to be able to study cellulose I structure. From a very early date, techniques such as X-ray diffraction (Meyer and Mark, 1928) and infrared spectroscopy (Tsuboi, 1957; Liang and Marchessault, 1959) have been used to study the crystalline structure of cellulose. X-ray diffraction was able to provide more information towards the three-dimensional structure of crystalline cellulose whereas infrared spectroscopy, with the aid of deuteration, has shown existence of crystalline and non-crystalline cellulose (Tsuboi, 1957). More modern techniques used to study cellulose I structure include Cross Polarization / Magic Angle Spinning Carbon 13 – Nuclear Magnetic Resonance - CP/MAS ^{13}C-NMR (Solid state NMR) (Atalla and VanderHart, 1984; 1999; Larsson *et al.*, 1997; Wickholm *et al.*, 1998) and Atomic Force Microscopy (AFM) (Fahlén and Salmén, 2005; Kontturi and Vuorinen, 2009). Solid state nuclear magnetic resonance spectroscopy utilizes the fact that various magnetic nuclei have different magnetic properties. By recording the differences in the magnetic properties it is possible to estimate the positions of the nuclei in the molecule. It is also possible to determine how many different environments there are in the molecule. Solid state NMR has been applied, initially, to the study of native celluloses where Atalla and VanderHart (1984) demonstrated the existence of two crystalline forms of cellulose I (Figure 1.1).

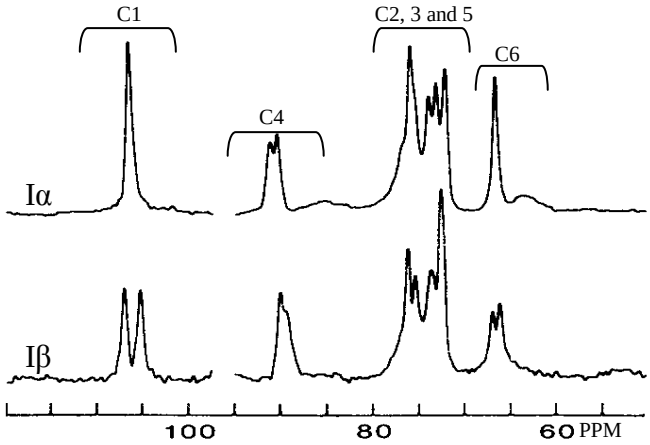

Figure 1.1: Approximate CP/MAS ^{13}C-NMR spectra of cellulose Iα and Iβ from plant celluloses (Atalla and VanderHart, 1984).

This pioneering research opened up the pathway for other researchers to follow (Newman and Hemmingson, 1994; Larsson *et al.*, 1995, 1997, 1999; Maunu, 2000; Duchesne *et al.*, 2001; Hult *et al.*, 2002; Virtanen *et al.*, 2008). Several years later Larsson and co-workers (1997) showed that, apart from the presence of cellulose Iα and Iβ, other non-crystalline forms also existed. The different components of the C4 region thus consisted of crystalline cellulose Iα, Iβ and I(α+β), paracrystalline cellulose, non-crystalline components. Mathematical fitting of the different regions in the spectrum, using Gaussian and Lorentian line shapes, made quantification of spectra possible. Numerous studies such as X-ray diffraction (Teeäär *et al.*, 1987), field emission scanning electron microscopy (Duchesne and Daniel, 2000), Atomic force microscopy studies (Fahlén and Salmén, 2005) have been carried out to support the applicability of solid state NMR to the study of cellulose supra-molecular structure (i.e. cellulose aggregation within the S2 layer of the dissolving pulp fibre wall). Using various experimental methods, a model of cellulose I was hypothesised, the 'Cellulose I Fibril Aggregate Model', showing the different regions in a cellulose I spectrum (Larsson *et al.*, 1997; Wickholm *et al.*, 1998).

The objective of the present study is to understand the effects of pulping, bleaching and drying on cellulose I structure at the supra-molecular level and also to assess the 'reactivity' of the different grades of dissolving pulp samples i.e. 91%, 92% and 96% α-cellulose to manufacture microcrystalline cellulose, viscose and cellulose acetate

respectively. The degree of cellulose aggregation in the fibre wall has been determined using solid state NMR. The model, developed by Larsson *et al.* (1997), has been applied to understand these effects. Fahlén and Salmén (2002, 2003, and 2005) have shown that AFM is a 'useful tool for transverse fibre wall characterisation on the nanoscale'. Together with image analysis, AFM can be used to quantify cellulose aggregate dimensions within the S2 layer of wood and dissolving pulp fibres (Fahlén and Salmén, 2003; 2005). Cellulose aggregate measurements using solid state NMR and AFM in addition to a range of wet chemical properties i.e. Estimate of degree of polymerisation (Viscosity), total hemicellulose and degraded cellulose content and total hemicellulose content (Solubility), Lignin content (K-number) etc. have been used to identify the drivers of the changes in supra-molecular structure during acid bi-sulphite pulping, bleaching and drying. In addition, the study has tried to identify any links between cellulose aggregation and 'reactivity' to the production of various cellulose derivatives. Studies have been conducted previously using solid state NMR and AFM on softwoods and kraft pulp (Larsson *et al.*, 1997; Wickholm *et al.*, 1998; Fahlén and Salmén, 2003; 2005); (Kontturi and Vuorinen, 2009). Very few researchers have studied pulping and bleaching on hardwood and acid bi-sulphite dissolving pulp. Nocanda *et al.*, (2007) have shown that the method developed by Larsson *et al.* (1997), for the quantification of cellulose aggregate dimensions in softwood kraft pulp samples, can be applied to hardwoods and dissolving pulp produced by acid bi-sulphite pulping. For the purpose of this thesis the 91%, 92% and 96% α-cellulose dissolving pulp samples will be represented as 91α, 92α and 96α respectively.

The present study is novel in its approach to study a single hardwood clone that has been acid bi-sulphite pulped, bleached to produce 3 different grades of dissolving pulp i.e. 91α, 92α and 96α. These dissolving pulp grades are used for the production of cellulose derivatives such as microcrystalline cellulose (91α), viscose (92α) and cellulose acetate (96α). The accessibility of cellulose to chemical reagents is of great importance in the manufacturing of cellulose derivatives since a homogeneous substitution of the hydroxyl functional groups in the cellulose I chain is desired in order to obtain high value products. However, the structure of cellulose I ultimately governs the accessibility to chemical reagents. The study will provide information on

the structure and accessibility of cellulose I and its effect on the chemical ‘reactivity’ of dissolving pulp produced from a single hardwood clone.

Chapter 2

2. Cellulose I

2.1 The cell wall ultra-structure

Wood is composed mainly of three types of material; cellulose, hemicellulose and lignin, with the relative composition varying in different species of trees (Fengel and Wegener, 1984). The wood cell wall is composed of the primary wall (P) and the secondary wall (S) (Figure 2.1).

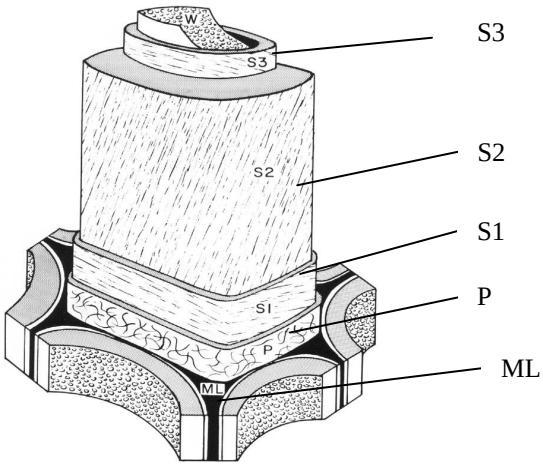

Figure 2.1: Simplified structure of the wood cell wall showing the middle lamella and the layers of the cell wall (P, S1, S2, S3, and L-lumen) (Côté, 1967)

The secondary wall (S) which is laid down after cell division can be subdivided into three layers. The outermost, S1, comprises approximately 10% wall thickness. The middle layer, S2, comprises approximately 85% of the wall thickness. The innermost layer, S3, comprises approximately 1% of the wall thickness (Fengel and Wegener, 1984; Sjöström, 1993). The lignin-rich middle lamella (ML) between the fibres serves to bind the fibres together. The secondary wall contains, mainly, cellulose, hemicellulose and lignin whereas the primary wall also contains a considerable amount of pectin, xyloglucan and protein (Fengel and Wegener, 1984; Sjöström, 1993). Knowledge of the ultra-structural arrangement within wood fibres is important

for understanding and controlling the ultra-structural changes that occur during pulp processing.

2.1.1 Cellulose, Hemicellulose and Lignin

Glucose is produced by the action of photosynthesis. Haworth, in the late 1920's, proposed that the glucose units polymerise with the adjacent glucose units to form a long glucan chain (Haworth, 1928) (Figure 2.2). Water is removed from the glucose in this process and so each individual unit is an anhydroglucose unit ($C_6H_{10}O_5$). The anhydroglucose unit is in the form of a six sided ring consisting of 5 carbon atoms and 1 oxygen atom, the former carrying side groups which play an important role in intra- and intermolecular bonding. Every alternate anhydroglucose unit along the glucan chain is rotated around the C(1) – C(4) axis by 180º (Krässig, 1996) resulting in a long, straight glucan chain.

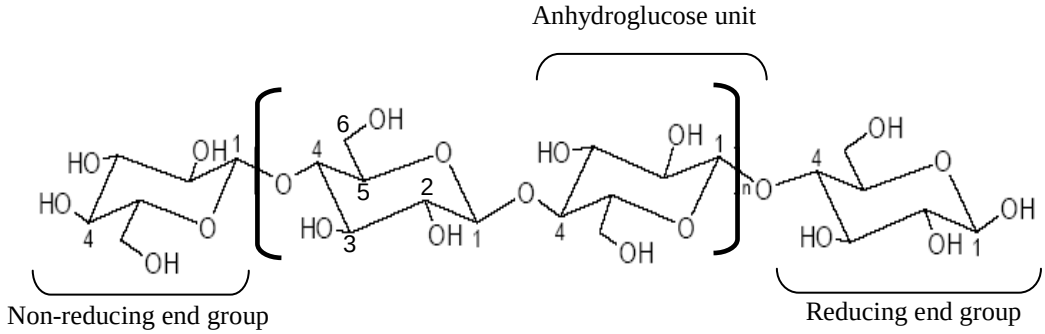

Figure 2.2: Cellulose, β-(1-4) linked homopolymer of anhydroglucose (Krässig, 1996)

The linear glucan chains are linked laterally by hydrogen bonds to form linear bundles (Sjöström, 1993), giving rise to cellulose. Payen, in 1838, was the first to determine the elemental composition of cellulose I and conclude that it had the empirical formulae of $C_6H_{10}O_5$ (Krässig, 1996; Kadla and Gilbert, 2000). Cellulose is the most abundant compound in the cell wall of plants and woods. Approximately 40 – 50% of the dry mass of wood is in the form of cellulose (Fengel and Wegener, 1984).

Hemicellulose is the second major component in a wood fibre. Hemicelluloses are a group of heterogeneous polymers that play a supporting role in the fibre wall. Twenty to thirty percent of the dry weight of wood consists of hemicellulose (Fengel and

Wegener, 1984). Hemicelluloses are branched, low-molecular-weight polymers composed of several different kinds of pentose and hexose sugar monomers (Miller, 1999). The main constituents are glucose, mannose, galactose, xylose and arabinose (Mauna, 2002) with the relative amounts varying markedly with species (Miller, 1999). The main hemicellulose in hardwood is xylan, more specifically an O-acetyl-4-O-methylglucurono-ß-D-xylan (Fengel and Wegener, 1984; Sjöström, 1993; Laine, 2005).

The third major component in a wood fibre is lignin. Although lignin occurs in wood throughout the cell wall, it is concentrated toward the outside of the cells and between cells (Miller, 1999). Lignin is often considered the 'cementing agent' that binds individual cells together (Miller, 1999). Lignin is a branched heterogeneous aromatic polymer formed of phenylpropane units linked together mainly by β-O-4 arylether linkages. These linkages constitute approximately 16 – 25% of the dry weight of wood. Lignin does not dissolve in water or other common solvents, but it can be made soluble by chemical action. Delignification that occurs during pulping is mainly due to nucleophillic reactions (Gierer, 1985). The reader is referred to the comprehensive books 'Pulping processes' by S. Rydholm (1965) and 'Lignins' edited by K. V. Sarkanen and C. H. Ludwig (1971). Both books contain chapters describing the most important delignification processes during pulping.

In addition to cellulose, hemicellulose and lignin, wood also contains minor, non-structural, extraneous components (Fengel and Wegener, 1984). It consists of both organic and inorganic extraneous materials. The organic component comprises extractives which contribute to the following wood properties: colour, odour, taste, decay resistance, density, hygroscopicity and flammability. Extractives include tannins and other polyphenolics, colouring matter, essential oils, fats, resins, waxes, gum starch and simple metabolic intermediates. Extractives can be removed from wood by extraction with solvents, such as water, alcohol, acetone, benzene, or ether. Extractives may constitute approximately 5 – 30% of the wood substance, depending on factors such as species, growth conditions, and time of year when the tree is cut (Miller, 1999). The inorganic component of extraneous material constitutes approximately 0.2 – 1.0% of wood. Calcium, potassium, and magnesium are the more abundant elemental constituents (Miller, 1999). Trace amounts (<100 parts per

million) of phosphorus, sodium, iron, silicon, manganese, copper, zinc are also present (Miller, 1999).

2.1.2 Cellulose I fibrils and fibril aggregates

In this study the term ‘glucan’ is used to describe the β-(1-4) linked homopolymer of anhydroglucose. Several glucan chains make up a ‘cellulose fibril’ and several cellulose fibrils make up a ‘cellulose fibril aggregate’. ‘Cellulose fibrils have cross sections of varying shape with widths in the range from a few nanometers to a few tenths of nanometers’ (Larsson, 2003). The arrangement of cellulose fibrils into cellulose fibril aggregates of varying diameters may influence the accessibility of cellulose to chemicals.

2.1.3 Cellulose I crystallinity

The conceptual structural framework of cellulose fibril aggregation is frequently discussed (Atalla, 1990). Krässig (1996) stated that ‘there is a high tendency of cellulose to organise into a parallel arrangement of crystallites and crystallite strands’. This is due to the ability of hydroxyl groups to form hydrogen bonds with one another (Sjöström 1993; Krässig, 1996). X-ray diffraction was used close to a century ago to study the crystalline structure of cellulose from wood, hemp and bamboo (Nishikawa and Ono, 1913). Further studies were inevitable and provided X-ray diffraction patterns of cellulose from different sources and eventually led to several cellulose structures being proposed. A crystalline cellulose molecular model originally developed by Meyer and Mark (1928) was a landmark for the molecular models to follow. Some of these models included work by Sarko and Muggli (1974), Gardner and Blackwell (1974) and Blackwell *et al.* (1977). More recently, the degree of crystallinity of wood pulp was evaluated using X-ray diffraction and solid state NMR measurements (VanderHart and Atalla, 1984; Teeäär *et al*., 1987). VanderHart and Atalla (1984) demonstrated the existence of two distinct cellulose crystalline allomorphs, Iα (triclinic) and Iβ (monoclinic), using solid state NMR. These allomorphs are believed to co-exist in the fibril with a different ratio, depending on the origin i.e. either plant or animal sources like trees or tunicates respectively

(VanderHart and Atalla, 1984). Unravelling the crystalline structure of cellulose I therefore requires the determination of not one but two crystalline structures i.e. cellulose Iα and cellulose Iβ (Figure 2.3). In both cellulose Iα and cellulose Iβ, there are relatively strong O3–H···O5 intra-chain hydrogen bonds (Nishiyama *et al.*, 2002; Nishiyama *et al.*, 2003). Nishiyama *et al.* (2003) described the partially occupied positions of the hydrogen atoms associated with the O2 and O6 atoms by two mutually exclusive hydrogen bonding networks. Their finding suggested that the intra-sheet bonding involving the O2 and O6 donors is disordered over the hydrogen bonding networks in both cellulose Iα and cellulose Iβ. They agreed with earlier suggestions by Blackwell *et al.* (1977) where van der Waals attraction between hydrogen bonded sheets were shown to contribute to cellulose I crystal cohesion and added that their results show that weak C–H···O hydrogen bonding also plays a role.

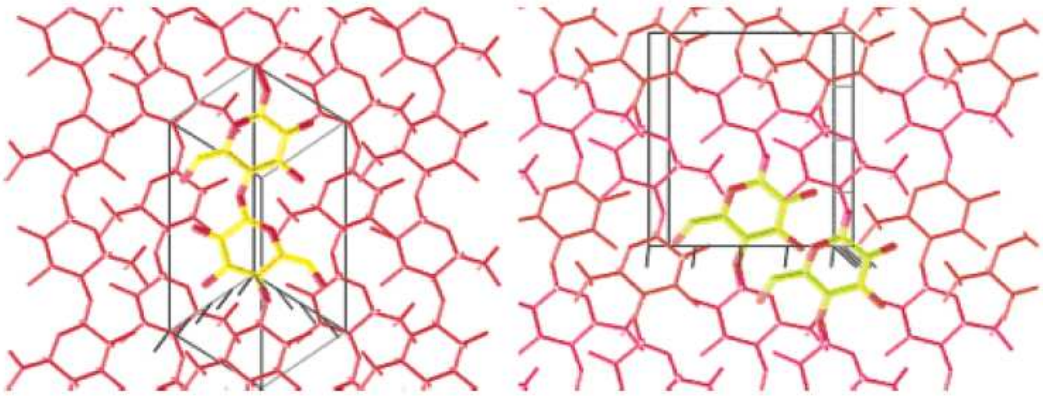

Figure 2.3 Cellulose Iα (left) and cellulose Iβ (right) chains represented by red skeletal models. The asymmetric unit of each structure is represented in thicker lines with carbons in yellow (Nishiyama *et al.*, 2003).

2.1.4 Cellulose I ‘reactivity’

The ‘reactivity’ of cellulose can refer to its capacity to participate in diverse chemical reactions. Each anhydroglucose unit in a cellulose polymer has three different hydroxyl groups. The hydroxyl groups at O(2) H, O(3) H and O(6) H are the main reactive groups susceptible to chemical modification (Verlhac and Dedier, 1990). When discussing reactivity of cellulose I the accessibility of the hydroxyl groups on the surface of fibrils or fibril aggregates to the chemical reagents is a crucial factor

(Krässig, 1996). The accessibility on the surface of fibrils or fibril aggregates is limited by the compact structure of cellulose I, which is determined by the presence of highly ordered regions formed by strong hydrogen bonds (Fengel and Wegener, 1984). With the advent of infrared spectroscopy, accessibility could be determined by deuteration (Tsuboi, 1957). Verlhac and Dedier (1990) described the O(3) H as 'unreactive' when the cellulose surface was highly ordered and 'reactive' when the cellulose surface was less ordered. They used the procedure described Rowland and Howley (1985) to calculate the availability of surface hydroxyl groups. More recently Horikawa and Sugiyama (2008) reported of a Fourier Transform Infrared (FTIR) spectroscopic method to measure the accessibility and size of cellulose fibrils from the cell wall of *Valonia ventricosa* by investigation of deuteration and rehydrogenation. Krässig (1996) proposed that the accessibility of cellulose I depends on the surface, as determined by the size of cellulose fibril aggregate, that is accessible; and the structure of the cellulose molecules, which will determine which hydroxyl groups are accessible; and the size and type of reagent. The method used in this study for assessing cellulose I structure and accessibility was to determine the dissolving pulp reactivity during cellulose derivative formation.

2.1.5 Cellulose I derivatives

The 91α, 92α and 96α dissolving pulp samples were used to manufacture the following cellulose derivatives viz. microcrystalline cellulose (MCC), viscose and cellulose acetate respectively. Each of these manufacturing processes is affected by the quality of the dissolving pulp samples. Christov *et al.* (1998) mentioned that the 'efficiency of conversion of cellulose into specific derivatives is dependant upon the lignin and hemicellulose content of dissolving pulp'. The presence of residual lignin in dissolving pulp contributes to the brightness of the pulp. The solubility of cellulose acetate in the acetate process, cellulose acetate filterability and solution haze can be affected by high concentrations of hemicellulose (Gubitz *et al*., 1998). In the viscose process, high amounts of hemicellulose in cellulose can affect viscose filterability, xanthation, viscose strength properties and final viscose yield (Rydholm, 1965). In the microcrystalline cellulose process, the degree of polymerisation (DP) of the 91α cellulose at the start of the process is critical in obtaining a final or level-off degree of

polymerisation (LODP) of ca. 250 anhydroglucose units. The term ‘level-off degree of polymerization’ refers to the relatively constant value of degree of polymerization which results when cellulose is subjected to severe acid hydrolysis (Belfort and Wortz, 1966). When pulp is hydrolysed with dilute acids at elevated temperatures, the non-crystalline regions of cellulose are destroyed, while the crystalline regions are more resilient to acid hydrolysis. The degree of polymerisation falls and reaches the LODP. The hydrolysed pulp is washed. After drying and grinding microcrystalline cellulose (MCC) powder is obtained (Battista, 1964).

Commercially, cellulose acetate is made from high purity 96α cellulose. The dissolving pulp is processed using acetic anhydride to form acetate flake.
During viscose manufacture high purity 92α cellulose is mixed with 18.5% sodium hydroxide for a period of 30 minutes. This process is known as steeping. In the next step the steeped (alkalized) pulp is ‘pressed’ to remove excess sodium hydroxide. The alkalized pulp is then shredded to increase the surface area for rapid ageing and subsequent xanthation. The xanthation reaction with carbon disulphide (CS_2) results in sodium cellulose xanthate. The sodium cellulose xanthate is then dissolved in sodium hydroxide to form viscose and thereafter ripened to give optimum degree of xanthate substitution for spinning. The product is run through a spinning mechanism and out of a slit into an acid bath, resulting in the formation of viscose filament or cellulose II (Schottler, 1988).

2.2 Isolation of Chemical cellulose I

2.2.1 Traditional methods: Sulphate (‘kraft’) pulping vs Sulphite (acid bi-sulphite) pulping

Sulphate pulping is the most common process and uses sodium sulphide and sodium hydroxide as its main chemical ingredients. The process produces a brown pulp often called ‘kraft’ pulp. The lignin macromolecule is depolymerised mainly through the cleavage of the ether linkages to become dissolved in the pulping liquor. The normal operating temperature during pulping is in the range 150 – 180ºC while under pressure. The temperature is critical to the rate of the pulping process. Pulping time is

generally up to 4 hours. The ‘kraft’ pulping process results in a pulp yield of between 45 – 60%. Kraft pulp fibres are normally used in bleached form in paper and board products, however with the addition of a preceding acid prehydrolysis stage the kraft process can also be used to produce dissolving pulp (Kordsachia *et al.*, 2004).

Sulphurous acid and bi-sulphite ions are the main ingredients during acid bi-sulphite pulping. The sulphite pulping cycle is divided into three main processes; the penetration period, the pulping period and the recovery period. Time must be allowed for the chemicals to penetrate the chips completely. The slowest chemical reaction determines the reaction rate (Fengel and Wegener, 1984). The temperature in the reaction vessel is raised slowly over a period of about 4 hours to 130ºC (Penetration period). Following the penetration period, the temperature is raised to the maximum, usually between 135ºC and 145ºC and pulping commences (Pulping period). The pressure is allowed to rise until it reaches about 800 kPa and then maintained constant by venting. The pulping period is varied between 43 minutes to 103 minutes depending on the amount of lignin removal required. When the pulping process ends, the pressure is reduced below 100 kPa during a period of about 90 minutes in order to recover chemicals (Recovery period). The pulping finishes during the recovery period, and at the end the pulp washed and screened. The total pulping time for acid bi-sulphite pulping is approximately 8.5 hours (Fengel and Wegener, 1984). Sulphite pulping takes longer but has a slightly higher yield than the ‘kraft’ pulping process (Karlsson, 2006). A disadvantage of the sulphite process, compared to the sulphate/‘kraft’ process, is the environmental concerns associated with it i.e. difficulty in chemical recovery during the process (Karlsson, 2006). The sulphite process is however characterised by its high flexibility compared to the ‘kraft’ process. In principle, the entire pH range can be used for sulphite pulping by changing the dosage and composition of the chemicals, whereas ‘kraft’ pulping can be carried out only with highly alkaline pulping liquor. Thus, the use of sulphite pulping permits the production of many different types and qualities of pulp samples for a broad range of applications. The sulphite process can be distinguished according to the pH into four different types of pulping namely Acid bi-sulphite, Bi-sulphite, Neutral sulphite (NSSC) and Alkaline sulphite. Table 2.1 presents the main pH ranges for different sulphite pulping processes.

Table 2.1: pH ranges for different sulphite pulping processes (Uhlmann, 1991)

Process	pH	Base	Active reagent	Pulping temperature ºC	Pulp yield %	Applications
Acid bi-sulphite	1-2	Ca^{2+}, Mg^{2+}, Na^{+}	SO_2 H_2O, H^{+}, HSO_3	125 – 143	40 – 50	Dissolving pulp, tissue, printing paper, special paper
Bi-sulphite	3-5	Mg^{2+}, Na^{+}	HSO_3^{-}, H^{+}	150 – 170	50 – 65	Printing paper, tissue
Neutral sulphite (NSSC)	5-7	Na^{+}, NH_4^{+}	HSO_3^{-}, SO_3^{2-}	160 – 180	75 – 90	Corrugated medium, semi-chemical pulp
Alkaline sulphite	9 – 13.5	Na^{+}	SO_3^{2-}, OH^{-}	160 - 180	45 – 60	'Kraft' – type pulp

2.2.2 Chemical pulping

"In a pulping process, wood is converted into fibres. This can be achieved mechanically, thermally, chemically or through a combination of these techniques" (Karlsson, 2006). For this study a single clone, *E. grandis* x *E. urophylla* clone (GU A380) was sampled from Zululand in Northern Kwa-Zulu Natal, South Africa, site quality 1*, high site index, was pulped using acid bi-sulphite pulping conditions. Chemical delignification, an important process during pulping, includes all processes resulting in partial or total removal of lignin from wood by the action of suitable chemicals (Gierer, 1985). The lignin macromolecule is depolymerised through the cleavage of the ether linkages to become dissolved in the pulping liquor. The α-hydroxyl and α-ether groups are readily cleaved under simultaneous formation of benzilium ions (Funaoka *et al.*, 1991). The cleavage of the open α-aryl ether linkages represents the fragmentation of lignin during acid sulphite pulping. The benzilium ions are sulphonated by attack of hydrated sulphur dioxide or bi-sulphite ions, resulting in the increased hydrophylic nature of the lignin molecule. The extent of delignification depends on the degree of sulphonation as well as the depolymerisation (Funaoka *et al.*, 1991). In summary the aim of pulping is to break down the lignin bonds between the fibres using chemicals and heat, enabling easy removal by washing, whilst not destroying the cellulose and hemicellulose components.

* Site Quality Classification based on Forest Land Types for Sappi Landholdings. (Pallett, 2001)

2.2.3 Dissolving pulp

The unbleached pulp that results after acid bi-sulphite pulping is used as raw material for dissolving pulp production. Lignin and hemicelluloses in the unbleached pulp are considered to be contaminants and are removed in order to produce high purity dissolving pulp samples. This can be done using oxygen delignification followed by a 4 step bleaching sequence. The bleaching sequence can either be Chlorine dioxide – Alkali extraction – Chlorine dioxide – Hypochlorite (D_1ED_2H) or Chlorine dioxide – Alkali extraction – Chlorine dioxide – Peroxide (D_1ED_2P) stage depending on the desired end product i.e. 91α, 92α or 96α dissolving pulp samples. "Dissolving pulp is a chemical pulp intended primarily for the preparation of chemical derivatives of cellulose. It is utilized for the chemical conversion into products such as microcrystalline cellulose, cellophane, cellulose acetate, cellulose nitrate" (Karlsson, 2006).

2.2.4 Bleaching

Bleaching is the chemical process performed on acid bi-sulphite pulp designed to remove hemicelluloses, residual lignin and at the same time improve the brightness of the pulp samples. Table 2.2 presents the shorthand of chemical treatments used in delignification and bleaching.

Table 2.2: Shorthand of chemical treatments used in delignification and bleaching

Stage	**Abbreviation**	**Process**
Oxygen	O	Delignification
Chlorine dioxide	D	Brightness
Alkali extraction stage	E	Extract hemicelluloses and solubilise lignin degradation products
Hypochlorite stage[a]	H	Polymer chain scission (control viscosity)
Peroxide stage[b]	P	Brightness and residual hemicellulose removal

[a] Used for 91α and 92α dissolving pulp production

[b] Used for 96α dissolving pulp production

Different grades of dissolving pulp require different bleaching conditions. Refer to the experimental design for details (Tables 3.4, 3.5 and 3.6, Chapter 3). Temperature, time, pressure and concentration of alkali are varied to produce the desired grade of dissolving pulp.

(i) O stage: Oxygen delignification under alkali conditions

The first commercial oxygen delignification installation was in South Africa during the 1970's (De Souza *et al*., 2002). It was seen as a cost effective and environmentally friendly method to reduce chemical consumption during bleaching. In the normal state oxygen is a weak reactant. The reactivity can be increased by increasing the temperature and providing a reactive substrate. The use of sodium hydroxide provides the alkaline conditions required to ionise free phenolic hydroxyl groups in residual lignin (Dence and Reeve, 1996).

$$HOROCH_3 + NaOH \rightarrow {}^{-}OROCH_3 + H_2O \qquad (1)$$

As a result of the above reactions (Equation 1, Dence and Reeve, 1996), lignin becomes oxidized and more hydrophilic making it easier to remove from the pulp. During oxygen delignification approximately 50% of residual lignin can be removed from the pulp (Dence and Reeve, 1996).

(ii) D Stage: Chlorine dioxide

The D stage uses chlorine dioxide as a bleaching agent. The primary function of this stage is to improve the brightness of the pulp. The principle of the brightening reaction is based on the reaction of the chlorine compounds, produced by chlorine dioxide, with chromophoric (colour generating) compounds in the pulp (i.e. Lignin). Chlorine dioxide is a radical bleaching agent and reacts with phenolic and non-phenolic lignin.

$$HOROCH_3 + ClO_2 + H_2O \rightarrow HOOROOCH_3 + ClO_2^{-} + HOCl + H^{+} \qquad (2)$$

It reacts slowly with non-phenolic lignin structures and more easily with phenolic lignin and ionized lignin structures. As chlorine dioxide oxidizes lignin it is reduced

to chlorite (Equation 2). The reaction products are more hydrophilic than the original compounds and therefore are easier to wash out of the pulp.

(iii) E Stage: Alkaline extraction

The chlorine dioxide stage is normally followed by an alkaline extraction stage to further remove lignin (Dence and Reeves, 1996). The Alkaline extraction stage functions to extract hemicelluloses and solubilise lignin degradation products which are subsequently washed out of the pulp. The amount of NaOH added at the alkaline extraction stage is dependant on the desired end product i.e. 91α, 92α or 96α dissolving pulp samples. A lower dose will target the 91α and 92α dissolving pulp samples whereas a higher dose will target the 96α dissolving pulp sample. This stage ensures that the chloro and oxidized lignin from the previous chlorine dioxide (D) stage are dissolved and removed. The reader is referred to a comprehensive book, 'Pulp bleaching – Principles and practices' edited by Dence and Reeves (1996), that details the reactions and mechanisms involved during alkaline extraction.

(iv) Hypochlorite stage (Final stage)

The hypochlorite stage is the final stage of bleaching used to produce both the 91α and 92α pulp samples. This stage uses hypochlorite under alkaline conditions at a temperature of 58ºC. The function of this stage is to control the viscosity of the pulp (i.e. the degree of polymerisation) whilst increasing the brightness of the pulp. Using a higher dose of hypochlorite e.g. in the 91α pulp sample, results in a lower viscosity and hence lower degree of polymerisation compared to the 92α pulp sample.

(v) Peroxide stage (Final stage)

'Hydrogen peroxide is a potent, relatively inexpensive oxidant that chemically degrades chromophoric components in pulp samples' (Poggi *et al*., 2005). The peroxide stage is used to target a 96α grade cellulose pulp. The use of hydrogen peroxide favours the partial or complete elimination of elemental chlorine from the final pulp (Resich, 1995; Johnson, 1994). 'The formation of the per-hydroxyl anion has been widely described as important for the bleaching reaction' (Zeronian and Inglesby, 1995), the concentration of which depends largely on the pH of the solution (Andrews, 1979). Hydrogen peroxide solutions react quite slowly at low temperatures and pH (Valko, 1955). This stage removes any residual hemicelluloses without

affecting the degree of polymerisation. The reader is referred to a review, 'Bleaching of cellulose by hydrogen peroxide' by Zeronian and Inglesby, 1995 and references therein, that details the reactions and mechanisms involved during hydrogen peroxide bleaching.

Thus far, the cell wall ultra-structure of wood; the supra-molecular structure of cellulose I fibrils and fibril aggregates; the concepts of cellulose accessibility and 'reactivity'; the importance of cellulose derivatives and the processes to manufacture them; the cellulose I isolation procedure that encompasses acid bi-sulphite pulping and the delignification and various bleaching involved required to produce dissolving pulp has been described. This study presents the following techniques, Cross-Polarization Magic Angle Spinning Carbon-13 Nuclear Magnetic Resonance (CP/MAS ^{13}C-NMR) spectroscopy and Atomic Force Microscopy for the purpose of understanding cellulose I structure, accessibility and 'reactivity'. The strength and limitations of the techniques to determine cellulose I structure, accessibility and 'reactivity' are also discussed.

2.3. Solid state NMR Spectroscopy for determining cellulose I supra-molecular structure

Application of Cross-Polarization Magic Angle Spinning Carbon-13 Nuclear Magnetic Resonance (CP/MAS ^{13}C-NMR) spectroscopy for the purpose of understanding the cellulose I structure was first reported by Atalla and VanderHart (1984). CP/MAS ^{13}C-NMR spectroscopy can detect changes in the fibre wall polymer interactions during chemical pulping, bleaching and drying. The degree of cellulose aggregation in the fibre wall can be determined by CP/MAS ^{13}C-NMR spectroscopy. When studying different allomorphs of cellulose by CP/MAS ^{13}C-NMR spectroscopy, various methods can be used to resolve the overlapping peaks, one of which is spectral fitting (Wickholm *et al*., 1998; Larsson *et al*., 1999). CP/MAS ^{13}C-NMR in conjunction with spectral fitting is capable of distinguishing between the different types of cellulose in pulp. These are the accessible fibril surfaces, paracrystalline regions, inaccessible fibril surfaces and crystalline (cellulose Iα + Iβ) components (Figure 2.4). The assignment of specific resonances has been obtained by studies on

celluloses from known sources; in particular *Valonia, Cladophora, Halocynthia* cellulose, cotton linters and birch (Wickholm *et al.*, 1998). NMR spectroscopy has shown potential for studying solid-state structures such as cellulose I. The introduction of Cross-Polarisation Magic Angle Spinning (CP/MAS) opened up new possibilities (Schaefer, 1977; Yannoni, 1982). Proton-carbon cross polarizations enhance the sensitivity and the magic angle spinning improves the resolution, resulting in well-resolved ^{13}C spectra (Schaefer, 1977; Yannoni, 1982).

2.3.1 Principles of CP/MAS ^{13}C-NMR spectroscopy

CP/MAS ^{13}C-NMR spectroscopy is a useful technique for studying the structure of semi-crystalline polymorphic solids. Solid state NMR has not always been used for structure determination because of line broadening. Broad lines characteristic of conventional NMR measurements on solid samples is attributed to two causes, static dipolar interactions between ^{13}C and ^{1}H and the chemical shift anisotropy. The strong dipolar interaction between ^{13}C and neighbouring protons can be removed by high-power proton decoupling. The second cause of line broadening, the chemical shift anisotropy is experimentally diminished by Magic Angle Spinning (MAS), which incorporates a rapid spinning (5 kHz) at an angle of 54.7 degrees with respect to the external magnetic field. Magic angle spinning will also average any residual dipolar broadening (Sanders and Hunter, 1987). Cross-Polarization (CP) is a pulse technique used to enhance the signal-to-noise ratio of the spectrum, since ^{13}C is a low abundance nuclei and its spin-lattice relaxation in solids is long (Schaefer and Stejskal, 1976). This enhancement is performed by first exciting the ^{1}H spins and then transferring the magnetism to the ^{13}C-spin system (Schaefer and Stejskal, 1976). Cross-polarization in combination with magic angle spinning and high power proton decoupling generates spectra with comparatively high resolution and good sensitivity (Schaefer and Stejskal, 1976). Typical CP/MAS ^{13}C-NMR spectra from cellulose I are made up of six signals from the anhydroglucose unit split into fine structure clusters due to the supra-molecular structure of the cellulose I fibril (Figure 2.4). The information content in this fine structure is high, but the accessibility of the information is hampered by a severe overlap of the signals (Larsson *et al.*, 1999). In order to obtain

quantitative information on the supra-molecular structure of cellulose, post-acquisition processing (spectral fitting) of the spectra is needed (Larsson *et al.*, 1999).

2.3.2 CP/MAS ^{13}C-NMR in combination with spectral fitting

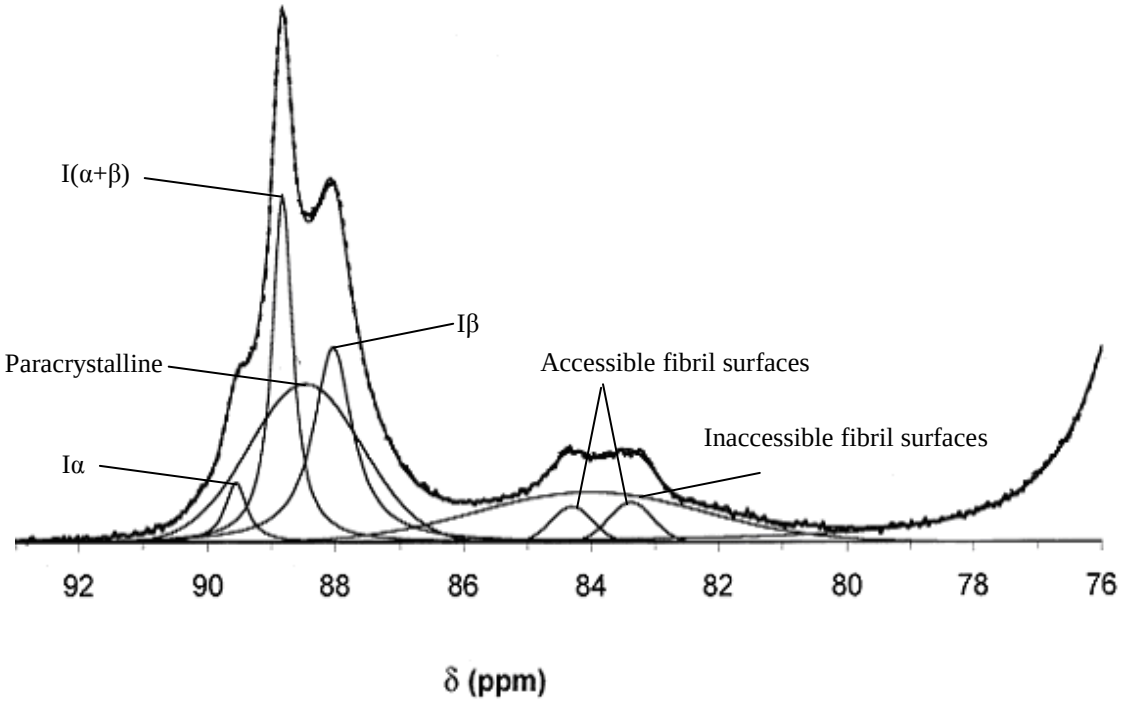

Figure 2.4: The fitting of the C-4 region of a CP/MAS ^{13}C-NMR spectrum recorded on chemically disintegrated cotton cellulose.

Figure 2.4 shows the experimental spectrum as a broken line. The fitted spectral lines and their superposition are shown as solid lines. The broken line of the experimental spectrum is partially hidden by the superimposed fitted spectrum. The model for the spectral C-4 region of cellulose I fibrils consists of seven distinct lines: three Lorentzian lines for the signals from the crystalline cellulose I allomorphs, cellulose Iα (89.5 ppm), I(α+β) (88.8 ppm), and I β (87.9 ppm), and four Gaussian lines for the remaining signals attributed to non-crystalline cellulose forms, paracrystalline cellulose (88.4 – 88.7 ppm), accessible fibril surfaces (84.3 and 83.3 ppm) and inaccessible fibril surfaces (approximately - 83.8 ppm) (Figure 2.4) (Larsson *et al.*, 1995; Larsson *et al.*, 1997; Wickholm *et al.*, 1998). The spectral fitting of the C-4

region in plant celluloses is performed by starting with the dominating signals for paracrystalline cellulose and cellulose at inaccessible fibril surfaces. After convergence at this level, additional lines are added to describe the crystalline allomorphs and cellulose at accessible fibril surfaces. After final convergence, the fitted result is evaluated with respect to the χ^2 – value (statistic measure used to characterize how well an experimentally observed distribution matches an expected distribution (Press *et al*., 1986)), agreement of chemical shifts and line-widths with an appropriate reference spectrum such as the spectrum of cotton linters (Cotton linters is approximately 99.9% pure cellulose I). If applicable, agreement between the obtained and the expected signal intensity ratios for cellulose Iα and cellulose Iβ is also a criterion for acceptance (Yamamoto and Horii, 1993). To describe the hemicellulose contribution in the spectra a minimum number of additional Gaussian lines are added to the cellulose C-4 region to obtain an acceptable fitting of the cellulose part of the spectrum and a χ^2-description of the overall spectrum (Hult *et al.*, 2001).

2.3.3 Cellulose I Fibril Aggregate Model

A model of aggregated cellulose I fibrils was constructed based on spectral fitting and spin diffusion experiments (Figure 2.5) (Wickholm, 2001). Two C-4 signals at 84.3 and 83.3 ppm are assigned to cellulose at accessible fibril surfaces in contact with water and the C-4 signal at 83.8 ppm is assigned to cellulose at water-inaccessible fibril surfaces, formed either by interior distortions or aggregation of fibrils (Hult, 2001). Paracrystalline cellulose can be partly explained as being due to distortions from the fibril-fibril contact surfaces reaching into the fibril interior (Hult, 2001) i.e. the result of fibrils forming fibril aggregates. This is schematically illustrated in Figure 2.5 where the paracrystalline cellulose is shown to penetrate one layer below the fibril surface. This is purely an arbitrary representation since penetration depth is dependent on the size and severity of the distortions induced at the fibril surfaces (Wickholm, 2001).

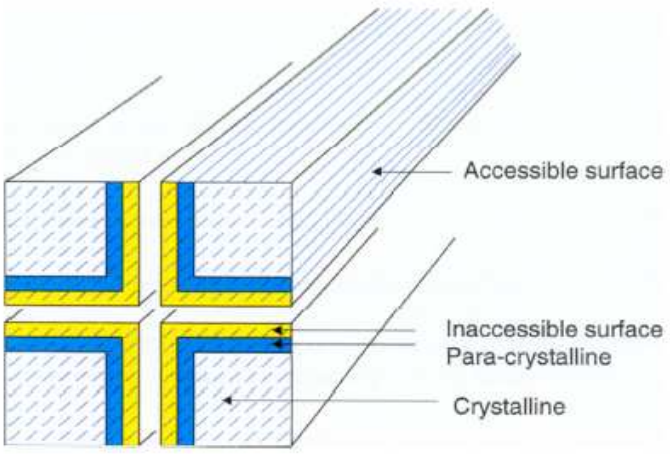

Figure 2.5: Schematic model of four aggregated cellulose I fibrils (Wickholm, 2001)

2.3.4 The application of solid state NMR for determining average lateral fibril dimensions (LFD) and lateral fibril aggregate dimensions (LFAD)

Fibrils have cross-sections of varying shape and widths in the range from a few nanometers to a few tenths of nanometers (Fengel and Wegener, 1984; Krässig, 1996; Atalla, 1999). There is a broad distribution of fibril aggregate structures in pulp probably due to the presence of hemicelluloses and short chain glucan in pulp samples. In order to calculate the average lateral fibril dimensions (LFD) and average lateral fibril aggregate dimensions (LFAD), spectral fitting has to be performed on lignin- and hemicellulose-free pulp samples (glucose content > 95 %) since interfering signals (signal overlap from hemicellulose and spinning side bands from the lignin) influence calculations (Hult *et al.*, 2001). From the assignment of the signals in the C-4 region of the CP/MAS ^{13}C-NMR spectra, lateral dimensions can be assigned. Assuming a square cross-section (Figure 2.5), the fraction of the signal intensity from accessible fibril surfaces (calculation of lateral fibril aggregate dimension) or the fraction of the signal intensity from accessible and inaccessible fibril surfaces (calculation of lateral fibril dimensions) are both denoted q and are given by the equation:

$$q = \frac{(4n-4)}{n^2} \qquad (3)$$

where n is the number of cellulose chains on the side of the square fibril cross-sections. A conversion factor of 0.57nm width per cellulose polymer has been used in the calculations (Sugiyama *et al*., 1991; Heiner *et al*., 1998; Newman, 1999).

2.3.5 Computation of specific surface area from Lateral Fibril Aggregate Dimensions (LFAD)

Differences in supra-molecular structure of cellulose produce materials with a changed amount of interior surface area.

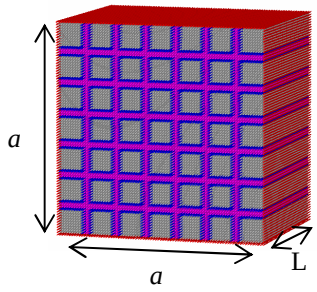

Figure 2.6: Schematic diagram of the fibril aggregate

Average density of cellulose molecule: $\rho \approx 1600$ kg/m^3

a = length along one side, in nm

Total surface area exposed: $A = a \times L \times 4$ (4)

Volume: $V = a^2 \times L$ (5)

Mass: $M = V \times \rho$

$= a^2 \times L \times \rho$ (6)

Specific surface area (σ): $\frac{A}{M} = \sigma = \frac{a \times L \times 4}{a^2 \times L \times \rho}$

$= \frac{4}{\rho \times a}$ (7)

Thus fibril aggregates with different dimensions produce different specific surface areas. However this theory is limited since infinitely large objects yield specific surface areas too small to measure.

Given that the hydroxyl groups on the fibril aggregate surface are the only functional groups available for further reaction, the question that arose from the above computation is whether the specific surface area measured using CP/MAS ^{13}C-NMR relates to a measure of chemical reactivity. To answer this, a series of reactivity studies were carried out on high purity pulp samples (i.e. 96α dissolving pulp and cotton linters).

2.3.6 The application of solid state NMR for determining initial reaction rates of dissolving pulp samples

To test the hypothesis that the specific surface area determined by the solid state NMR technique relates to chemical characteristic of the material, an attempt was made to correlate reaction rate ratios to ratios of specific surface areas determined by NMR. Acetylation experiments were performed with commercial 96α Eucalyptus dissolving pulp and cotton linters. These samples are of high purity with respect to cellulose and differ significantly in their specific surface areas. Both samples were oven dried preceding the acetylation reaction. The hypothesis was based on the assumption that during the heterogeneous acetylation of cellulose, only hydroxyl groups situated at the surface of fibril aggregates are directly exposed to the surrounding liquid and hence, initially accessible to the reagent. Other hydroxyl groups resides either in the interior of fibrils or in the interior of fibril aggregates making them less accessible or inaccessible to the reagent.

The reaction scheme is illustrated below

$$ROH + (CH_3CO)_2O \underset{k_{-1}}{\overset{k_1}{=}} ROCOCH_3 + CH_3COOH \qquad (8)$$

ROH denotes the accessible hydroxyl groups on the cellulose, *$(CH_3CO)_2O$* denotes the acetic anhydride (*AA*), *$ROCOCH_3$* denotes the formed cellulose acetate (*CA*) and *CH_3COOH* denotes the formed acetic acid (*HAc*). *k_1* and *k_{-1}* denotes the forward and

reverse reaction rates respectively. The general rate expression for the formation cellulose acetate can be given as (using abbreviations, brackets indicating concentrations)

$$\frac{d[CA]}{dt} = k_1[ROH]^a[AA]^b - k_{-1}[CA]^c[HAc]^d \quad (9)$$

The experimental setup used a constant amount of cellulose for all reaction times, a large excess of acetic anhydride (*AA*) and measured formed amounts of cellulose acetate (*CA*) only for short reaction times. The short reaction time effectively means that only a small fraction of all accessible hydroxyl groups were acetylated and that any reverse reaction rate can be neglected. The large excess of acetic anhydride used makes the concentration of acetic anhydride essentially constant throughout the course of the reaction. This allows for the following approximations to be introduced.

$$\frac{d[ROH]}{dt} \approx 0 \quad (10)$$

$$\frac{d[AA]}{dt} \approx 0 \quad (11)$$

$$-k_{-1}[CA]^c[HAc]^d \approx 0 \quad (12)$$

Using these approximations pseudo-zero order reaction kinetics can be realized

$$\frac{d[CA]}{dt} = k_1[ROH]^a[AA]^b \approx k'[ROH]^a \approx k'' \quad (13)$$

The connection between the pseudo zero-order reaction rate (*k"*) and the specific surface area, as determined from NMR LFAD measurements is given below, under the assumption that the exponent *a* in Equation (13) is equal to one.

$$k'[ROH] \approx k' \frac{\sigma MN}{V} = k'' \quad (14)$$

[*ROH*] denotes the average volumetric concentration of accessible hydroxyl groups, σ denotes the specific surface area, *N* denotes the number of moles of hydroxyl groups

per unit surface area and finally *V* denotes the sample volume. Keeping experimental conditions in agreement with the introduced approximations, keeping all parameters under experimental control equal only changing the cellulose substrate, a meaningful ratio of pseudo-zero order reaction rates can be formed. For substrates labelled A and B

$$\frac{k_A''}{k_B''} = \frac{k' \frac{\sigma_A MN}{V}}{k' \frac{\sigma_B MN}{V}} = \frac{\sigma_A}{\sigma_B} \qquad (15)$$

Equation (15) relates the ratio of pseudo-zero order reaction rate determined from the kinetic experiments directly to the specific surface area determined from NMR LFAD measurements. This means that it is possible to test if the physical measure LFAD carries any information that is relevant to the chemical characteristics of the cellulose material, i.e. its behaviour during chemical modification. The system used for the acetylation was formulated in agreement with the theoretical assumptions made to reach pseudo zero-order kinetics (Equations 8-15).

2.3.7 Computation of degree of substitution (DS) of surfaces

Using the information obtained from the specific surface area determination and the reactivity experiments, the degree of substitution for high purity pulp sample during the acetylation reaction could be estimated.

Degree of Substitution = no. of substituted hydroxyl groups per anhydroglucose unit

$$= \frac{n\left(r_{OH}\right)}{n\ (Anhydroglucose\ unit)} \qquad (16)$$

From CP/MAS ^{13}C-NMR:

Total average Degree of Substitution =

$$\frac{Total\ \ Intensity\ methyl\ carbon}{Total\ Intensity\ \ from\ one\ anhydroglucose\ unit} \qquad (17)$$

The total intensity from one anhydroglucose unit and one methyl carbon in the acetyl group are shown in Figure 2.7.

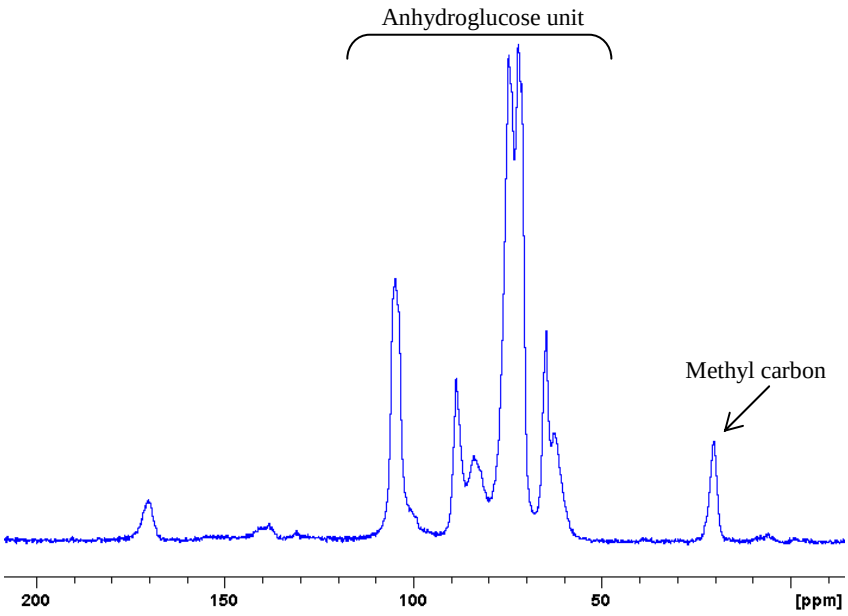

Figure 2.7: CP/MAS ^{13}C-NMR spectrum showing the anhydroglucose unit and the methyl carbon in the acetyl group

Spectral integrals were determined for the methyl signal (around 20 ppm) and the collective signals from cellulose (about 120-40 ppm) (Figure 2.7). The integration results were combined with the NMR measurements of LFAD to compute the average degree of substitution of the glucan chains present at fibril aggregate surface areas (<DS>$_S$) using the following equation (Equation 18):

$$\langle \mathrm{DS} \rangle_S = \frac{I(Me)}{I(C)} \frac{N^2}{(4N-4)} \qquad (18)$$

Where *I(Me)* and *I(C)* are the integrated intensities over the methyl signal (about 20 ppm) and the cellulose signal region (about 120-40 ppm) respectively, *N* the number of glucan polymers along one side of the assumed square cross section of the fibril aggregate.

2.4 Atomic Force Microscopy in wood and ultra-structural research

Atomic Force Microscopy (AFM) has recently been applied to structural studies on cell wall characteristics of wood fibres from different environments (Fahlén and Salmén, 2002, 2003, 2005; Poggi *et al.*, 2005; Pereira *et al*., 2001); unbleached pulp and pulp components like cellulose, hemicellulose and lignin (Gustafsson, 2002); during different stages of dissolving pulp production (Chunilall *et al*., 2006) and even after drying dissolving pulp (Chunilall *et al.*, 2008; Kontturi and Vuorinen, 2009). The present study uses AFM to examine the morphological arrangement of cellulose fibril aggregates within the secondary wall of raw pulp fibres, fully bleached pulp fibres and fully bleached pulp fibres after oven drying. Lateral fibril aggregate dimensions (LFAD) were measured within the secondary wall of the fibre. This was done in order to confirm the results obtained using solid state NMR showing the ultra-structural changes that occur during acid bi-sulphite pulping, chemical bleaching and drying.

The application of AFM for surface characterisation of wood, fibres, pulp and paper is still at an early stage; although the technique has been tested in almost every part of the value chain ranging from wood to printed paper (Hanley and Gray, 1995; Béland, 1997; Niemi and Paulapuro, 2002). The removal of hemicelluloses closely associated with cellulose fibrils in the kraft fibre wall during the bleaching process has been suggested to favour an increase in cellulose fibril aggregate diameter measured using solid state NMR (Duchesne *et al.*, 2001; Hult *et al*., 2001). AFM was used to identify changes in cellulose fibril aggregation during acid bi-sulphite pulping, bleaching and drying and was used to validate solid state NMR findings.

2.4.1 Principle of Atomic Force Microscopy (AFM)

The basic principle of the AFM is the measurement of forces between the sample surface and a sharp tip (Figure 2.8). The sample is mounted on a piezoelectric stage that provides sub-Ångstrom resolution. The tip is secured to the end of the cantilever and moves in an *x-y* direction across the sample. Changes in topography cause the tip and cantilever to deflect with this deflection measured by reflecting a laser beam from the back of the cantilever to a position sensitive photodiode (Meyer and Amer, 1988; Alexander *et al.*, 1989; Hanley *et al.*, 1995).

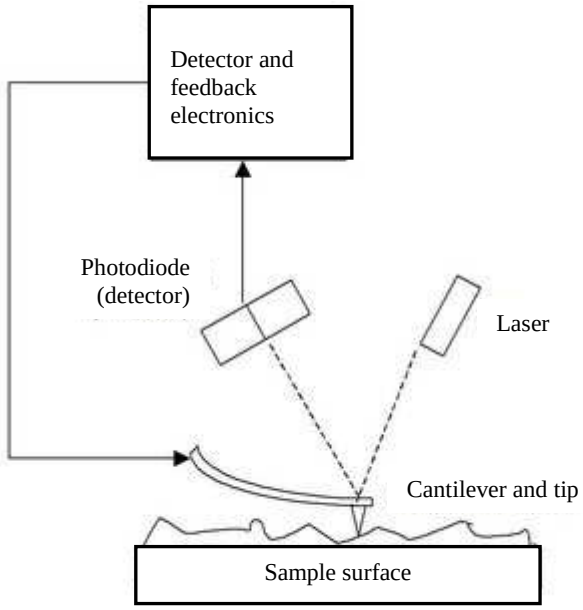

Figure 2.8: Schematic diagram of the Atomic Force Microscope

2.4.2 Imaging modes

The primary modes of AFM are contact mode and Tapping Mode™. In contact mode operation, the probe is in direct contact with the surface as it scans at a constant vertical force (Jena and Horber, 2002). In contact mode the signal of primary interest is the cantilever deflection signal with cantilever selection determining the range and resolution of applicable forces between the tip and substrate. Since the tip is in contact with the substrate while they move laterally there is a possibility that the tip may 'rupture' a surface. In the Tapping Mode™, the cantilever resonates i.e. oscillated at or close to its fundamental resonance frequency, and the tip of the probe makes intermittent contact with the sample surface (Jena and Horber, 2002). Hence the

Tapping Mode™ is preferred for ‘soft’ materials preventing surface deformation during scanning. The oscillation amplitude, phase and resonance frequency are modified by tip-sample interaction forces; these changes in oscillation with respect to the external reference oscillation provide information about the sample topography (Jena and Horber, 2002).

2.4.2.1 Application of Tapping Mode™

The Tapping Mode™ (Zhong *et al*., 1993) is a development of the contact mode AFM. In the Tapping Mode™, the oscillation of the cantilever is driven by a constant driving force. Amplitude oscillation of the cantilever is monitored and, in contrast to the contact mode, it is the primary signal of the Tapping Mode™. The tip touches the surface at the bottom of each oscillation, and this reduces the oscillation amplitude of the cantilever (Puttman *et al*., 1994). The feedback control loop of the system then maintains this new amplitude constant as the oscillating (tapping) tip scans the surface. The information in a Tapping Mode™ height image corresponds in principle to the information in the Contact Mode. Since the tip only makes intermittent contact with the surface, tip-surface interactions are much ‘gentler’ than contact mode AFM. Lateral and shear forces are thus reduced in Tapping Mode™ AFM (Nagao and Dvorak, 1999). The result of scanning in the Tapping Mode™ is an amplitude image.

Phase imaging is an extension of Tapping Mode™. The phase lag between the cantilever oscillation and the detected oscillation signal is used to create a topography image (Nagao and Dvorak, 1999). Phase imaging is not possible in the Contact Mode since it requires the oscillation and amplitude feedback loop of the Tapping Mode™. The acquisition of a phase image is based on information directly from the detector, which improves image resolution.

2.4.3 Image analysis

The phase images from AFM reveal fibril aggregates. Once a scan is obtained (Figure 2.9a) image analysis is performed using Image-Pro® Plus (Version 6.0) (MediaCybernetics®). A greyscale image of the scan is then obtained (Figure 2.9b). Thereafter a 3D morphological filter is applied, i.e. watershed segmentation (Figure

2.9c). The fourth step involves a mask being created of the areas that are most likely to be fibrils aggregates (Figure 2.9d). The fifth step is to measure the mean fibril aggregate diameter. The fibril aggregates are ringed in red and one of the many fibril aggregates has been highlighted in green (Figure 2.9e). The objects or aggregates on the perimeter are not included in the measurement.

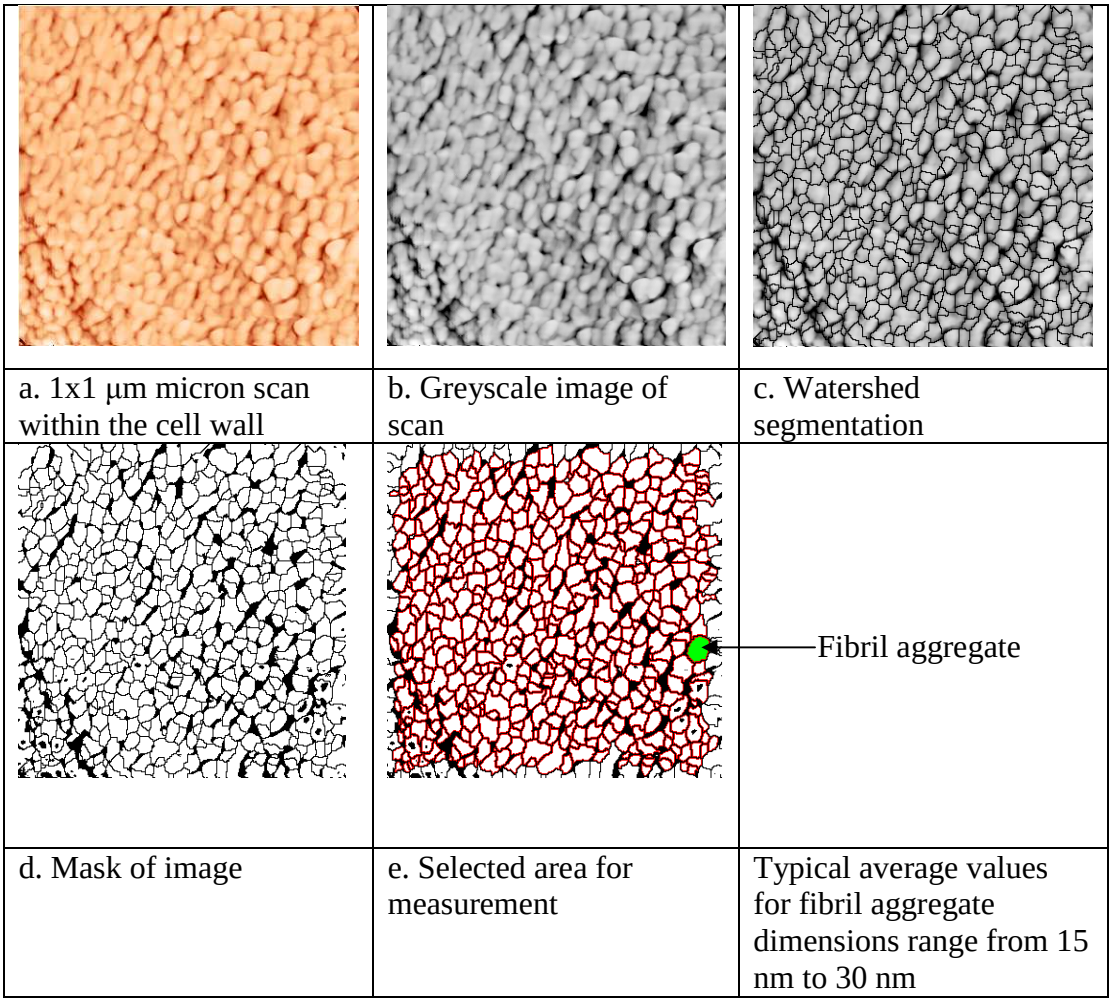

a. 1x1 µm micron scan within the cell wall	b. Greyscale image of scan	c. Watershed segmentation
d. Mask of image	e. Selected area for measurement	Typical average values for fibril aggregate dimensions range from 15 nm to 30 nm

Figure 2.9: Image analysis using Image Pro Plus

Image analysis reveals the mean fibril aggregate diameter or lateral fibril aggregate diameter in nanometers. This measurement is however incomplete since the tip enlargement effect was not taken into consideration during the measurement. Wang and Chen (2007) reported that "the finite size of the tip apex, no matter how small, will lead to a systematic enlargement of the lateral size of any surface features". The surface roughness (Rq) value is used in calculating the tip enlargement effect (x).The image is initially flattened (1^{st} to 3^{rd} order) and the surface roughness is determined.

The angle of the tip (y) is determined by scanning electron microscopy (SEM) (Figure 2.10).

This value is substituted into the following equation:

$$x = Rq \times \tan y \qquad (21)$$

Where x = the tip enlargement effect

Rq = surface roughness (roughness coefficient)

tan y = size of the tip

In order to get a true estimate of the lateral fibril aggregate dimensions the tip enlargement effect is calculated and subtracted from the original LFAD measurement. The mean of the distribution is computed and the error in the mean is reported.

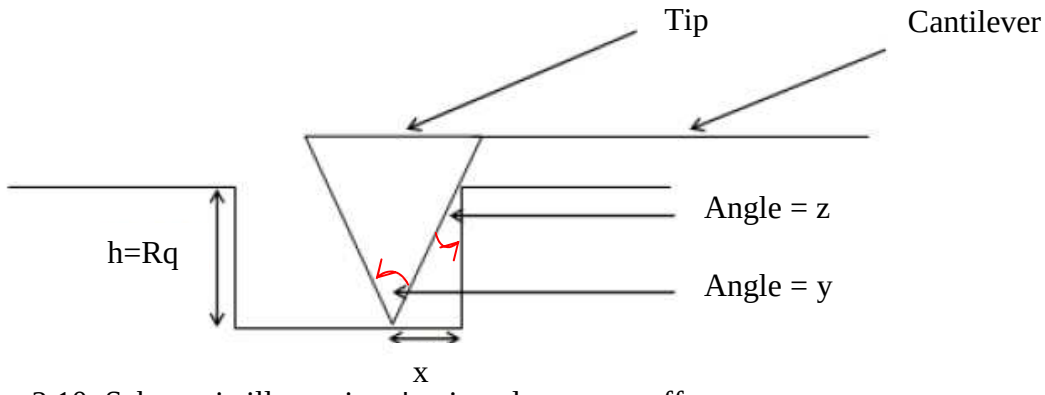

Figure 2.10: Schematic illustrating the tip enlargement effect

2.4.4 Advantages and disadvantages of using the Atomic force microscope for ultra-structural research

AFM has several advantages:

- AFM provides a three dimensional surface profile of a sample.
- There is non-destruction of sample surface by scanning in the Tapping Mode™.
- AFM has the ability to study surfaces in vacuum, air and liquid environments (Yamada, 2007).

- High resolution AFM (ca. 1Å) is comparable to Scanning Tunneling Microscopy and Transmission Electron Microscopy.

Some of the disadvantages are as follows:

- The maximum scanner dimensions in the XY plane range from 100 to 150 microns, maximum height Z on the order of 2 microns.
- An incorrect choice of tip for the required resolution can lead to image artefacts.
- The sample preparation procedure leading up to scanning high resolution images requires approximately 3 days.
- An average of 10 fibres are scanned with the LFAD results thus having limited statistics

Chapter 3

3 Experimental design

3.1 Experimental design

For this study a single *E. grandis* x *E. urophylla* (GU A380) clone sampled from a single site was selected in order to minimize the effects of genetics and the environment on dissolving pulp quality. Stands of GU A380 (Site quality 1*) were selected from a compartment in Futalulu, Zululand (Figure 3.1). The trees were sampled at age 9 years, chipped with an industrial chipper and air dried to a moisture content of approximately 12%. Figure 3.2 shows a schematic of the experimental design and highlights the Raw material, Processing, Samples for analysis and the Analysis methods.

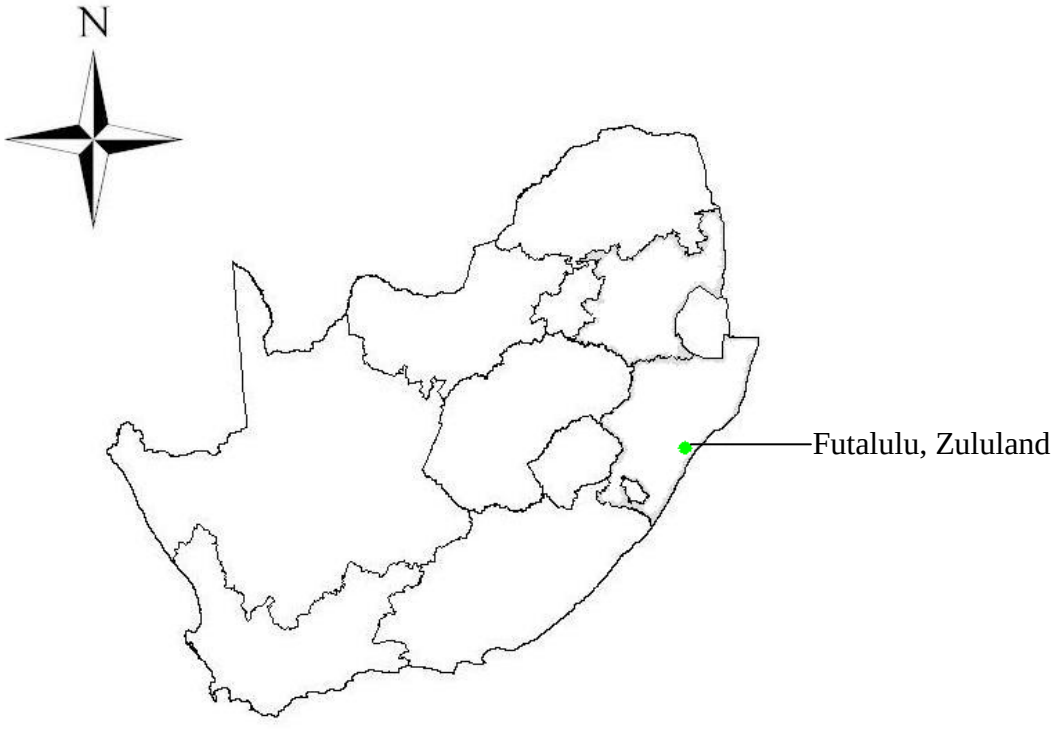

Figure 3.1: Map of South Africa highlighting Futalulu in Zululand

* Site Quality Classification based on Forest Land Types for Sappi Landholdings. (Pallett, 2001)

Raw Material

Eucalyptus grandis x *urophylla*

(Site quality 1: High site; Zululand;

Age: 9 years)

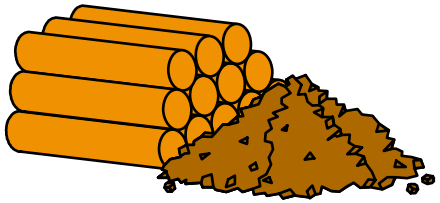

Logs were debarked, chipped and air dried for 3 months

Processing

Delignification (3 pulp samples)
Acid bi-sulphite pulping
Oxygen delignification (O_2 - Stage)

Bleaching Sequence (3 pulp samples)
Chlorine dioxide (D_1- Stage)
Alkali extraction (E- Stage)
Chlorine dioxide (D_2 - Stage)
Hypochlorite (H-Stage)
Peroxide (P-Stage)

Samples for analysis

Wood holocellulose
Subject to sodium chlorite treatment for 3 hours

Bleaching strategies

91 α – Raw, D_1, E, H
92 α – Raw, D_1, E, H
96 α – Raw, D_1, E, P
Pulp samples were stored wet prior to analysis

Drying strategies

91α, 92α, 96α final pulp samples subject to:

Condition drying – 5 days at 23 ºC and 50% relative humidity

Air drying – 5 days at room temperature and 70% relative humidity

Oven drying – 12 hours in an oven at 104 ºC

Reactivity strategies

96α – Evaluating Cellulose Acetate formation on Commercial 96α and Cotton linters cellulose

- Acetylation at 40ºC – 3, 6, 9 and 12 minute intervals
- Acetylation at 60ºC – 2, 3, 4 and 5 minute intervals

92α – Evaluating Viscose formation on two laboratory pulp samples different in terms of reactivity towards viscose manufacture
Alkcel samples removed after:

- 15 minutes of 'steeping'
- 30 minutes of 'steeping'
- 30 minutes of 'steeping' and 3 ½ hours of aging

91α – Evaluating MCC formation on 2 pulp samples with different LODP

- Pulp sample after 5 minutes of acid hydrolysis
- Pulp sample after 60 minutes of acid hydrolysis

Analysis

Lignin content by K-Number analysis;

Solubility – Total extractable material (hemicellulose and degraded cellulose content) i.e. S_{10}%, Total hemicellulose content i.e. S_{18}%, degraded cellulose content, α – cellulose content;

Viscosity;

Reducing- end groups by Copper number analysis;

Molecular weight distribution analysis by SEC-MALLS

Physical measure of supra-molecular structure (LFAD) by solid state NMR analysis confirmed on a Bruker 300 MHz and Varian 500 MHz

Validation of physical measure by AFM analysis 92α and 96α pulp samples during the bleaching process and after oven drying

Initial reaction rate constant for the acetylation reaction determined by solid state NMR and solution state NMR

Figure 3.2: Schematic diagram of the experimental design

3.2 Delignification

Delignification was carried out in two parts;

- Firstly acid bi-sulphite pulping followed by
- The oxygen (O_2) delignification step.

3.2.1 Laboratory acid bi-sulphite pulping

Laboratory acid bi-sulphite pulping is a scaled down version of the commercial process and is based on the use of aqueous sulphur dioxide (SO_2) and a base i.e. magnesium oxide.

3.2.2 Pulping liquor preparation

The pulping liquor is made by bubbling sulphur dioxide into 7 litres of a water and magnesium oxide slurry. The sulphur dioxide reacts with water to give sulphurous acid (Holzer, 1954).

$$SO_2 + H_2O \rightleftharpoons H_2SO_3 \quad (1)$$

Thereafter the magnesium oxide reacts with sulphurous acid to form sulphite via the following equations:

$$MgO + 2H_2SO_3 \rightarrow Mg(HSO_3)_2 + H_2O \quad (2)$$
$$Mg(HSO_3)_2 + MgO \rightarrow 2MgSO_3 + 2H_2O \quad (3)$$

The pH range for the pulping liquor was 1-2. Approximately 1700 g of air-dried wood chips were loaded into a flow-through digester. This reaction vessel was pressurised to 850 KPa, and the temperature ramped to 140ºC over 5 h 17 minutes. The reaction vessel (8 litre capacity) was held at 140ºC for 43 minutes. These conditions are shown in Table 3.1 below.

Table 3.1: Acid bi-sulphite pulping conditions

Reagents	**Conditions**
SO_2	8.0 % - 8.5% (v/v)
MgO	0.75% - 0.85% (m/v)
Pressure	850 KPa
Liquor/Wood Ratio	4.3
Ramp time	5h17 min
Pulping time at 140ºC	43 min

After completion of the pulping, the spent liquor was neutralized with base and disposed of down the drain. The pulp sample was removed from the reaction vessel and washed repeatedly with water to remove solubilzed lignin and excess acid. The pulp samples were then screened through a 0.020 inch mesh to remove rejects and unreacted wood chips. The oven-dry weight was determined and the percentage yield determined by the following equation:

$$\text{Percentage yield} = \frac{mass\ of\ \ pulp\ (oven\ dried)}{mass\ of\ \ wood\ \ chips\ (oven\ dried)} \times 100\% \qquad (4)$$

3.2.3 Oxygen delignification (O_2)

Table 3.2 presents the laboratory O_2 delignification conditions adapted from the commercial scale for the three grades of dissolving pulp samples. The time, temperature and pressure were kept constant and the concentration of sodium hydroxide (NaOH) varied i.e. 1%, 2% and 4% for the 91α, 92α and 96α respectively (Table 3.2).

Table 3.2: O_2 delignification conditions used for the three grades of dissolving pulp samples

	Reagent	**91α**	**92 α**	**96 α**
Concentration (%) (m/v)	NaOH	1	2	4
Consistency* (%)		11	11	10
Temperature (ºC)		100	100	100
Pressure (KPa)	O_2	300	300	300
Time (minutes)		60	60	60

*Consistency – percentage solid content of pulp

3.3 Pulp bleaching

The laboratory bleaching sequence was a scaled down version of the commercial process. The results obtained for the viscosity and lignin content (K-number) at the O_2 delignification stage were used to adjust the bleaching conditions. The aim of adjusting the bleaching was to produce pulp that conformed to the quality control parameters for α-cellulose, viscosity, solubility ranges prescribed commercially for the 91α, 92α and 96α dissolving pulp grades. Tables 3.3 – 3.5 present the bleaching conditions utilized in the laboratory to produce 91α, 92α and 96α dissolving pulp samples. The concentration of reagents; consistency of pulp samples; temperature and duration at which the bleaching stage was completed were varied during the 4 stage bleaching cycles.

Table 3.3: Hypochlorite bleaching of 91α

Stage	Reagent	Concentration (%) (m/v)	Consistency (%)	Temperature (°C)	Time (min)
D_1	ClO_2	0.9	10	57	60
E	NaOH	0.5	11	85	120
D_2	ClO_2	0.6	11	70	180
Hypo	OCl^-	1.5	12	58	150
	NaOH	0.3	-	-	-

Table 3.4: Hypochlorite bleaching of 92α

Stage	Reagent	Concentration (%) (m/v)	Consistency (%)	Temperature (°C)	Time (min)
D_1	ClO_2	0.9	10	57	60
E	NaOH	3.2	11	100	120
D_2	ClO_2	0.6	11	70	180
Hypo	OCl^-	0.6	12	58	150
	NaOH	0.25	-	-	-

Table 3.5: Peroxide bleaching of 96α

Stage	Reagent	Concentration (%) (m/v)	Temperature (°C)	Time (min)
D_1	ClO_2	1	57	47
E	NaOH	9	130	120
	O_2(KPa)	100	-	-
	$MgSO_4$	5	-	-
D_2	ClO_2	2	58	150
Peroxide	H_2O_2	0.3	63	150
	NaOH	0.2	-	-
	$MgSO_4$	0.3	-	-

Consistency = 10%

3.4 Wet chemistry analysis

In the current study the following chemical properties were measured:
The permanganate number (K-number method) was used to assess the lignin content after each stage of processing. The principle of the method is based on the direct oxidation of lignin in pulp by standard potassium permanganate and back-titrating the excess permanganate with ferrous ammonium sulphate (Mohr's salt) standard solution (Tappi method, UM 251). The procedure for permanganate number determination is as follows: Approximately 20 mL of 10% sulphuric acid and 180 mL of water is added to 1 g of pulp sample in a conical flask. The mixture is then stirred using a magnetic stirrer. Twenty five millilitres of 0.1N potassium permanganate is added and after 3 minutes 25 mL of 0.1N ferrous ammonium sulphate is added followed by 10 drops of N-phenyl anthranilic acid indicator. The excess is back titrated with 0.1N potassium permanganate. A blank is also carried out with the exception of the pulp sample. The following calculation is used for permanganate number determination:

Permanganate number = (Sample titre – Blank titre) x 0.355 (5)

The acid insoluble lignin content (klason lignin) in wood and raw pulp was determined by gravimetric analysis (Tappi method, TM 222). The klason lignin content is described as the constituent that is insoluble in 72% (m/m) sulphuric acid. The klason lignin content in wood and raw pulp was determined as follow: 0.35g of extractive free wood sawdust (40 mesh) is added to 3 mL of sulphuric acid in a test tube with stirring. The test tube is placed in a water bath at 30ºC for 1 hour. The contents of the test tube are then placed in a Schott bottle with 84 mL of water. The Schott bottle is then placed in an autoclave set at a temperature of 100ºC and pressure of 103 kPa for 1 hour. After an hour the contents are allowed to cool and then transferred to a 200 mL volumetric flask and diluted to the mark. The sample is then filtered using 0.45 μm filter and placed in an oven at 105ºC overnight. The filter paper is then cooled and weighed to determine the percentage klason lignin. For pulp the weight of sample used is 0.2g and 15 mL of sulphuric acid is used. The rest of the experimental procedure is as for the wood sample.

The viscosity of a pulp sample provides an estimate of the degree of polymerisation (DP) of the cellulose chain. Viscosity determination of pulp is one of the most informative procedures that is carried out to characterise a polymer i.e. this test gives an indication of the degree of degradation (decrease in molecular weight of the polymer, i.e. cellulose) resulting from the pulping and bleaching processes. The viscosity measure involves dispersing 1g of dissolving pulp sample (cellulose I) in a mixture of (15 mL) sodium hydroxide and (80 mL) cuprammonium solution (concentration of ammonia 166 g/L and concentration of copper sulphate 94 g/L) for a period of 1 hour. The dispersed cellulose I is allowed to equilibrate at 20ºC for 1 hour and is then siphoned into an Ostwald viscometer. The time taken for it to flow between two measured points is recorded and the viscosity is calculated using the specific viscosity constant at the corresponding temperature. Viscosity in this study was determined according to (TAPPI method, T230 om-94).

Pulping and bleaching is known to affect cellulose structure by the generation of oxidised positions and subsequent chain cleavage in pulp samples **(**Röhrling *et al.*, 2002). The copper number gives an indication of the reducing end groups in a pulp sample. The copper number is a measure of the reducing properties of the pulp and is defined as the number of grams of metallic copper reduced from the cupric to cuprous state in alkaline solution by 100g cellulose under standard conditions. The copper number is inversely proportional to the viscosity of the pulp samples i.e. with a decrease in viscosity there is increased chain cleavage and hence more reducing end groups. The copper number also serves as an index of reducing impurities in pulp, such as oxycellulose, hydrocellulose, lignin and monosaccharides which possess reducing power. The procedure for determining copper number is as follows: 2.5 g of disintegrated pulp is mixed with a carbonate/bicarbonate (2.6/1, w/w) and 0.4N copper sulphate solution (95/5, v/v) for exactly 3 hours. Thereafter the pulp is filtered and washed with 5% sodium carbonate followed by hot deionised water. Cuprous acid is dissolved by treating the cellulose on the filter with 45 mL of 0.2N ferric ammonium sulphate. This is left for 10 minutes then filtered off. The pulp is then washed with 250 mL of 2N sulphuric acid. The filtrate is then titrated with 0.04N $KMnO_4$. The blank is subtracted from the titre value to yield the number of grams of reduced copper in the pulp sample (TAPPI method, T430 OM 94).

Low molecular weight carbohydrates (hemicellulose and degraded cellulose) can be extracted from pulp samples with sodium hydroxide. Solubility of a pulp in alkali thus provides information on the degradation of cellulose and loss or retention of hemicellulose during the pulping and bleaching processes. The solubility gives an indication of the amount of degraded cellulose/short chain glucan and hemicellulose present in the pulp. S_{10} (%) and S_{18} (%) indicate that proportion of low molecular weight carbohydrates that is soluble in 10% and 18% sodium hydroxide respectively. S_{10} (%) alkali solubility gives an indication of the total extractable material i.e. degraded cellulose/short chain glucan and hemicellulose content in a pulp sample. S_{18} (%) alkali solubility gives an indication of the total hemicellulose content of the pulp sample and is also known as the percentage gamma (γ %) cellulose content of pulp samples.

The quantity of degraded cellulose/short chain glucan, also known as percentage Beta (β %) cellulose, was determined by the difference in S_{10} (%) and S_{18} (%) alkali solubilities, i.e.

$$\text{Degraded cellulose/short chain glucan} = S_{10}(\%) - S_{18}(\%) \quad (6)$$

The α-cellulose content is given by the following equation

$$\alpha\text{-cellulose} = 100 - \left(\frac{S_{10}\% + S_{18}\%}{2} \right) \quad (7)$$

S_{10} (%) and S_{18} (%) alkali solubilities were determined according to TAPPI method T235 OM- 60 (1960). The principle of the method is based on the extraction of carbohydrates with sodium hydroxide followed by oxidation with potassium dichromate (TAPPI method T235 OM- 60, 1960). The procedure for S_{10} (%) alkali solubilities determination is as follows: 1.6g of the pulp sample is placed in 100 mL of 10 % sodium hydroxide (18 % sodium hydroxide for S_{18} (%) determination). The pulp and solution are stirred for a period of 3 minutes and thereafter left at 20ºC for a period of an hour. The pulp sample is filtered under vacuum using a sintered glass crucible (G3). Ten millilitres of 0.4N potassium dichromate and 30 mL of concentrated sulphuric acid is added to 10 mL of the filtrate. Therafter 500 mL of

deionised water is added and the solution is cooled. Approximately 20 mL of 10% potassium iodide is added to the cool solution and 5 minutes therafter the solution is titrated with 0.1N sodium thiosulphate. A blank sample, without pulp sample, is also titrated to give the blank titre. The alkali solubility is given by the following equation:

$$\text{Alkali solubility} = \frac{(Blank\ titre - Sample\ titre) \times 0.685\%}{Weight\ of\ \ pulp\ sample} \quad (8)$$

Table 3.6 presents ranges for the different wet chemical properties of industrially approved 91α, 92α and 96α final dissolving pulp grades. The quality requirements are linked to the end use application for the particular pulp grade.

Table 3.6: Ranges of standard wet chemical properties for industrial 91α, 92α and 96α final dissolving pulp grades

Final pulp	**91α**	**92 α**	**96 α**
k-number	0.3	0.3	0.25
Viscosity (cP)	10 – 14	9 – 20	28 – 35
Copper number	1.05 – 1.34	1.11 – 1.39	0.43 – 0.54
S_{10} (%)	11.5 – 12.9	9.5 – 10 .1	6.4 – 7.0
S_{18} (%)	5.8 – 6.2	4.6 – 5.1	2.7 – 3.3
S_{10} (%) –S_{18} (%)	5.7 – 6.7	4.9 – 5	3.7
α-cellulose	90.8	92.5	95.3

The polysaccharides in the 91α, 92α and 96α pulp after each stage of processing were measured after their conversion to monosaccharides via a two step hydrolysis procedure with 72% sulphuric acid. The first step in the hydrolysis process is the addition of 3 mL of sulphuric acid to 0.2g of oven dried pulp in a test tube with stirring. The contents of the test tube are then quantitatively transferred into a Schott bottle with 84 mL of water. The second step in the hydrolysis process involves placing the Schott bottle in an autoclave set at a temperature of 121 ºC and pressure of 103 kPa for 1 hour. After an hour the contents are allowed to cool and then filtered using a 0.45 µm filter. The filtrate is then transferred to a 200 mL volumetric flask and diluted to the mark. 50 µl of the sample is placed in a vial and diluted with 500 µl of water. Twenty microlitres of 1mg/ml fucose (internal standard) is added using the autosampler. The monosaccharide constituents (glucose, mannose, xylose, arabinose etc.) were analysed using high performance liquid chromatography coupled with

pulsed amperometric detection (Davis, 1998). Reference standards of glucose, xylose, arabinose, galactose, and mannose were prepared. The standards were treated in the same way as the sample and analysed using high performance liquid chromatography coupled with pulsed amperometric detection. The concentrations of the monosaccharide constituents were obtained from the calibration curves of the standards.

Molecular weight distribution analysis was performed using Size Exclusion Chromatography coupled with Multi-Angle Laser Light Scattering (SEC-MALLS) on fully bleached 91α, 92α and 96α samples after conversion to cellulose nitrate (Fischer *et al*., 1999). Nitration acid was prepared by adding 76g of phosphorous pentoxide (P_2O_5, AR grade) to 40 mL of 84% ortho phosphoric acid (AR grade) in small portions. The reaction was cooled in an ice bath with continuous stirring. The mixture was allowed to cool down for 3 hours with occasional shaking. Thereafter 61 mL of fuming nitric acid (AR grade) was added to the mixture with stirring. It was stored at 0ºC. The pulp samples were dried at room temperature for 12 hours and then flayed using a blender. The pulp was extracted with acetone for 8 hours using a Soxhlet extractor and then dried at 50ºC for 2 hours. Fifteen millilitres of the nitration acid was added to 0.15 g of pulp which was pre-cooled in ice. The mixture was cooled on ice for 3 hours with regular shaking. It was then filtered by gravity through a sintered glass crucible (No.1). Excess acid was neutralised by washing with 150 mL of 2% (w/v) aqueous $NaCO_3$ without suction. The sample was washed again with 800 ml deionised water without suction. The remaining water in the sample was drawn off by suction and the sample was stabilised for 2 hours by covering it with methanol (room temperature). The methanol was filtered off using suction and cellulose nitrate was dried over P_2O_5 at room temperature for at least 15 hours. Five milligrams is dissolved in 10 ml of THF. The solution was left on a shaker for 2 hours. Two millilitres of sample with a glass syringe attached to a 0.45 μm PTFE filter is injected (Fischer *et al*., 1999). Table 3.7 presents the SEC-MALLS column conditions used.

Table 3.7: SEC-MALLS column conditions

PSS columns	Porosity 10^4 and 10^6 Å, 20 μm particle size, 20 x 600 mm
Guard column	SDV 07921
dn/dc	0.078
Flow rate	0.8 ml/min
Dawn calibration constant	5.25×10^{-5}
Aux1 calibration constant	1.63×10^{-5}
Solvent RI	1.409
Temperature of the column, light scattering detector and the RI detector	25ºC

3.5 Physical measures of structure and accessibility

Lateral fibril dimensions (LFD) and lateral fibril aggregate dimensions (LFAD) (nanometre scale) of cellulose I were determined using solid state NMR. In order to validate results obtained using the solid state NMR, AFM analysis was performed on the same pulp samples. The samples analysed were wood holocellulose; unbleached pulp samples; D_1, E, hypochlorite and peroxide stages for the 92α and 96α respectively. A further comparison was made between the final bleached pulp samples i.e. 91α, 92α and 96α. The wood holocellulose was prepared as follows: The sawdust sample was subject sodium chlorite treatment (0.5g of sodium chlorite/g of sawdust) under acid conditions (pH 4-5) at 60ºC for three hours. After 3 hours the sawdust sample was washed repeatedly under vacuum using a Buchner funnel and Whatman No. 2 filter paper. This process was repeated until the Klason lignin content was < 10%. The wood holocellulose and pulp samples were stored wet in airtight bags at room temperature prior to analysis.

The experiment studying the effect of drying on cellulose I supra-molecular structure was conducted on dissolving pulp samples dried using three methods viz. oven dried, air dried and condition dried. Oven dried pulp samples were prepared by placing dissolving pulp into the oven at 104ºC for 18 hours. Condition dried pulp was placed in a conditioned room at 23ºC with relative humidity of 50% for 5 days. The pulp samples were thereafter sealed in airtight bags ready for analysis.

3.5.1 CP/MAS ^{13}C-NMR data acquisition

All pulp samples were wetted with deionised water (40% to 60% water content) and packed uniformly in a zirconium oxide rotor. Recording spectra on wet samples gives a higher apparent resolution compared to dry samples (Newman, 1993). The CP/MAS ^{13}C-NMR spectra were recorded in a Bruker Avance AQS 300 WB instrument operating at 7.04 T. All measurements were performed at 290 ± 1 K. The MAS rate was 5 kHz. A double air-bearing probe was applied. Acquisition was performed with a CP pulse sequence, by a 4.3 μs proton 90 degree pulse, 800 μs ramped (100 – 50%) falling contact pulse and a 2.5 s delay between repetitions. A TPPM15 pulse sequence was used for ^{1}H decoupling. Hartman-Hahn matching procedure is based on glycine. The chemical shift is related, as usual, to TMS ($(CH_3)_4Si$). The data point of maximum intensity in glycine carbonyl line was assigned a chemical shift of 176.03 ppm. The software for spectral fitting was developed at STFI-Packforsk AB and is based on a Levenberg-Marquardt algorithm (Larsson *et al.*, 1997). All computations are based on integrated signal intensities as obtained from the spectral fitting (Wickholm *et al.*, 1998). Further comparative solid state NMR data sets were recorded in a Varian 500MHz solid state NMR instrument, equipped with two channels using a 6mm HX MAS probe (15N-31P). The operating parameters were identical to that used at STFI.

3.5.2 Atomic Force Microscopy (AFM)

Our interest centred on scanning fibres, initially 15x15 μm and then in the 1x1 μm range within the S2 layer of the fibre wall. The Solver P47H was equipped with a scanner that could provide resolution in the 5 nm – 15 μm range. The tip used was specifically manufactured for Tapping Mode™ application and had a tip radius of 2 nm. In order to obtain LFAD measurements using the Atomic Force Microscope, the dissolving pulp samples have to be prepared in a manner suitable for scanning. A number of different fibre drying techniques are available for the preparation of fibres with a more or less preserved ultra-structure. These include air-drying, freeze-drying, and critical-point drying. It has been reported that freeze-drying and critical-point drying preserve the fibre wall very well and give similar results, while air-drying changes the ultra-structure considerably (Daniel and Duchesne, 1998). Freeze drying

has hence been selected as the sample preparation procedure and involves immobilising the dissolving pulp at low temperature (<-60ºC), after which it is placed under vacuum to remove water by sublimation. This freeze drying process prevents structural rearrangements before the sample is completely dry, after which it can be brought safely to atmospheric pressure and temperature. Samples are aligned before freezing to aid in obtaining cross-sections after freeze drying. Fibre bundles are placed on a $1cm^2$ piece of foil and kept on a moist filter paper in a Petri dish with paper towel in it to prevent premature drying. Liquid nitrogen is used to freeze the samples rapidly after which they are placed on the stage of the freeze drying apparatus previously cooled to -60ºC and kept under vacuum for 24 hours in the freeze drying apparatus. Freeze dried samples are infiltrated with epoxy resin under mild vacuum, placed in silicon moulds, after which they are polymerised in an oven at 70ºC for 8 hours preserving the ultra-structure of the pulp samples. The preferred epoxy resin for AFM sample preparation was Spurr's resin (Spurr, 1969). Samples in polymerised blocks are sectioned transversely with a section thickness of 0.5 μm – 1.0 μm. Sections are collected from the trough of glass microtome knives and dried on cover slips for AFM observation. Originally a diamond knife was used to section the sample blocks. It was presumed that this would produce much 'smoother' sections for AFM imaging. This presumption was abandoned when AFM scans of the sections prepared using a diamond knife showed signs of chatter'. 'Chatter' is defined as a mechanical vibration that shows on the sections as marks or wrinkles parallel to the knife edge. This 'chatter' interferes with the measurement of the fibril aggregate dimensions and is therefore undesirable in the image. A glass knife was used to section the sample blocks. This method removed the chatter from AFM scans creating a better resolved AFM image. Sectioning with a glass knife was the adopted methodology used throughout this study.

Atomic Force Microscopy (AFM) was performed with Solver P47H base with a SMENA head, manufactured by NT-MDT. The cantilever of choice was SuperSharpSilicon™ SPM-Sensors (SSS-NCLR, Nanosensors™) with a resonance frequency of 146-236 kHz were used; Force constant of 21-98 N/m; Tip radius 2nm (typical), the scan rate ranged from 0.6-1.6 Hz. The entire fibre wall has to be scanned prior to obtaining a scan of 1x1 μm within the S2 layer of the fibre. The step wise

scanning begins with the entire fibre ~15x15 μm, then a ~8x8 μm of the fibre wall. The next scan is a ~3x3 μm scan of the fibre wall and finally a 1x1 μm scan is taken within the S2 layer of the fibre wall. Scanning has to be performed in this manner in order to minimize deviation from the scan area of interest i.e. the S2 layer. Although the scanning of the 1x1 μm takes ca. 15 minutes the entire process to obtain a single scan takes ca. 2 hours. Scans were taken in both height mode, in which the deflection of the cantilever was directly use to measure the z position (Height image) and in phase mode, where the phase lag of the cantilever was used to determine the differences in material stiffness (Phase image). All scans were conducted in air (climate controlled) at 512x512 pixels and analysed by Image Pro® Plus (Version 6.0) software. A minimum of 10 scans per sample were completed with all presented quantitative data extracted from phase images.

3.6 Chemical measure of reactivity

The study involves the assessment of the structure, accessibility and reactivity using three grades of dissolving pulp (i.e., 91α, 92α and 96α) which are used to manufacture microcrystalline (MCC), viscose and cellulose acetate respectively. The processes applied to the pulp samples are unique for each dissolving pulp grade and therefore separate reactivity indicators need to be identified for each grade of dissolving pulp in order to suitably address the question of accessibility and reactivity.

Two pulp samples with different supra-molecular structure (i.e. specific surface area measured using solid state NMR) were used in the acetylation reaction i.e. 96α commercial pulp and cotton linters cellulose to determine initial reaction rate constants. The hypothesis is such that if the initial reaction rate constant ratio is proportional to the specific surface area ratio for the two different cellulose pulp samples then chemical reactivity for the acetylation reaction can be estimated using the solid state NMR. LFAD measurements obtained from solid state NMR can be converted to specific surface area (SSA) for surfaces. The 96α was acetylated and run on the solid state NMR using the conditions outlined below.

3.6.1 Acetylation of dissolving pulp samples for solid state NMR analysis

Re-slushed pulp samples; 96α dissolving pulp samples and cotton linters cellulose (>99% glucose); were dried in a heating cabinet over night at 105ºC. The dry sample (about 0.5g) was taken out of the heating cabinet and immediately submerged in 50 mL of a mixture of glacial acetic acid (Merck p.a.) and acetic anhydride (Merck p.a.) (20/80 v/v) kept at the desired temperature (40ºC or 60ºC) using a thermostat. After 1 minute in the mixture (mild stirring), 20 uL of sulphuric acid (95-97 % Merck) was added as a catalyst starting the reaction. The acetylation at 40ºC is carried out at 3, 6, 9 and 12 minutes intervals. The acetylation at 60ºC is carried out at 2, 3, 4 and 5 minutes intervals. After the desired reaction time the reaction mixture was poured into 400 mL of deionised water, stopping the reaction and subsequently washed repeatedly with 400 mL batches of deionised water until the pH of the washing water was about 5. The washed sample was dried for two days at room temperature prior to recording solid state NMR spectra on the dry samples. The sample is run dry because cellulose acetate domains may swell in the presence of a liquid in a way that pure cellulose do not. Swelling can thus induce mobility in these domains leading to signal intensity discrimination. The data acquisition parameters were the same as that for dissolving pulp samples. The initial reaction rate constant ratio was determined using the methyl intensity determined by solid state NMR. In the spectrum the cellulose acetate and the methyl, in the acetyl groups, intensity is shown. The cellulose signal is set to 1 and the relative intensity of the methyl signal is determined. The graph of methyl intensity vs. time gives the initial reaction rate constant. For two materials with different specific surface areas a ratio of the initial reaction rate can be determined.

3.6.2 Acetylation of dissolving pulp samples for proton NMR analysis

The acetylation procedure is identical to that for solid state NMR however the acetylation times are different. Preliminary experiments showed that reaction times at 40ºC (3, 6 and 9 minutes) do not provide any signal intensity on the proton NMR spectrum. The times were adjusted to maintain the initial reaction rate viz., 10, 11, 12, 13 and 15 minutes. The pulp samples acetylated included the laboratory 96α and cotton linters. The dried acetylated pulp samples were placed in deuterated chloroform. In theory, the acetylated surfaces should dissolve in deuterated

chloroform with the solid or unacetylated material filtered. The dissolved acetylated pulp is then analysed on the solution state NMR. The graph of acetyl intensity (cellulose triacetate) vs. time gives the initial acetylation reaction rate constant (Goodlett *et al.*, 1971).

3.6.3 Solid state NMR and SEC-MALLS analysis of alkaline cellulose (92α)

Tracking the conversion of cellulose I to cellulose II

Two 92α laboratory dissolving pulp samples were further processed to the viscose film at Sappi/Saiccor (Chapter 2, Section 2.1.5). The two pulp samples differed in terms of their reactivity towards viscose manufacture. Alkaline cellulose (Alkcel) samples were removed at different stages in the viscose process for analysis by solid state NMR and SEC-MALLS. The first alkcel sample was removed after 15 minutes of 'steeping' and the second was removed after 30 minutes of 'steeping' (Chapter 2, Section 2.1.5). The third and final sample was the viscose film. Each of the samples were analysed on the solid state NMR and SEC-MALLS using the acquisition conditions listed above.

3.6.4 Solid state NMR analysis of microcrystalline cellulose (91α)

Two 91α laboratory pulp samples were further processed to microcrystalline cellulose, using acid hydrolysis, at Sappi/Saiccor. The laboratory pulp samples were removed at 5 minutes and 60 minutes during the acid hydrolysis procedure. The hydrolysed cellulose samples were analysed by solid state NMR using the acquisition conditions listed above.

Chapter 4

4. Results and discussion

Cross Polarization/Magic Angle Spinning Carbon 13-Nuclear Magnetic Resonance (CP/MAS ^{13}C-NMR or solid state NMR) and Atomic Force Microscopy (AFM) has been applied to study the supra-molecular structure of cellulose I during pulping, bleaching and drying. In this study, the Cellulose Fibril Aggregate Model developed by Larsson *et al.* (1997) was applied to determine the lateral fibril dimensions (LFD) and lateral fibril aggregate dimensions (LFAD). Newman (1999) presented an alternate method for estimating the lateral dimensions of cellulose crystallites and compared the estimated dimensions with results from wide angle X-ray scattering. Although he was able to show a strong correlation between the two sets of lateral dimensions, those measured by the WAXS were lower than that estimated by NMR. This study acknowledges the existence of other methods for estimating lateral dimensions of cellulose crystallites but uses the method developed Larsson *et al.* (1997) to determine the lateral fibril dimensions (LFD) and lateral fibril aggregate dimensions (LFAD).

This chapter presents results for the wood material through the delignification stages of acid bi-sulphite pulping and O_2 delignification; followed by D_1, E, D_2 and Final Hypochlorite or Peroxide bleaching sequence to produce three different grades of dissolving pulp i.e. 91α, 92α and 96α. The influence of different drying strategies on LFAD; an evaluation of the reactivity of the 91α grade to the microcrystalline cellulose; the 92α to swelling and viscose and the 96α to acetylation in cellulose acetate production. Where necessary, wet chemical properties and size exclusion chromatography coupled with multi-angle laser light scattering (SEC-MALLS) are presented to try and understand the chemical properties/drivers governing changes in lateral fibril aggregate dimensions during pulping, bleaching and drying.

4.1 Wood holocellulose

Due to the complexity of wood and the sensitivity of the solid state NMR to determining the structure of cellulose the wood material had to be ‘lignin free’. Wood holocellulose can be described as ‘lignin-free’ fibre material prepared from wood by severe chlorite delignification. The intention of holocellulose preparation was to maintain the structure of cellulose close to the native form. The wood holocellulose has a klason lignin content of 7.2% which is a decrease from the original value of 29% in the wood sample (Table 4.1). The glucose and xylose content, determined by HPLC analysis, for the wood sample was 47% and 10.5% respectively (Table 4.1). The glucose and xylose content for the wood holocellulose sample was 52% and 12% respectively (Table 4.1). The total recovery (sum of klason lignin, glucose, xylose, galactose, mannose, rhamnose and arabinose) for the wood holocellulose sample was however ca. 72%. Similar recoveries were also noticed by Inari *et al.*, (2007) and could possibly be explained by the degradation of lignin and glucose due to the severe chlorite delignification. Using the method developed by Larsson *et al.* (1997) the $LFAD_{NMR}$ for the wood holocellulose was determined. The LFAD measurement for the wood holocellulose sample was 22.9 ± 2.7 nm (Table 4.1) with the NMR spectrum shown in Figure 4.1. This result establishes the LFAD value for the starting wood material. Table 4.1 highlights the properties of wood, wood holocellulose and never dried unbleached pulp samples that result from the chemical pulping

Table 4.1: Properties of wood, wood holocellulose and never dried unbleached pulp samples that result from the chemical pulping (NR – not recorded)

	Wood	**Wood holocellulose**	**43 minute pulp**	**103 minute pulp**	**Commercially pulped GU A380**
Total extractable material S_{10} (%)	NR	NR	10.8	9.2	10.2
Hemicelluloses-S_{18}(%)	NR	NR	7.6	6.3	6.8
Klason lignin (%)	29	7.2	1.8	1.6	2.8
$LFAD_{NMR}$ (nm)	NR	22.9 ± 2.7	17.6 ± 0.5	24.0 ± 0.9	16.0 ± 0.3
$LFAD_{AFM}$ (nm)	NR	NR	22.0 ± 5.3	33.6 ± 0.9	19.6 ± 1.2
Glucose (%)	47	51	95.1	97.3	95.4
Xylose (%)	10.5	12	3.5	2.7	2.4
Galactose (%)	0.9	0.9	0	0	0
Mannose (%)	0.7	1.0	1.4	0	1.5
Rhamnose (%)	0.3	0.2	0	0	0
Arabinose (%)	0.2	0.2	0	0	0
Degraded cellulose/short chain glucan (%)	NR	NR	3.2	2.9	3.4

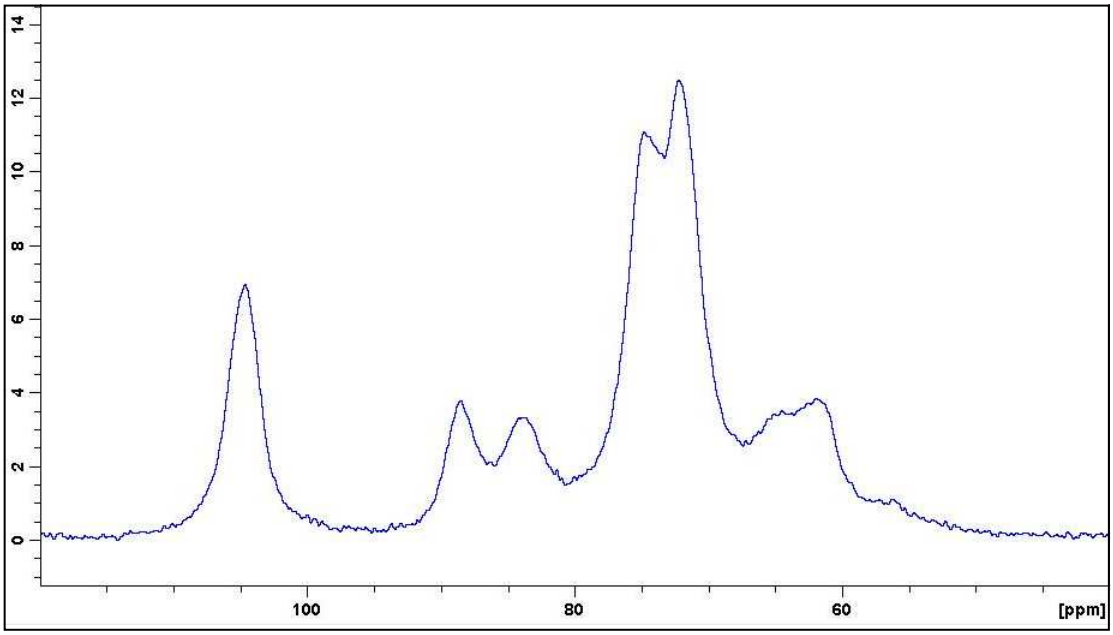

Figure 4.1: The wood holocellulose spectrum recorded using the Bruker 300 MHz

4.2 Delignification

The predominant delignification stage is during pulping were the bulk of the lignin is removed. The majority of the residual lignin is then removed in the second oxygen (O_2) stage of delignification.

4.2.1 Acid bi-sulphite pulping

The acid bi-sulphite pulping conditions, presented in Chapter 3, were used to produce pulp material. The effect of pulping time on total extractable material i.e. hemicelluloses and degraded cellulose/short chain glucan – S_{10} (%); hemicelluloses – S_{18} (%); degraded cellulose/short chain glucan i.e. S_{10} (%) – S_{18} (%) and lateral fibril aggregate dimensions (LFAD) was investigated. Three wood pulp samples were produced i.e. the wood pulped in the laboratory for 43 minutes; the wood pulped in the laboratory for 103 minutes and the wood commercially pulped for 43 minutes. The spectra recorded are shown in Figure 4.2 highlighting the differences between the 43 minute and 103 minute laboratory pulped sample and also the similarities between the 43 minute laboratory and commercially pulped sample.

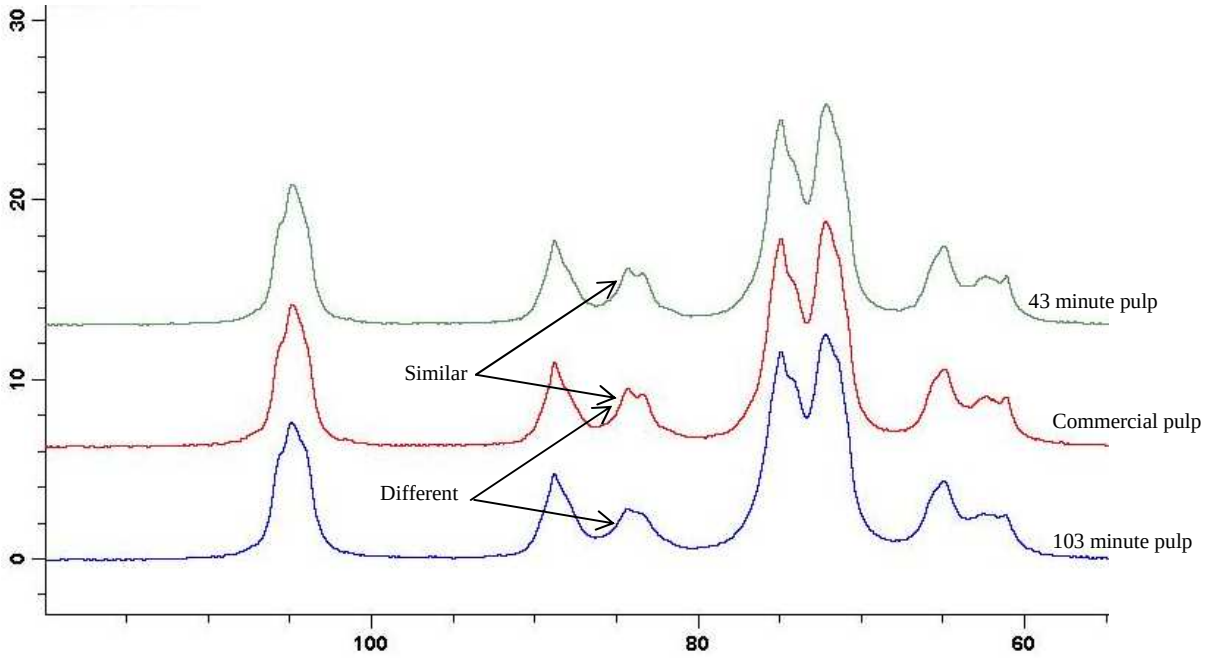

Figure 4.2: The pulp spectra, recorded using solid state NMR, for the laboratory produced unbleached pulp samples

The $LFAD_{NMR}$ results between the wood holocellulose and the 103 minute pulp sample are similar within analysis error, i.e. 22.9 ± 2.7 nm and 24.0 ± 0.9 nm respectively (Table 4.1). It is however known that hemicellulose and lignin interferes with the solid state NMR spectral resolution hence the error in the fit may be larger than that determined (Wickholm *et al.*, 1998; Newman, 1999). This is the case for the wood holocellulose sample which has a xylose content (hemicellulose content) of 12% and klason lignin content of 7.2%. By comparison the 103 minute pulp sample has a hemicellulose content of 2.7% and klason lignin content of 1.6% and the spectrum is relatively free from interference. The 103 minute pulp sample is thus more accurate in terms of the $LFAD_{NMR}$ measure. The 43 minute pulp sample and commercial pulp sample had similar $LFAD_{NMR}$ (17.6 ± 0.5 nm and 16.0 ± 0.3 nm respectively) and $LFAD_{AFM}$ (22.0 ± 3.2 nm and 19.6 ± 1.2 nm respectively). Wet chemical properties show that 43 minute pulp sample and commercial pulp sample share similar glucose, xylose, degraded cellulose/short chain glucan, total extractable material S_{10}% and hemicellulose S_{18}% content as well (Table 4.1). This shows that the LFAD measured by solid state NMR or AFM may depend on the pulp wet chemical properties. Laboratory pulping for 103 minutes showed that there was an increase in $LFAD_{NMR}$ (24.0 ± 0.9 nm) and $LFAD_{AFM}$ (33.6 ± 0.9 nm) compared to the laboratory 43 minute pulp sample. Laboratory pulping for 103 minutes also had an effect on the wet chemical properties such as xylose, degraded cellulose/short chain glucan, total extractable material S_{10}% and hemicellulose S_{18}% content i.e. the properties decreased upon laboratory pulping for 103 minutes (Table 4.1). Although it may seem evident that LFAD determined by solid state NMR and AFM may be dependent on the wet chemical properties of the pulp samples, it is also possible that both the LFAD and wet chemical properties depend independently on the severity of the degradation during acid bi-sulphite pulping.

4.2.2 O stage delignification

The next step after acid bi-sulphite pulping is the O stage delignification. Three different O stages i.e. using 91α, 92α and 96α bleaching conditions are aimed at reducing the lignin content of the unbleached pulp sample by 50%.

Table 4.2: Klason lignin (%), K-number (%) and degraded cellulose/short chain glucan (%) [S_{10} (%) – S_{18} (%)] for unbleached and 3 different Oxygen stages

		Unbleached pulp	**O stage**
91α bleaching conditions	Klason lignin (%)	3.4	0.9
	K-number (%)	2.5	1.9
	Total extractable material S_{10} (%)	10.3	10.4
	Hemicelluloses S_{18} (%)	7.9	6.7
	Degraded cellulose/short chain glucan	2.4	3.7
92α bleaching conditions	Klason lignin (%)	3.4	1.1
	K-number (%)	2.5	1.8
	Total extractable material S_{10} (%)	10.9	8.1
	Hemicelluloses S_{18} (%)	7.9	6.7
	Degraded cellulose/short chain glucan	2.4	3.2
96α bleaching conditions	Klason lignin (%)	4.3	2.0
	K-number (%)	3.9	2.0
	Total extractable material S_{10} (%)	9.8	8.1
	Hemicelluloses S_{18} (%)	7.2	6.0
	Degraded cellulose/short chain glucan	2.6	2.1

Table 4.2 highlights the klason lignin content; K-number; S_{10} (%) 'Total extractable material' which includes hemicellulose and degraded cellulose/short chain glucan content and S_{18} (%) 'Total extractable hemicellulose' content. Table 4.2 shows that the decrease in lignin content (klason lignin (%) and K-number (%)), in the unbleached pulp samples after the O stage, was in the approximate range of 25% - 70% for the pulp samples. Apart from the residual lignin that is removed during the O_2 $^{91\alpha}$ O_2 $^{92\alpha}$ and O_2 $^{96\alpha}$ delignification stage, there is a change in the total extractable material S_{10} (%) i.e. hemicellulose and degraded cellulose/short chain glucan content. The total extractable material content S_{10} (%) for the pulp bleached using O_2 $^{91\alpha}$ delignification conditions changed marginally whereas the total extractable material S_{10} (%) content and total extractable hemicellulose S_{18} (%) content for the pulp samples bleached using O_2 $^{92\alpha}$ and O_2 $^{96\alpha}$ conditions decreased. There is an increase in degraded cellulose/short chain glucan content for the pulp samples delignified using O_2 $^{91\alpha}$ delignification conditions (degraded cellulose/short chain glucan content increased from 2.4 – 3.7%) and O_2 $^{92\alpha}$ delignification conditions (degraded cellulose/short chain glucan content increased from 2.4 – 3.2%) (Table 4.2). The pulp sample delignified using O_2 $^{96\alpha}$ conditions showed a decrease in degraded cellulose/short chain glucan content (2.6 – 2.1%, Table 4.2). This could

possibly be attributed to the use of magnesium sulphate ($MgSO_4$) in the O_2 $^{96\alpha}$ delignification step compared to the O_2 $^{91\alpha}$ and O_2 $^{92\alpha}$ delignification conditions which does not use magnesium sulphate. Magnesium sulphate has been used as a protecting group and prevents excessive cellulose degradation (Chen and Lucia, 2002).

4.3 Bleaching

Following the O_2 stage, delignified pulp samples were bleached using 91α, 92α and 96α bleaching conditions (Tables 3.3, 3.4 and 3.5, Chapter 3). Bleaching of the acid bi-sulphite pulp samples were performed in three bleaching sequences: $D_1E_o^{91\alpha}D_2H^{91\alpha}$ and $D_1E_o^{92\alpha}D_2H^{92\alpha}$ for the 91α and 92α respectively, $D_1E_o^{96\alpha}$ D_2P for the 96α (Chapter 3). The effect of changing the final stage in the 96α production from peroxide to hypochlorite was also investigated. The sequence used was the $D_1E_o^{96\alpha}D_2H^{92\alpha}$.

Lateral fibril aggregate dimensions measured using solid state NMR and AFM were recorded for the unbleached pulp; after bleaching stages D_1, $E_o^{91\alpha}$, $E_o^{92\alpha}$, $E_o^{96\alpha}$, $H^{91\alpha}$, $H^{92\alpha}$, $P^{96\alpha}$ (Table 4.3). This was done in order to identify a stage at which a change, if any, in LFAD occurs. A change in LFAD would translate to a change in cellulose supra-molecular structure. The average LFAD values are obtained using the 600 MHz and 500 MHz solid state NMR is shown in Table 4.3, Figure 4.3.

Table 4.3: LFAD (nm), measured using solid state NMR, through the bleaching stages

	LFAD (nm)			
	Unbleached	**D_1**	**E**	**Final**
91α conditions	18.5 ± 0.8	19.9 ± 0.7	19.5 ± 0.8	20.5 ± 0.8
92α conditions	18.8 ± 0.8	18.4 ± 0.7	20.5 ± 0.9	22.2 ± 1.4
96α conditions	18.8 ± 0.9	21.0 ± 1.0	25.3 ± 1.2	25.8 ± 1.3

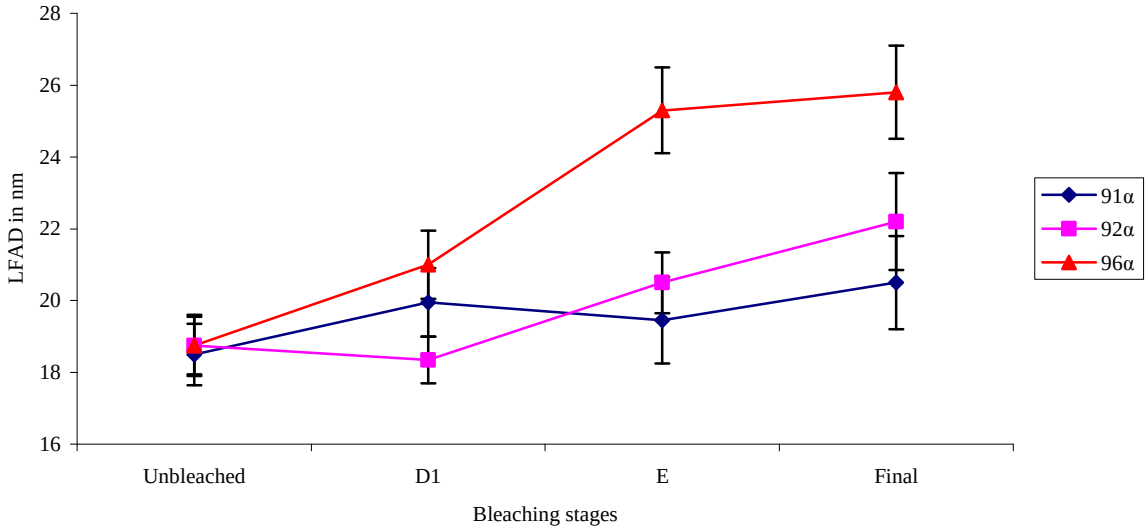

Figure 4.3: Effect of bleaching conditions on $LFAD_{NMR}$

The variation in $LFAD_{NMR}$ with processing is shown in Figure 4.3. The change in LFAD from unbleached pulp to fully bleached dissolving pulp for the 91α was from 18.5 ± 0.8 nm to 20.5 ± 0.8 nm and for the 92α was from 18.8 ± 0.8 nm to 22.2 ± 1.4 nm. The similar profiles suggest that the pulp samples share a similar supra-molecular structure during the bleaching process. During bleaching there is a pronounced increase in $LFAD_{NMR}$ after the $E_o^{96\alpha}$ stage. The $LFAD_{NMR}$ levels off at the final peroxide stage, 25.3 ± 1.2 nm to 25.8 ± 1.3 nm. Substituting the peroxide bleach for a hypochlorite (H) bleach had a marginal effect on LFAD. The $LFAD_{NMR}$ for the $H^{96\alpha}$ was 23.7 ± 0.6 nm.

Table 4.4: $LFAD_{AFM}$ (nm), measured using, through the bleaching stages

	$LFAD_{AFM}$ (nm)*			
	Unbleached	**D_1**	**E**	**Final**
92α Hypochlorite	38 ± 2	31 ± 2	18 ± 2	23 ± 2
96α Peroxide	38 ± 2	21 ± 2	23 ± 2	30 ± 2

*Results are from 10 AFM scans with the error in the aggregate dimension measurement reported

Table 4.5 presents $LFAD_{AFM}$ results for the unbleached and samples produced after D_1, $E_o^{92\alpha/96\alpha}$ and final P or H stage during 92α and 96α dissolving pulp production.

Figure 4.4 and Figure 4.5 show the 1x1 micron phase images for the unbleached, D_1, $E_o^{92\alpha}$ $E_o^{96\alpha}$ and final samples for the 92α and 96α bleaching processes. Lighter areas correspond to regions of higher stiffness (Meyer *et al*., 2004) and are therefore associated with cellulose (Fahlén and Salmén, 2003; Mark, 1967). The darker structures hence may be considered to be predominantly 'matrix' material (lignin and hemicelluloses).

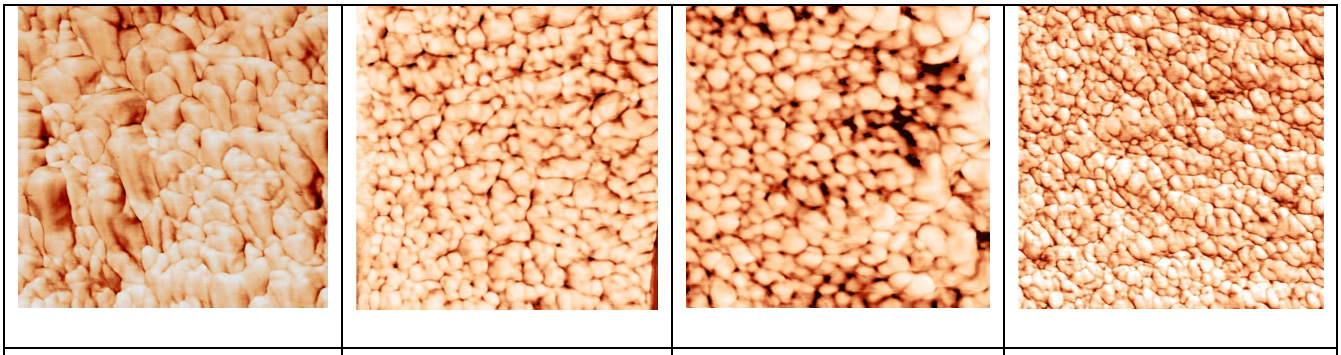

Unbleached	D_1 Stage	E stage	Final

Figure 4.4: 1x1µm scans within the S2 layer for the unbleached pulp, after $D_1^{92\alpha}$, $E_o^{92\alpha}$, and final 92α

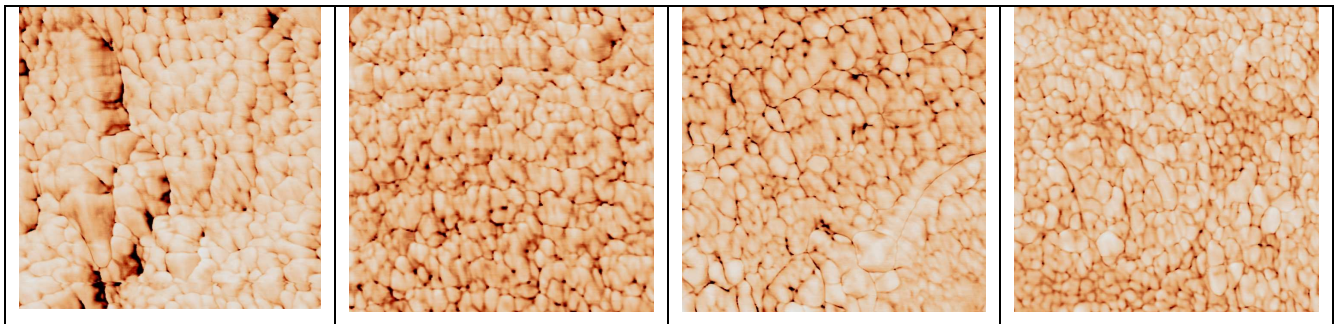

Unbleached	D_1 Stage	E stage	Final

Figure 4.5: 1x1µm scans within the S2 layer for the unbleached pulp, after $D_1^{96\alpha}$, $E_o^{96\alpha}$, and final 96α

Image Pro® Plus with watershed segmentation was used for processing the images and calculating the $LFAD_{AFM}$. The unbleached pulp sample has a higher LFAD (38 ± 2 nm) compared to the in-process and final pulp samples bleached using 92α and 96α bleaching conditions. A marginal increase in LFAD was evident for the 92α pulp from the E stage to the Hypochlorite stage samples i.e. 18 ± 2 nm to 23 ± 2 nm.

The 96α pulp sample however showed a significant increase in LFAD from the E stage to the Peroxide stage i.e. 23 ± 2 nm to 30 ± 2 nm. Although the absolute measure of LFAD by AFM is shown, it is the trends observed that are important. The trends in $LFAD_{AFM}$ during the latter stages of the bleaching sequence mimic the trends observed for the $LFAD_{NMR}$ on the same pulp samples. A few possibilities exist for the variation in the $LFAD_{AFM}$ and $LFAD_{NMR}$: a. the variation may be due to the number of samples analysed by the two techniques. The $LFAD_{NMR}$ gives an average based on ca. 100000 fibres whereas $LFAD_{AFM}$ gives an average of 10 fibres scanned and b. for the unbleached pulp sample, the variation may be due to the influence of hemicellulose and lignin on tip. It may be possible that changes in material stiffness, due to presence of hemicellulose and lignin, resulted in an exaggeration in LFAD measured by the AFM.

A closer look at the wet chemical properties, at each of the bleaching stages, is thus necessary in order to understand the results from solid state NMR and AFM. Table 4.5 presents the wet chemical properties for the pulp samples processed using 91α, 92α and 96α bleaching conditions, after pulping, O_2 delignification and subsequent bleaching steps to produce 91α, 92α, 96α P and 96α H.

Table 4.5: Wet chemical properties at the delignification, bleaching and final steps during dissolving pulp production

	Delignification		**Bleaching**			
91α conditions	**Unbleached pulp**	**O**	**D_1**	**E_o**	**D_2**	**Final**
Lignin (K-number)	2.5	1.9	1.7	1.6	1.1	0.8
Total extractable material S_{10} (%)	10.3	10.4	7.0	10.7	7.2	12.0
Total hemicellulose S_{18} (%)	7.9	6.7	5.1	6.7	5.1	7.6
Degraded cellulose/short chain glucan	2.4	3.7	1.9	4.0	2.1	4.4
92α conditions						
Lignin (K-number)	2.5	1.8	1.4	1.0	0.8	0.6
Total extractable material S_{10} (%)	10.9	8.1	10.8	8.7	6.2	8.9
Total hemicellulose S_{18} (%)	7.9	6.7	6.5	5.2	7.8	5.0
Degraded cellulose/short chain glucan	3.0	1.4	4.3	3.5		3.9
96α P - conditions						
Lignin (K-number)	3.9	2.0	1.5	0.7	0.5	0.4
Total extractable material S_{10} (%)	9.8	8.1	11.0	6.0	6.2	6.5
Total hemicellulose S_{18} (%)	7.2	6.0	6.6	3.9	4.0	3.8
Degraded cellulose/short chain glucan	2.6	2.1	4.4	2.1	2.2	2.7
96α H - conditions						
Lignin (K-number)	2.5	1.9	1.2	1.1	0.8	0.7
Total extractable material S_{10} (%)	9.8	9.0	11.0	6.0	4.5	5.0
Total hemicellulose S_{18} (%)	7.5	6.3	6.3	2.8	3.0	2.7
Degraded cellulose/short chain glucan	2.3	2.7	4.7	3.2	1.5	2.3

S_{18}(%) = Total extractable hemicellulose; S_{10} (%) = Total extractable Hemicellulose and Degraded cellulose/short chain glucan

Table 4.5 highlights the following wet chemical properties of the pulp samples: K-number; S_{18} (%) 'total extractable hemicellulose' content and S_{10} (%) 'total extractable hemicellulose' content and degraded cellulose/short chain glucan content. The $LFAD_{NMR}$ was measured after the first stage of bleaching, after the E stage and after the final stage i.e. D_1, E, and P or H respectively. The $LFAD_{NMR}$ measurements for the raw unbleached 91α, 92α and 96α pulp samples, on average, varied between 18.5 ± 0.8 nm for the 91α to 18.8 ± 0.9 nm for the 96α (Table 4.3). A similar trend was noticed at the D_1 stage for the 91α, 92α and 96α pulp samples, which on average, varied between 18.4 ± 0.7 nm for the 92α to 21.0 ± 1.0 nm for the 96α (Table 4.3). A significant increase in aggregate dimension is noticed at the $E_o^{96\alpha}$ (Table 4.3, Figure 4.3). This increase in $LFAD_{NMR}$ was not as pronounced in the $E_o^{91\alpha}$ and $E_o^{92\alpha}$. The increase in $LFAD_{NMR}$ at the $E_o^{96\alpha}$ stage could be attributed to either total

extractable material S_{10} (%), total extractable hemicellulose S_{18} (%) or degraded cellulose/short chain glucan content. Bleaching tables (Chapter 3) show that the concentration of sodium hydroxide, temperature and processing time, used during the E-stage, for each of the pulp grades was different. A three-fold increase in sodium hydroxide (1% to 3.2%) during E-stage of bleaching did not have a noticeable affect on the $LFAD_{NMR}$ (supra-molecular structure) of pulp samples under the $E_o^{91\alpha}$ and $E_o^{92\alpha}$ conditions (Table 4.3, Figure 4.3). However a nine-fold increase in the sodium hydroxide concentration (1% to 9%) resulted in a marked increase in $LFAD_{NMR}$ for the pulp sample bleached using $E_o^{96\alpha}$ conditions (Table 4.3, Figure 4.3). On inspection of the wet chemical properties (Table 4.5) it is evident that there was a change in total extractable material S_{10} (%), total extractable hemicellulose S_{18} (%), and degraded cellulose/short chain glucan for each of the pulp grades at the E-stage that could be related to the changes in $LFAD_{NMR}$. Figure 4.6 shows a comparison of total extractable material S_{10} (%), total extractable hemicellulose S_{18} (%), and degraded cellulose/short chain glucan to $LFAD_{NMR}$ through the 92α bleaching sequence.

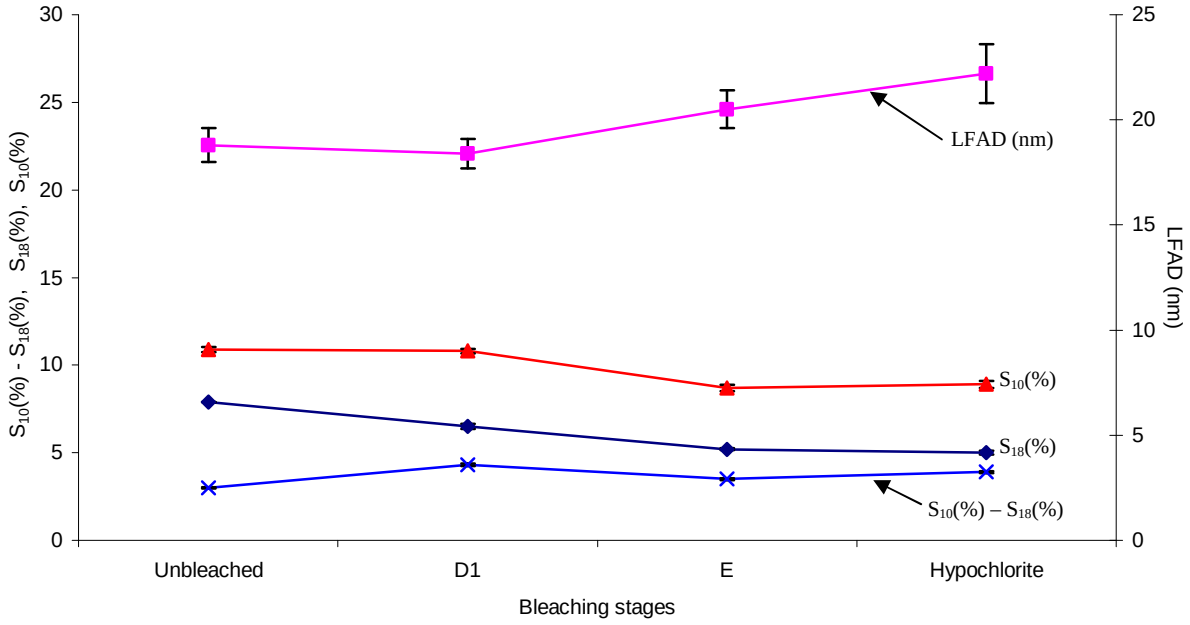

Figure 4.6: Comparison of degraded cellulose/short chain glucan, total extractable material S_{10} (%), total hemicellulose content S_{18} (%) and $LFAD_{NMR}$ during the 92α bleaching sequence

An overview of the $LFAD_{NMR}$ (Table 4.3) and wet chemical properties (Table 4.5) shows that the increase in caustic dose (NaOH) from 1% to 3% at the $E_o^{91\alpha}$ $E_o^{92\alpha}$ had an effect on the total extractable material, total extractable hemicellulose, and degraded cellulose/short chain glucan (Table 4.5). However, the increase in caustic dose did not have a noticeable effect on the $LFAD_{NMR}$.

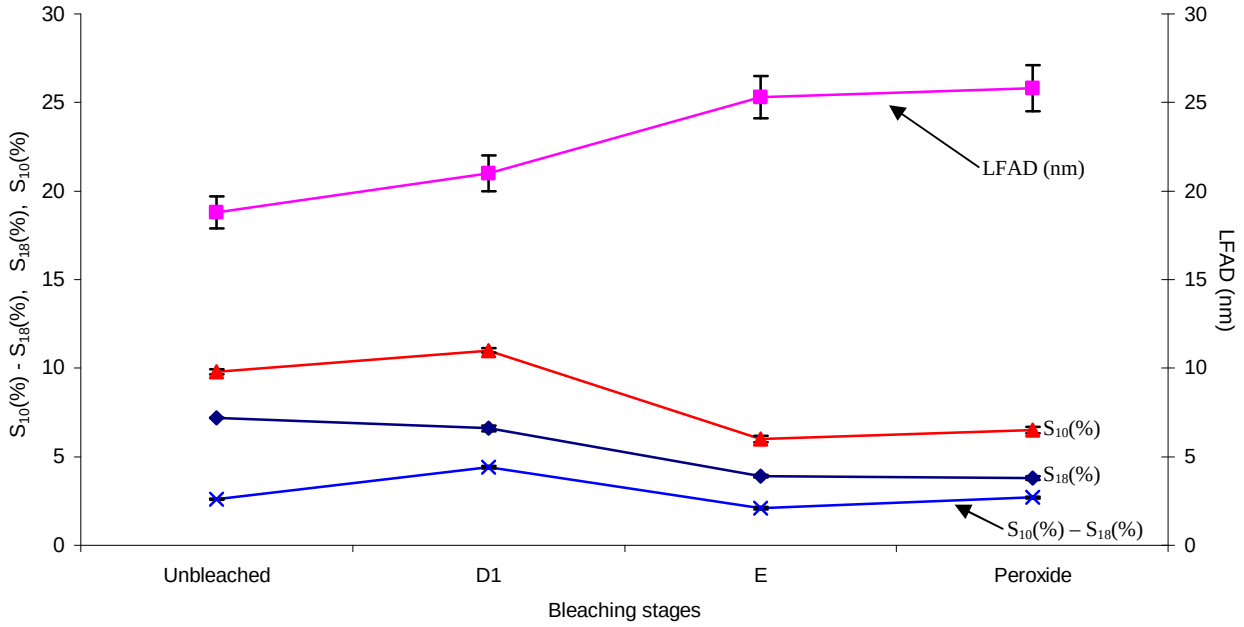

Figure 4.7: Comparison of degraded cellulose/short chain glucan, total extractable material S_{10} (%), total hemicellulose content S_{18} (%) and LFAD during the 96α bleaching sequence

From Figure 4.7 it is evident that a decrease in total extractable material S_{10} (%), total extractable hemicellulose S_{18} (%), and degraded cellulose/short chain glucan results in an increase in $LFAD_{NMR}$ at $E_o^{96\alpha}$ stage. An increase from 1% to 9% however had a pronounced effect on total extractable material, total extractable hemicellulose, degraded cellulose/short chain glucan content and $LFAD_{NMR}$. There thus seems to be a threshold value for the pulp samples, with respect to the change in total extractable material S_{10} (%), total extractable hemicellulose S_{18} (%), degraded cellulose/short chain glucan content from the D_1 stage to the E stage that either results in an increase in $LFAD_{NMR}$ or not. A change of ca. 25% in total extractable material S_{10} (%), total extractable hemicellulose S_{18} (%), degraded cellulose/short chain glucan content for the 92α results in a marginal change in $LFAD_{NMR}$. A change of ca. 70% in total extractable hemicellulose S_{10} (%), 80% in total extractable material S_{18} (%) and 100%

in degraded cellulose/short chain glucan content respectively results in a substantial increase in $LFAD_{NMR}$. The threshold values for total extractable material S_{10} (%), total extractable hemicellulose S_{18} (%), degraded cellulose/short chain glucan content should thus be in the range 25% to 70%.

A second D stage ($D_2^{91\alpha}$, $D_2^{92\alpha}$, $D_2^{96\alpha}$) using 0.6% – 2% chlorine dioxide was introduced to improve the brightness of the dissolving pulp samples after the E-stages. Chlorine dioxide solubilises residual lignin which is subsequently washed away. Table 4.5 shows that the lignin content decreased after the D_2 stage for 91α, 92α and 96α bleaching sequence. Since the D_2 stage is essentially a washing stage, $LFAD_{NMR}$ was not determined on the pulp samples, it was determined at the final bleaching stage where changes in cellulose supra-molecular structure were anticipated.

The chemical (i.e. hypochlorite or peroxide) used in the final bleaching stage depended on the grade of pulp being used. The pulp samples bleached using 91α and 92α conditions utilised hypochlorite in the final stage whereas the pulp sample bleached using the 96α conditions utilised peroxide in the final stage. Hypochlorite is used to control the degree of polymerisation (DP) of the cellulose molecules. The DP in this study is represented by the viscosity of the pulp sample. The use of hypochlorite increases cellulose molecule chain scission and also increases degradation (i.e. an increase in total extractable material S_{10} (%) and degraded cellulose/short chain glucan). The peroxide used during the final stage 96α bleaching conditions 'scavengers' and destroys elemental chlorine (Johnson, 1994; Reisch, 1995) resulting in pulp samples with a higher percentage of cellulose with little to no contamination from chlorine.

Table 4.6: Viscosity of the pulp samples at the D_2 and final bleaching stages

	Viscosity (cP)		**$LFAD_{NMR}$ (nm)**
	D_2	**Final**	**Final**
91α Hypochlorite	24	24	20.5 ± 0.8
92α Hypochlorite	40	30	22.2 ± 1.4
96α Peroxide	21	20	25.8 ± 1.3
96α Hypochlorite	40	20	23.7± 0.6

The use of hypochlorite increased cellulose molecular chain scission resulting in lower viscosity values (40 cP - 30 cP for the 92α, Table 4.6) at the final bleaching stage compared to D_2 stage. This was not evident for the 91α pulp sample which had a D_2 stage and Hypochlorite stage viscosity of 24 cP. The reason for lack of change in viscosity could be the dose of hypochlorite used. The 91α pulp sample uses a dose of hypochlorite smaller than that used for the 92α and 96α pulp sample. The peroxide did not affect the viscosity of the 96α, i.e. 21 cP at the D_2 stage to 20 cP at the peroxide stage. The use of hypochlorite instead of peroxide in the final bleaching stage for the 96α resulted in a 50% reduction in viscosity at the final stage in the bleaching sequence i.e. 40cP at the D_2 to 20cP at the hypochlorite stage (Table 4.6). The effect of hypochlorite on the supra-molecular structure of 91α, 92α and 96α was also evaluated. From Table 4.6 it is evident that the peroxide had a greater effect on $LFAD_{NMR}$ than hypochlorite i.e. 25.8 ± 1.3 nm and 23.7 ± 0.6 nm respectively for the 96α dissolving pulp sample.

The differences in wet chemical properties and $LFAD_{NMR}$ for each of the pulp samples is due to different process conditions used to make the respective dissolving pulp grades i.e. 91α, 92α and 96α. Paradoxically, this implies that attempts to remove lignin and extractable hemicellulose, during the production of 96α dissolving pulp, is accompanied by a corresponding increase in lateral fibril aggregate dimensions. One explanation that has been proposed is that degraded cellulose/short chain glucan, abundant in 91α and 92α pulp samples (Table 4.7), may exert steric hindrance and prevent cooperative large area contacts between surfaces of neighbouring fibril aggregates (Larsson, 2003). This will result in a low degree of aggregation in the 91α and 92α pulp samples (Table 4.3). The 96α with low levels of degraded cellulose/short chain glucan content show a higher degree of aggregation in the final pulp sample relative to the 91α and 92α pulp samples (Table 4.3).

Table 4.7: Degraded cellulose/short chain glucan content for final dissolving pulp samples

	Degraded cellulose/short chain glucan content [S_{10} (%) – S_{18} (%)]
91α Hypochlorite	4.4
92α Hypochlorite	3.9
96α Peroxide	2.7
96α Hypochlorite	2.7

4.4 Controlling fibril aggregation

The final 91α, 92α and 96α dissolving pulp samples were initially run on the solid state NMR in the wet state (never dried). The samples were then subject to drying via two strategies, viz. oven and condition drying. Oven dried pulp samples were prepared by placing dissolving pulp into the oven at 104ºC for 18 hours. Condition dried pulp samples were prepared by placing pulp in a conditioned room at 23ºC with 50% RH for 5 days. The dried pulp samples were re-wetted and analysed by solid state NMR. Table 4.8 show the LFAD measurements of the never dried pulp samples and the pulp samples after condition drying and oven drying.

Table 4.8: Total extractable material S_{10} (%), $LFAD_{NMR}$ (nm), of final dissolving pulp samples subject to different drying strategies

Pulp sample	**S_{10} (%)**	**$LFAD_{NMR}$ (nm)**		
		Never dried	**Condition dried**	**Oven dried**
91α Hypochlorite	11.4 ± 0.4	17.5 ± 0.6	21.2 ± 1.6	26.1 ± 1.9
92α Hypochlorite	9.1 ± 0.4	18.3 ± 0.5	22.3 ± 1.6	28.0 ± 2.1
96α Peroxide	6.7 ± 0.5	22.5 ± 0.7	28.0 ± 2.6	34.7 ± 2.6

Inspection of the data in Table 4.8 shows that there was a change in LFAD upon condition drying e.g. 17.5 ± 0.6 nm to 21.2 ± 1.6 nm for the 91α; 18.3 ± 0.5 nm to 22.3 ± 1.6 nm for the 92α and 22.5 ± 0.7 nm to 28.0 ± 2.6 nm for the 96α. The 91α and 92α pulp samples (Figures 4.8 and 4.9) show an increase in lateral fibril aggregation upon oven drying, 17.5 ± 0.5 nm to 26.1 ± 1.9 nm and 18.3 ± 0.5 nm to 28.0 ± 2.1 nm respectively. The 96α pulp sample (Figure 4.10) shows an increase in aggregate dimensions from 22.5 ± 0.7 nm to 34.7 ± 2.6 nm. Although the three grades of pulp samples show similar trends upon oven drying, the increase in aggregate dimensions is the largest during oven drying. The increase in $LFAD_{NMR}$ was greater for the 96α followed by the 92α and 91α with the aggregate dimensions being 34.7 ± 2.6 nm, 28.0 ± 2.1 nm and 26.1 ± 1.9 nm respectively. First time drying, oven or condition drying, induced a degree of irreversible aggregation of the cellulose fibrils i.e. ‘hornification’. Hornification, a term introduced by Jayme (Jayme, 1944), is used in wood and pulp literature to describe the ‘stiffening of a polymer structure’ taking place in lignocellulosic (cellulose containing lignin) material upon drying or

water removal (Diniz *et al.*, 2004). Wetting the samples, prior to running on the solid state NMR, does not return the LFAD to the original never dried state hence aggregation is irreversible.

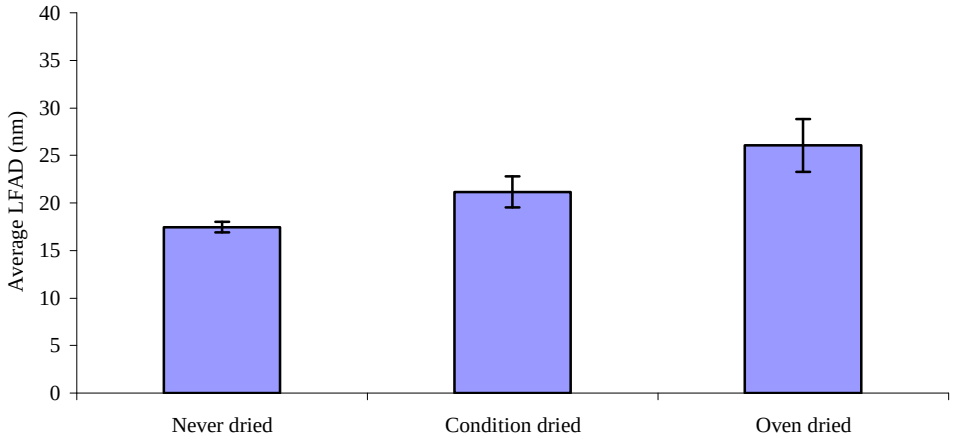

Figure 4.8: Average LFAD (nm) for the '91α' using the different drying strategies

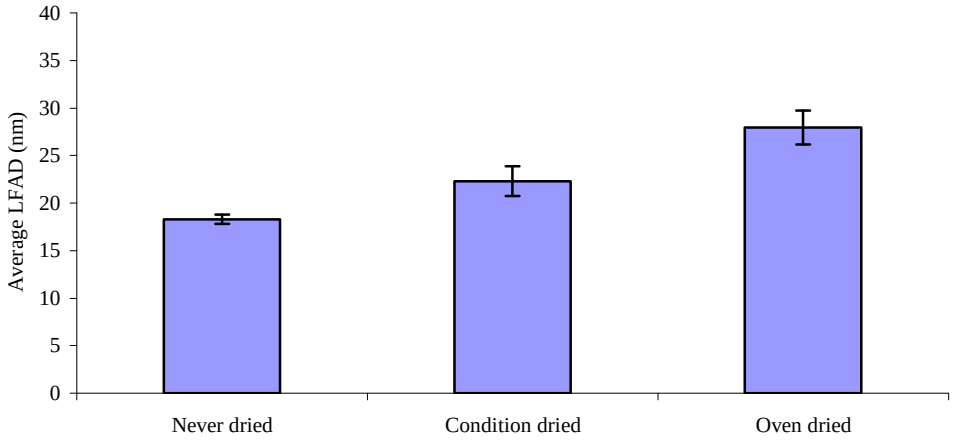

Figure 4.9: Average LFAD (nm) for the '92α' using the different drying strategies

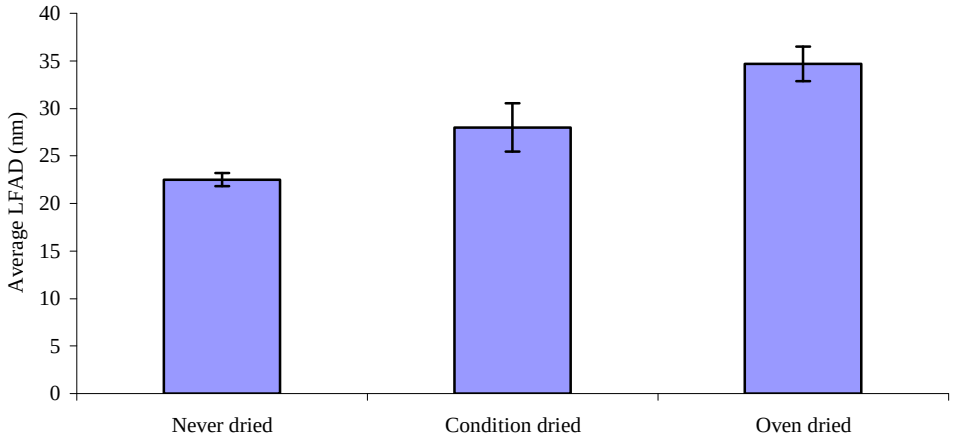

Figure 4.10: Average LFAD (nm) for the '96α' using the different drying strategies

The results thus far point to the possibility of controlling $LFAD_{NMR}$ by using different drying strategies. Condition drying the pulp samples is a possible method that can be used to control fibril aggregation. A plausible explanation for this method of drying is that the slow rate of water removal (period of 5 days), at a relative humidity of 50% and 23ºC limits the movement of the fibrils thereby preventing restructuring of the fibril aggregates. Oven drying presents a relatively rapid form of drying where the high temperature e.g. during oven drying (104ºC) increases the rate at which water is removed and the movement of the fibrils. This possibly leads to a random restructure of the fibril aggregates and an increase in lateral fibril aggregate dimension. If $LFAD_{NMR}$ can be controlled then it can be used to provide dissolving pulp samples with pre-defined specific surface area. Since the extractable hemicellulose and degraded cellulose/short chain glucan content influence the LFAD during acid bi-sulphite pulping and bleaching, there is a possibility that it can have an influence on fibril aggregation during drying. This increase in aggregate dimensions upon drying is supported by LFAD results obtained on another Eucalyptus clone studied by Nocanda *et al.* (2007). They showed that for a total extractable material S_{10} (%) and total hemicellulose S_{18} (%) content of 6.7 and 2.8 respectively there is an increase in aggregate dimensions from 22.8 nm to 30.3 nm upon drying for a 96α pulp sample (Nocanda *et al.*, 2007).

Table 4.9 presents the LFAD measurements recorded using the AFM on never dried and oven dried pulp samples. Table 4.9 shows that there is an increase in $LFAD_{AFM}$ for both the 92α and 96α never dried fully bleached 'final' dissolving pulp samples. This trend upon oven drying supports the solid state NMR trend for the same pulp samples.

Table 4.9: $LFAD_{AFM}$ (nm)* of dissolving pulp samples subject to oven drying

Pulp sample	**$LFAD_{AFM}$ (nm)**	
	Never dried	**Oven dried**
92α Hypochlorite	24.1 ± 1.9	28.9 ± 1.8
96α Peroxide	26.7 ± 1.6	32.2 ± 1.7

* Results are from 10 AFM scans with the error in the aggregate dimension measurement reported

Figure 4.11 and Figure 4.12 show the 1x1 μm scans of the never dried and oven dried 92α and 96α pulp samples. A visual inspection of Figure 4.11 and Figure 4.12 shows that upon oven drying, there is an increase in LFAD especially for the 96α pulp sample.

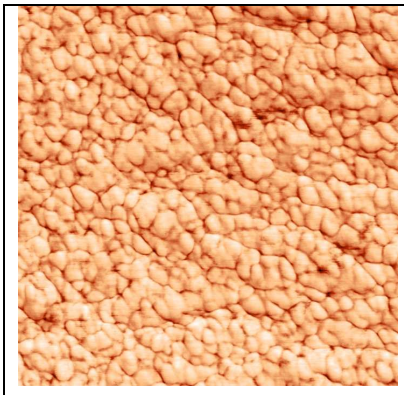

Never dried

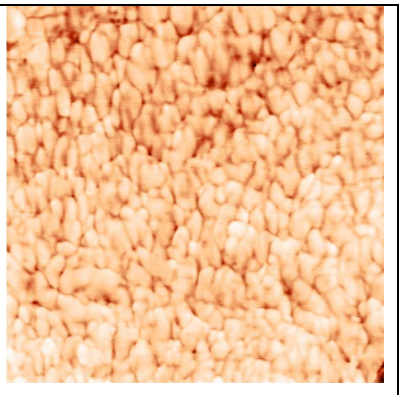

Oven dried

Figure 4.11: 1x1 μm scans within the S2 layer of never dried and oven dried final 92α pulp samples

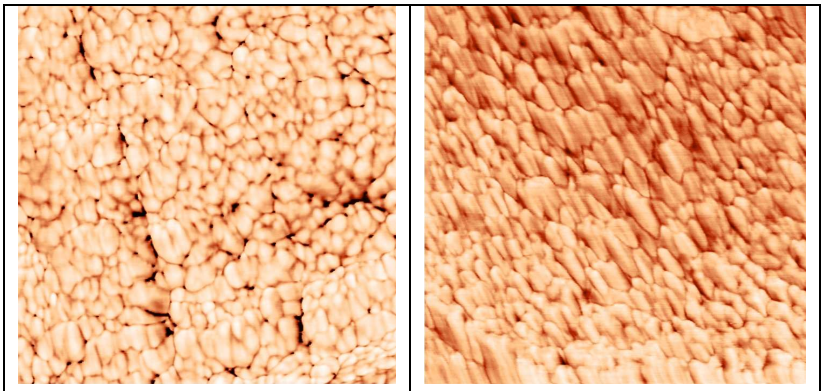

Never dried	Oven dried

Figure 4.12: 1x1 μm scans within the S2 layer of never dried and oven dried final 96α pulp samples

Table 4.10 shows the wet chemical properties of the 3 dissolving pulp grades used to evaluate the effect of drying strategies on LFAD.

Table 4.10: Wet chemical properties of the dissolving pulp samples used to evaluate the effect of drying strategies on LFAD

Wet chemical property	**91α**	**92α**	**96α**
K-number % (lignin)	0.28	0.28	0.32
S_{10} (%) 'Hemicellulose' and degraded cellulose/short chain glucan	11.4	9.1	6.7
S_{18} (%) 'Hemicellulose'	5.9	4.6	2.4
Degraded cellulose/short chain glucan (%)	5.5	4.5	3.6
Viscosity (cP)	16	17	36
Cu –Number (%)	1.1	0.9	0.4

As expected, the Cu-number is related to the viscosity of the pulp samples. At low viscosity levels i.e. 16 cP, for the 91α pulp, the Cu-number is 1.1%. At high viscosity levels i.e. 36 cp, for the 96α pulp, the Cu-number is 0.4%. Cu-number may also be regarded as an index of impurities (oxycellulose, hydrocellulose etc.) in pulp samples (Tappi T430, 2009) hence the 91α has a higher content of impurities than the 92α and 96α. An increase in aggregate dimension due to drying seems to correlate with the total extractable material S_{10} (%) i.e. hemicellulose [(S_{18} (%)] and degraded cellulose/short chain glucan [S_{10} (%) - S_{18} (%)]. During drying, an increased contact between the cellulose fibril surfaces is established (Oksanen *et al.*, 1997; Newman, 2004) and it seems that the Eucalypt acid bi-sulphite pulp samples with a higher total

extractable material have a lower tendency for cellulose fibrils to aggregate during drying. A possible explanation for the phenomenon, i.e. an increase in aggregate dimensions upon drying, is shown in Figure 4.13 and Figure 4.14 below.

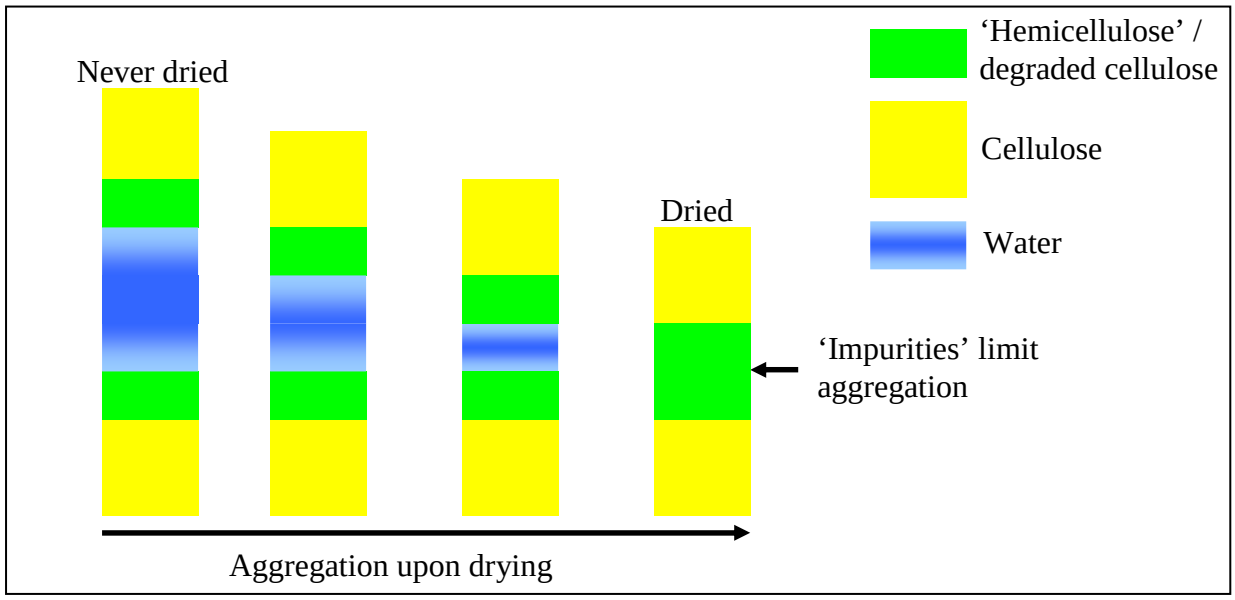

Figure 4.13: Aggregation of fibrils in the presence of extractable hemicellulose and/or degraded cellulose/short chain glucan.

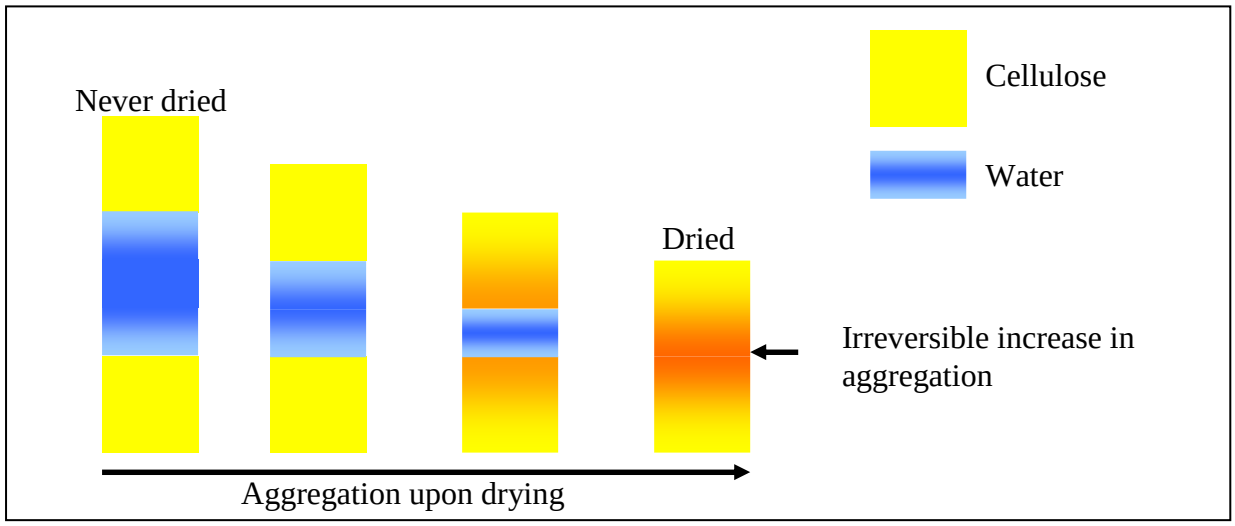

Figure 4.14: Aggregation of fibrils in the absence of extractable hemicellulose and/or degraded cellulose/short chain glucan

Drying pulp samples results in an irreversible change in lateral fibril aggregate dimensions irrespective of the drying strategies employed. The change can be marginal, as in the case of condition drying, or substantial as in the case of oven drying the pulp samples. Figure 4.13 shows the aggregation of fibrils upon drying in the presence of the total extractable content S_{10} (%) i.e. hemicellulose and degraded cellulose/short chain glucan ('impurities'). It is however evident, Figure 4.13, that the measurement of the fibril dimension for the dried material is going to be similar to the never dried material due to the presence of the 'impurities'. Rebuzzi and Evtuguin (2006) recently showed the effect 4-O-methylglucuronxylan has on fibril aggregation during drying. They showed that the presence of 4-O-methylglucuronxylan in the pulp samples diminished the fibril aggregation and hence hornification during drying. This scenario resembles that prevalent in the 91α and 92α pulp samples where the amounts of extractable hemicellulose and degraded cellulose/short chain glucan could possibly affect fibril aggregation.

The second scenario, Figure 4.14, shows the aggregation of fibrils upon drying in the absence or presence of small quantities of 'impurities'. Drying removes water from pores between the cellulose molecules facilitating their aggregation, however the absence or presence of small quantities of 'impurities' does not prevent the aggregation of fibrils. This scenario resembles the drying of 96α pulp were small quantities of extractable hemicellulose and degraded cellulose/short chain glucan do not inhibit the aggregation of fibrils. While this study shows the changes in LFAD upon drying in the radial direction of the fibril, there have been studies that showed that relatively pure forms of cellulose (cellulose nanocrystals) also experience changes in the longitudinal direction upon drying (Konturri and Vuorinen, 2009). Table 4.11 presents a summary of total extractable material S_{10} (%) and corresponding LFAD results for 91α, 92α and 96α used in this study.

Table 4.11: $LFAD_{NMR}$ (nm) and total extractable material S_{10} (%) for never dried final pulp samples

Pulp sample		**LFAD (nm)**	**S_{10} (%)**
91α Hypochlorite	Run 1	18.6 ± 0.4	12.0 ± 0.5
	Run 2	19.1 ± 0.5	11.4 ± 0.4
92α Hypochlorite	Run 1	18.9 ± 0.4	9.0 ± 0.4
	Run 2	19.8 ± 0.4	9.1 ± 0.4
96α Peroxide	Run 1	22.6 ± 0.7	6.5 ± 0.6
	Run 1	23.6 ± 0.6	6.7 ± 0.5
96α Hypochlorite	Run 2	23.7 ± 0.6	5.0 ± 0.5

Figure 4.15 highlights the relationship between total extractable material and LFAD for the pulp samples. A decrease in total extractable material corresponds to an increase in LFAD for the pulp samples.

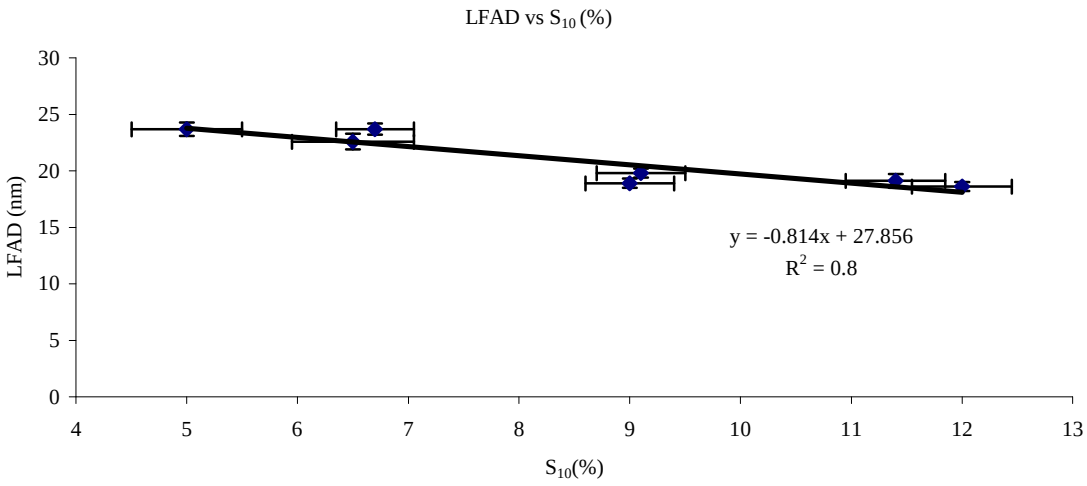

Figure 4.15: $LFAD_{NMR}$ (nm) and final total extractable material S_{10}% for never dried 91α, 92α and 96α pulp samples

This finding suggests that it should be possible to predict never dried LFAD measurements based on S_{10} (%) values for 91α, 92α and 96α final never dried dissolving pulp samples using the following equation:

$$y= -0814x + 27.856 \quad (1)$$

where $x = S_{10}$% and y = predicted LFAD in nm

Table 4.12 presents a set of total extractable material S_{10} (%) values for 91α, 92α and 96α pulp samples and corresponding predicted and actual LFAD.

Table 4.12: Total extractable material S_{10} (%), $LFAD_{predicted}$ (nm) and $LFAD_{actual}$ (nm) for the never dried final pulp samples

	S_{10}(%)	**$LFAD_{predicted}$ (nm)**	**$LFAD_{actual}$ (nm)**
91α	11.8 ± 1.5	18.2 ± 1.2	15.8 ± 0.6
92α	8.8 ± 0.5	20.7 ± 0.4	16.8 ± 0.6
96α	6.2 ± 0.9	22.8 ± 0.7	21.4 ± 0.9

The $LFAD_{predicted}$ (nm) trends for final never dried dissolving pulp samples, shown in Table 4.12, mimic the $LFAD_{actual}$ (nm) trends, i.e. a decrease in total extractable material results in a corresponding increase in LFAD.

Table 4.13: Total extractable material S_{10} (%) and percentage change in $LFAD_{NMR}$ upon drying

		Percentage change in $LFAD_{NMR}$	
	S_{10} (%)	**Condition dried**	**Oven dried**
91α	11.4 ±0.4	21.2 ± 2.0	49.3 ± 2.4
92α	9.1 ± 0.4	21.9 ± 2.1	52.7 ± 3.3
96α	6.7 ± 0.5	24.4 ± 2.7	54.2 ± 2.7

Table 4.13 presents the percentage change in LFAD upon condition and oven drying the 91α, 92α and 96α pulp samples. Figure 4.16 summarizes the correlation between the 3 pulp samples upon condition and oven drying to the total extractable material S_{10} (%) content.

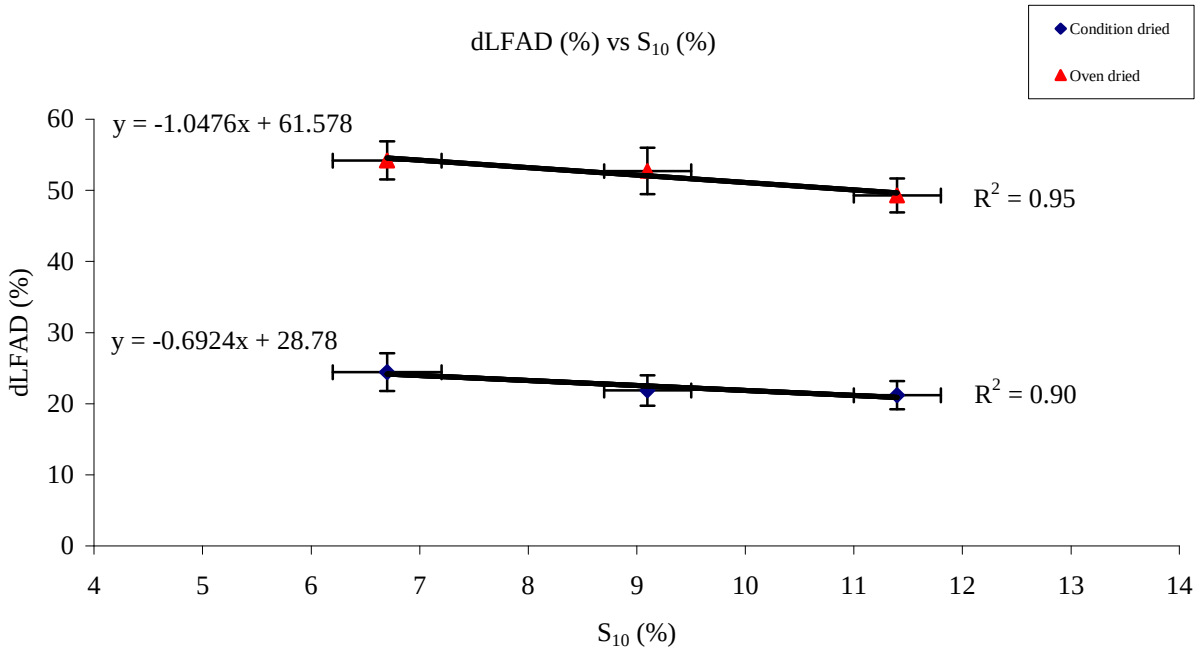

Figure 4.16: The percentage increase in fibril aggregate dimension upon oven and condition drying plotted against total extractable material S_{10} (%)

Table 4.13 and Figure 4.16 re-affirm that the method used to dry the pulp sample affects the percentage increase in fibril aggregate dimensions for each of the 3 pulp grades. The percentage increase in fibril aggregate dimension upon oven drying > condition drying, with the percentage change increasing with decreasing total extractable material S_{10} (%) i.e. hemicellulose and degraded cellulose/short chain glucan content. As discussed earlier, condition drying probably presents a situation where there is no, or very little, restructuring of the fibrils into fibril aggregates whereas oven drying allows for the restructuring of fibrils into larger fibril aggregates. The three dissolving pulp grades have different percentages of total extractable material S_{10} (%) i.e. 11.4%, 9.1% and 6.7% for the 91α, 92α and 96α respectively (Table 4.13). As discussed earlier, pulp samples with a higher total extractable material S_{10} (%) have a lower tendency for the cellulose fibrils to aggregate during drying. In summary, there are two distinct phenomena that seem to influence $LFAD_{NMR}$ and the change in $LFAD_{NMR}$ on drying; namely the total extractable material S_{10} (%) present before drying and the method in which the pulp sample is dried.

The results suggest that it is possible to predict the percentage change in LFAD upon drying for pulp samples if the total extractable content S_{10} (%) is known. This is vital commercially since predicting how a pulp is going to behave upon drying may also help predict how a particular pulp sample is going to behave during further chemical reactions towards for e.g. microcrystalline cellulose, viscose and cellulose acetate. Using the following equations obtained from Figure 4.16:

Condition dried: $y = -0.6924x + 28.78$ (2)

Oven dried: $y = -1.0476x + 61.578$ (3)

the predicted percentage changes in LFAD upon condition and oven drying for a known S_{10}(%) are shown in Table 4.14.

Table 4.14: Total extractable material S_{10} (%) and predicted percentage change in LFAD upon drying for the pulp samples

		Predicted percentage change in LFAD	
	S_{10} (%)	**Condition dried**	**Oven dried**
91α	10.8	21.3	50.3
92α	8.4	23.0	52.8
96α	6.9	24.0	54.4

The predicted values (Table 4.14), based on total extractable material S_{10} (%), mimic the trends as shown in Table 4.13 in that the way the sample is dried and percentage of total extractable material affects the percentage change in LFAD.

There is further evidence to suggest that there are different amounts of extractable hemicellulose and degraded cellulose/short chain glucan in the pulp samples. Size exclusion chromatography (SEC-MALLS) of the 92α and 96α cellulose show that the molecular mass distributions of the pulp samples are different (Figure 4.17). The 96α has a smaller amount of low molecular weight fractions whereas the 92α has a higher amount of low molecular weight fractions i.e. degraded cellulose/short chain glucan and hemicellulose. The probable reason for the difference in molecular weight distributions between the 92α and 96α, is that the hypochlorite bleaching step is used

during 92α dissolving pulp production. The result of which is chain scission which lowers the degree of polymerisation of the glucan chain thereby creating lower molecular weight glucan chains. The peroxide bleaching step used during production of the 96α pulp does not produce lower molecular weight glucan chains and results in a higher level of molecular ordering i.e. high molecular weight fractions.

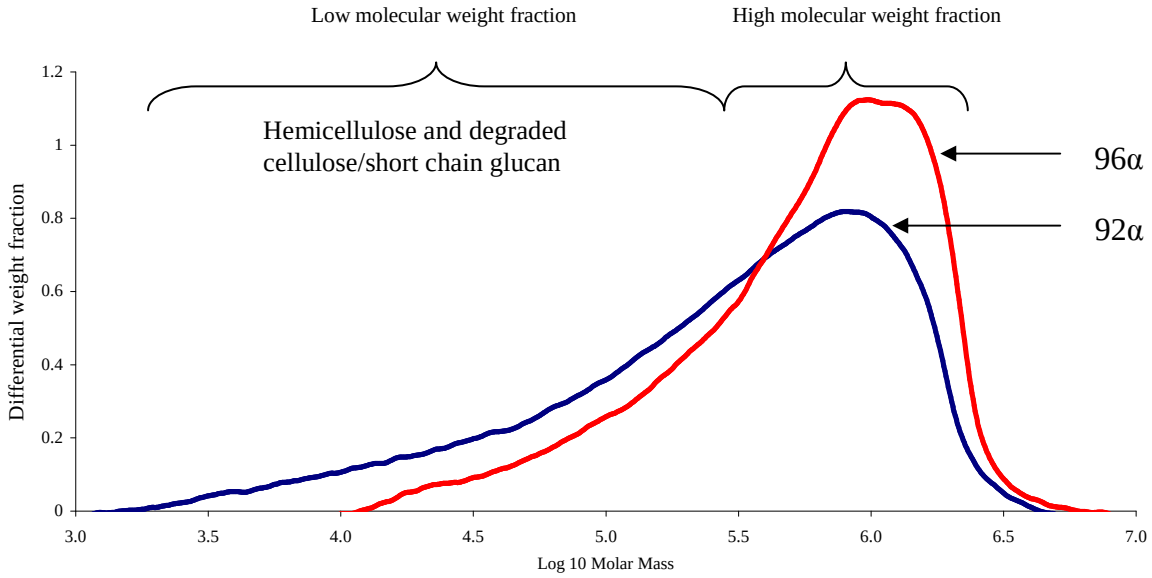

Figure 4.17: SEC-MALLS analysis of 92α and 96α

4.5 Chemical 'reactivity'

The 'reactivity' of dissolving pulp is often seen as the most significant quality parameter (Krässig, 1996). The 96α pulp was acetylated using acetic anhydride to form acetate flake. The 92α was treated with sodium hydroxide and then mixed with carbon disulfide (CS_2). The resulting cellulose xanthate was dissolved into more sodium hydroxide towards the formation of viscose. The 91α pulp was hydrolysed with dilute acids at elevated temperatures; the non-crystalline domains of cellulose were preferentially hydrolysed, while the crystalline ones remained intact. Attempts at estimating the reactivity of the pulp samples in each of the chemical processes were carried out using solid state NMR, ^{1}H-NMR and SEC-MALLS.

4.5.1 Acetylation studies using 96α grade dissolving pulp

The specific surface area ratio, determined using solid state NMR, was compared to the pseudo first order reaction rate ratio which was determined from the degree of acetylation. The question to be addressed was: does the supra-molecular structure of cellulose I, present in the 96α grade dissolving pulp, influence the reactivity towards acetylation? This study used two pulp samples with different LFAD in the acetylation reaction i.e. 96α commercial pulp and cotton linters cellulose. They were subject to acetylation at 40ºC and 60ºC. It was anticipated that the different pulp samples would have different specific surface areas and hence perform differently in the acetylation reactions. The aim of the experiment was to ascertain whether the ratio of specific surface areas for two 'different' dissolving pulp samples is similar to the ratio of the pseudo first order initial reaction rate constants. Table 4.15 presents the lateral fibril dimensions (LFD) and LFAD measurements, specific surface areas, pseudo first order initial reaction rate constant (k) at 40ºC and 60ºC for the cotton and commercial 96α dissolving pulp samples. The graph of methyl intensity versus time reveals the pseudo first order initial reaction rate constant for each of the dissolving pulp samples.

Table 4.15: LFD_{NMR} (nm), $LFAD_{NMR}$ (nm) and Specific Surface Area (SSA) in m^2/g for dissolving pulp samples

	LFD (nm)	**LFAD (nm)**	**SSA (m^2/g)**	**k at 40°C**	**k at 60°C**
Cotton linters	7.1 ± 0.1	47 ± 2	53	$1.4 \times 10^{-3} \pm 2 \times 10^{-4}$	$6 \times 10^{-3} \pm 6 \times 10^{-4}$
Commercial 96α	4.04 ± 0.04	28 ± 1	89	$2.4 \times 10^{-3} \pm 3 \times 10^{-4}$	$11 \times 10^{-3} \pm 2 \times 10^{-3}$

The LFD for the cotton linters cellulose is 7.1 nm. The native cellulose LFD is larger than the commercial produced dissolving pulp sample (average ca. 4 nm). The LFAD for the cotton linters cellulose was 47 ± 2 nm compared to the commercial dissolving pulp sample i.e. 28 ± 1 nm. For a larger LFAD, evident in Table 4.15, there is a smaller specific surface area. This implies that there is a smaller specific surface area available for chemical reaction. This is reflected in the pseudo first order initial reaction rate constants which are lower for smaller specific surface areas (Table 4.15).

Table 4.16: Summary of specific surface area ratio compared to initial reaction rate constant ratio computed from $LFAD_{NMR}$ and density of cellulose

	Specific surface area ratio	**Initial rate constant ratio 40°C**	**Initial rate constant ratio 60°C**
Cotton linters / Commercial 96α pulp	0.59 ± 0.06	0.59 ± 0.07	0.58 ± 0.09

The pseudo first order initial reaction rate constant ratio and specific surface area ratio for the commercial 96α and cotton linters cellulose are presented in Table 4.16. The results show that the pseudo-zero order rate constant ratio is 0.59 ± 0.06 with the ratio of specific surface area at 40ºC being 0.59 ± 0.07 and at 60ºC being 0.58 ± 0.09. This shows that the ratio of initial reaction rate constants, k(cotton linters)/k(commercial 96α), reproduce the ratio of specific surface area for both 40ºC and 60ºC reaction temperatures. This implies that:

1. Pseudo first order initial reaction rate ratio is related to specific surface area ratio for two different substrates and
2. The pseudo first order initial reaction rate constant ratio is independent of the temperature at which the acetylation reaction is performed.

A further comparison of acetylated sample analysis involved the use of ^{1}H-NMR. It was envisaged that it would provide a rapid result for the initial reaction rate constant compared to solid state NMR. The dried acetylated pulp samples were placed in deuterated chloroform. In theory, the acetylated surfaces should dissolve in deuterated chloroform with the solid or unacetylated material filtered. The dissolved acetylated pulp is then analysed by solution state NMR. The graph of acetyl intensity (cellulose triacetate) vs. time gives the initial reaction rate constant (Goodlett *et al*., 1971). Table 4.17 shows a comparison of the different processes involved in the analysis of acetylated material by solid state NMR and ^{1}H-NMR.

Table 4.17: Comparison of sample preparation and analysis

Solid state NMR	**^{1}H-NMR**
1. Commercial 96α pulp Cotton linters	1. Laboratory 96α pulp Cotton linters.
2. Acetylated at 40ºC for 3, 6, 9 and 12 minutes.	2. Acetylated at 40ºC for 10, 15, 20 and 25 minutes, dissolved in deuterated chloroform, undissolved material filtered off, Goodlett *et al.*, (1971).
3. Packed in the rotor and run on the solid state NMR at ca. 6 hours a sample.	3. Run on the Proton NMR at ca. 2 minutes a sample.

The preliminary ^{1}H-NMR reactivity study carried out on 96α pulp samples and cotton linters showed that the short reaction times, 3; 6 and 9 minutes, did not provide any signal intensity. The experiment was thus performed at 10, 15, 20 and 25 minutes. Following first order reaction kinetics at the short reaction times, the initial reaction rate constant was determined from a linear plot of cellulose triacetate signal intensity against time.

Table 4.18: Summary of results for specific surface area ratio vs. initial reaction rate constant ratio determined by solid state-NMR and ^{1}H-NMR at 40ºC

	Specific surface area ratio (m^2/g)	**Initial reaction rate constant ratio determined by solid state -NMR**	**Initial reaction rate constant ratio determined by ^{1}H-NMR**
Cotton linters / Commercial 96α pulp	0.59 ± 0.06	0.55 ± 0.12	0.60 ± 0.05

Table 4.18 highlights the results showing the comparison of the two techniques to determine initial reaction rate constant ratios. The specific surface area was determined from LFAD measurements using solid state NMR. The pseudo initial rate constant ratio determined by solid state NMR (0.55 ± 0.12) and first order reaction rate constant ratio determined by solution state ^{1}H-NMR (0.60 ± 0.05) is related to the ratio of specific surface area (0.59 ± 0.06) of the acetylated materials. Results indicate that the initial reaction rate constant ratio is proportional to the specific surface area ratio for the cellulose pulp samples. This shows that specific surface area is related to

initial reactivity to acetylation. It is thus possible to use solution state ^{1}H-NMR to give an indication of initial reaction rate constants for acetylation.

4.5.2 Alkaline cellulose (Alkcell) preparation using 92α grade dissolving pulp

Alkaline cellulose preparation is the first step in the viscose manufacturing process. 92α dissolving pulp, with extractable hemicellulose in the range of 4.6% – 5.1%, was used to produce alkcell. The first step in the process is steeping. Steeping is the process whereby 18.5% sodium hydroxide is mixed with pulp at 53ºC for a defined period of time to form alkali cellulose (Sappi Saiccor, Visc001/2004). Samples are removed after 15 minutes and 30 minutes of 'steeping' for chemical analysis. Excess sodium hydroxide is pressed out of the sample. Further material was sampled at 30 minutes after 'steeping' with 3 ½ hours of ageing. Ageing is the process whereby steeped alkcell, after pressing and shredding, is dried in an oven in the temperature range of 50ºC – 55ºC (Sappi Saiccor, Visc003/2004). Ageing the alkcell sample results in a product which has a specific degree of polymerisation (DP). The DP is imperative in the viscose manufacturing process. Other steps involved in the viscose manufacturing process include cellulose xanthate formation, ripening and spinning. The final product of the process is viscose. The 92α dissolving pulp and alkcell samples were initially analysed by solid state NMR and then SEC-MALLS.

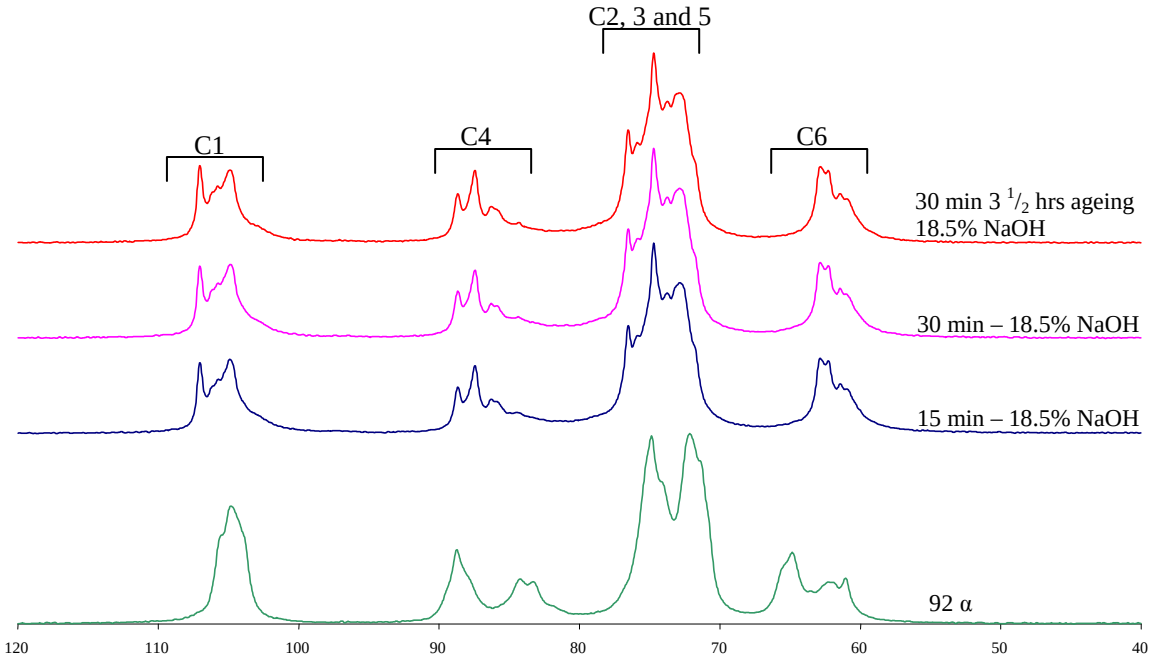

Figure 4.18: Solid state NMR spectra of 92α compared to alkcell material

The laboratory alkcell material was washed thoroughly with deionised water before recording a spectrum. Figure 4.18 shows a comparison of spectra for the starting 92α as well as the alkcell after 15 minutes and 30 minutes steeping and also 30 minutes steeping after 3 ½ hours of ageing. The starting material is cellulose I and has structure and aggregate dimensions which are measurable using the spectral fitting model applied to dissolving pulp samples. Figure 4.19 shows that there is a difference between the 92α spectrum and the 3 alkcell spectra. Figure 4.19 clearly shows this difference in the C1, C2, C3, C4, C5 and C6 regions with the overlaid spectra of the 92α compared to alkcell material.

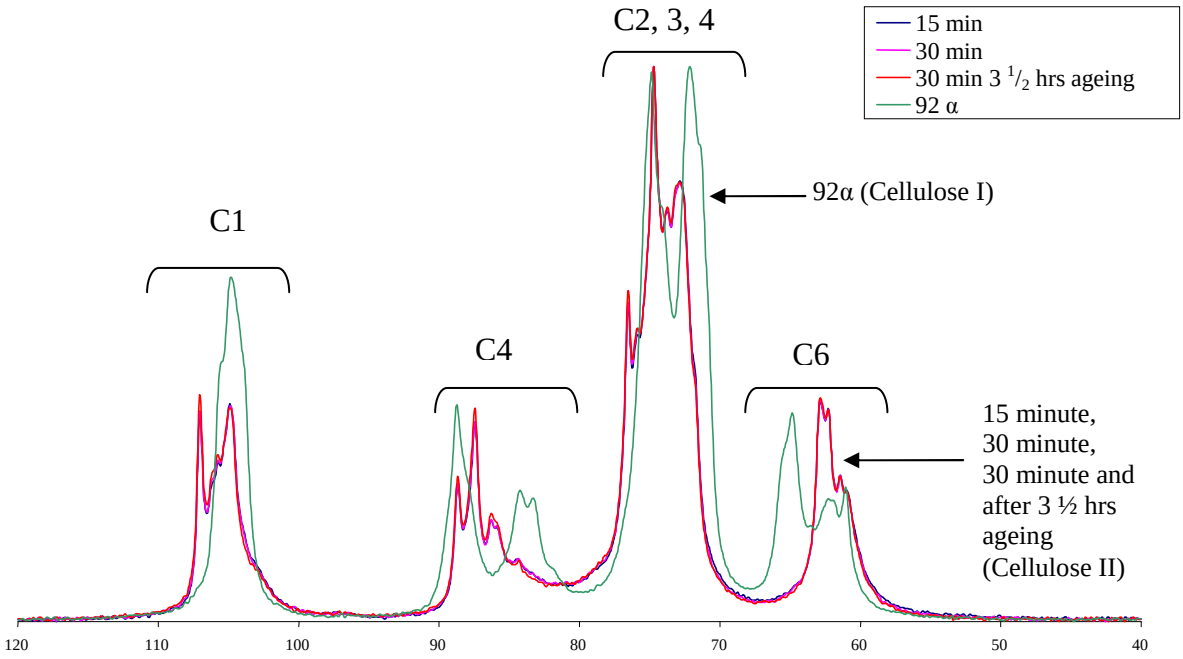

Figure 4.19: Overlaid solid state NMR spectra, recorded on a Bruker 300 MHz, of 92α compared to alkcell material

Figure 4.19 shows there is a conversion of cellulose I to cellulose II and the solid state NMR can differentiate between the two forms. It also highlights that the conversion from cellulose I to cellulose II is complete after 15 minutes of steeping, i.e., the spectrum for the alkcell sample (Figure 4.20) is consistent with a spectrum obtained for cellulose II (Koch *et al*., 2000).

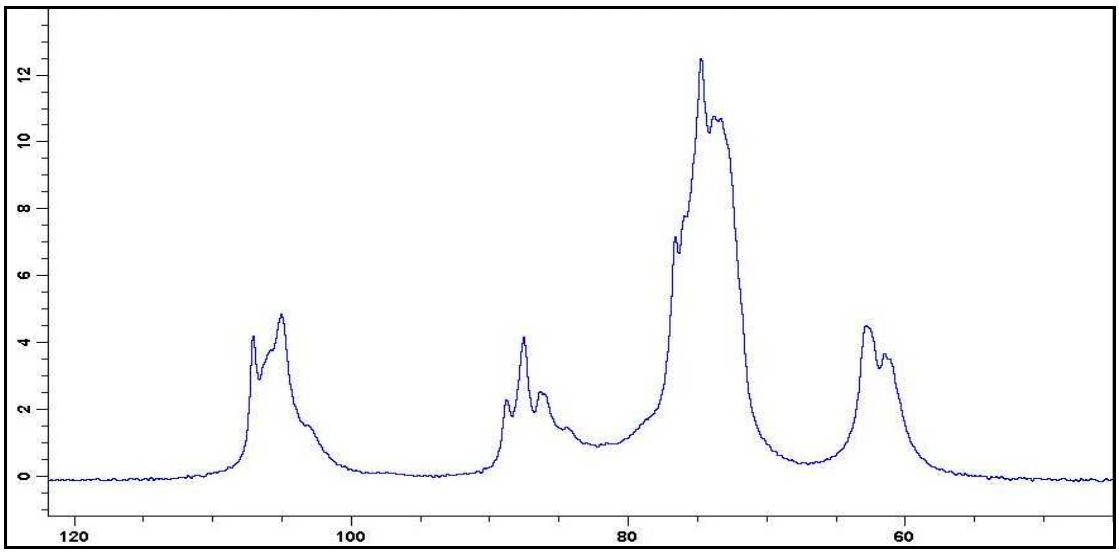

Figure 4.20: ^{13}C-NMR spectra for cellulose II

By comparison of spectra, solid state NMR can detect minor differences in supra-molecular structure. However, currently a limitation of the existing Cellulose Fibril Aggregate Model is that it is not possible to quantitatively determine the structural difference between cellulose II samples as was done with cellulose I. SEC-MALLS was thus used as a tool to gauge if it could detect differences between 92α pulp and alkcell samples. Figure 4.21 presents the SEC-MALLS analysis of the 92α pulp sample and also the alkcell material removed at the different stages in the process.

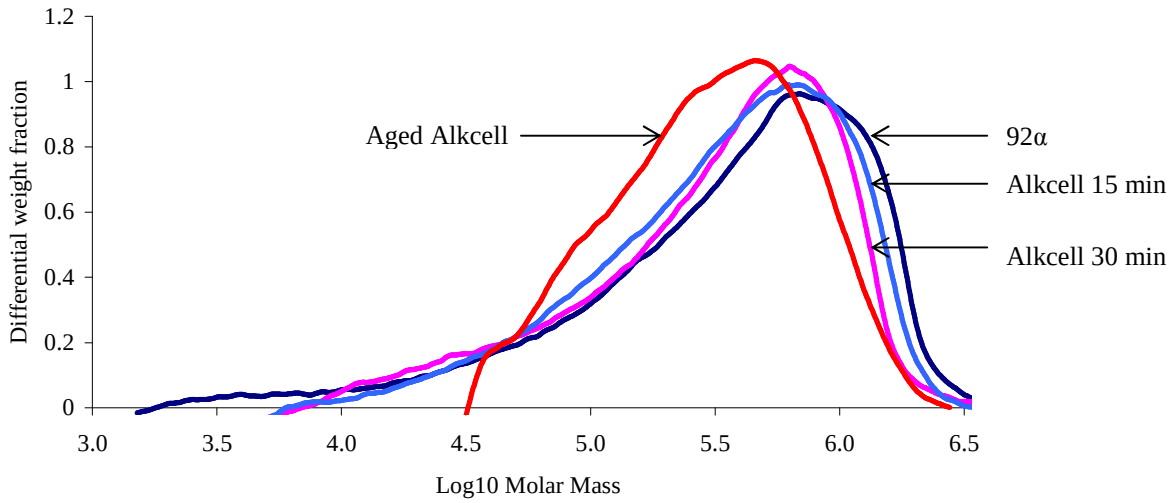

Figure 4.21: SEC-MALLS distributions for laboratory 92α pulp sample, 15 minutes and 30 minutes alkcell samples after steeping before ageing and 30 minute alkcell after 3 ½ hour aging

Figure 4.21 shows that there is a difference in molecular weight distribution between the 92α pulp sample and the alkcell material. The aged alkcell shows the narrowest molecular weight due to uniform molecular weight fragments. Figure 4.22 highlights a commercial pulp sample that was deemed highly reactive in the viscose manufacturing process. By comparison the shift in molecular weight distribution during steeping is more pronounced in the commercial dissolving pulp sample than the laboratory produced pulp sample.

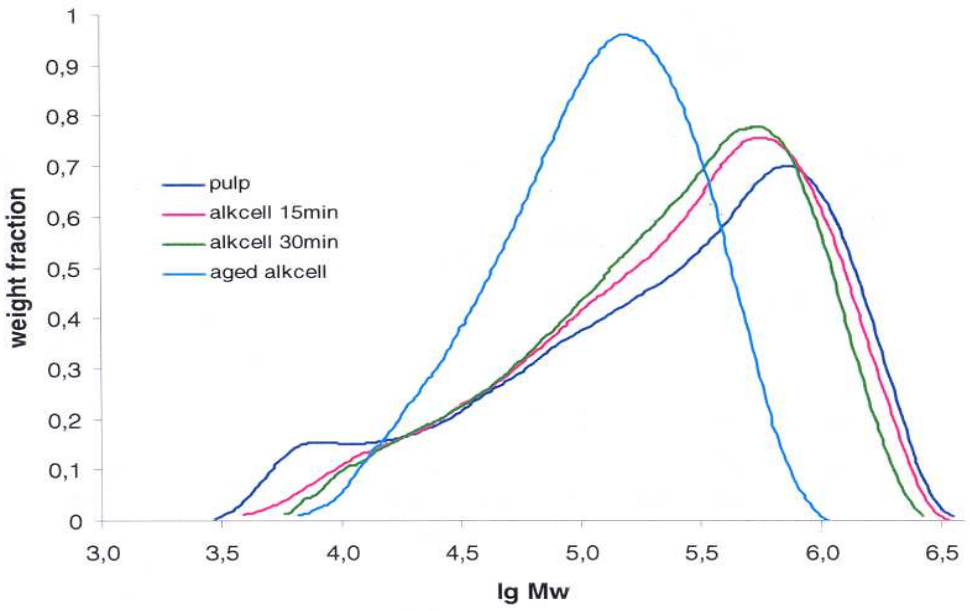

Figure 4.22: Commercial dissolving pulp samples showing a shift in molecular weight distribution upon steeping

It is apparent in Figure 4.22 that dissolving pulp with an acceptable reactivity to steeping and aging in the viscose process shows a noticeable shift in the molecular weight distribution after steeping and aging. This is possibly due to the conversion of cellulose I in the pulp to cellulose II in the alkcell and aged alkcell. SEC-MALLS can thus be used to gauge the reactivity of 92α pulp samples in the viscose manufacturing process and overcome the solid state NMR limitation of differentiating between pulp samples of low and high reactivity.

4.5.3 Microcrystalline cellulose (MCC) preparation from 91α grade dissolving pulp

Microcrystalline cellulose is produced by acid hydrolysis of 91α grade dissolving pulp where almost all non-cellulose material is removed and the cellulose I is depolymerised.

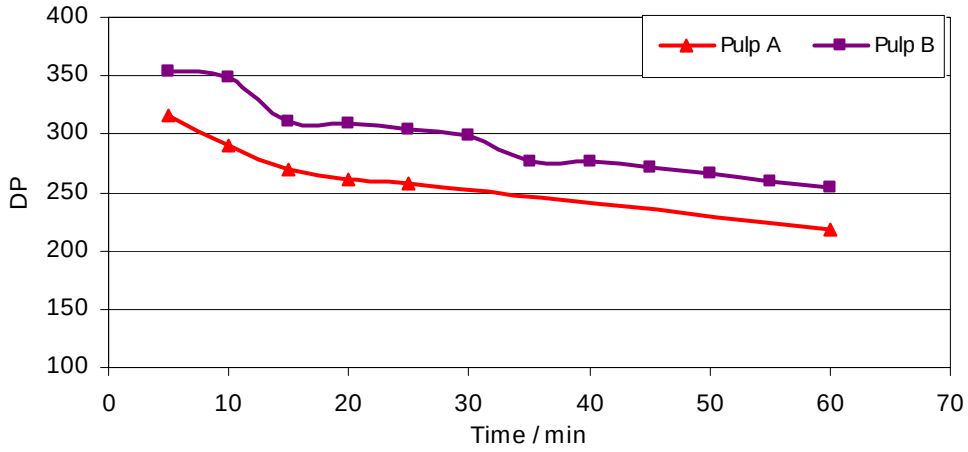

Figure 4.23: Variation of degree of polymerization with time after acid hydrolysis for two 91α laboratory produced dissolving pulp samples

Figure 4.23 shows the results for the acid hydrolysis experiments performed on two 91α pulp samples (Pulp A and Pulp B). Pulp A and Pulp B were selected based on the difference in DP after the final stage of bleaching i.e. the hypochlorite stage where the hypochlorite dose dictated the DP of the final pulp sample. From Figure 4.23 it is evident that the degree of polymerisation (DP) of the final pulp sample dictates the final DP or levelling off degree of polymerisation (LODP) i.e. the final DP of the cellulose molecule after acid hydrolysis. The standard 91α LODP is in the range 170 to 190. In order to achieve this, the starting DP should be in the 230 to 290 range.

The laboratory produced 91α, 91α after 5 minutes acid hydrolysis and MCC after 60 minutes of acid hydrolysis were further analysed using solid state NMR. Figure 4.24 show the individual spectra and Figure 4.25 shows the overlaid spectra.

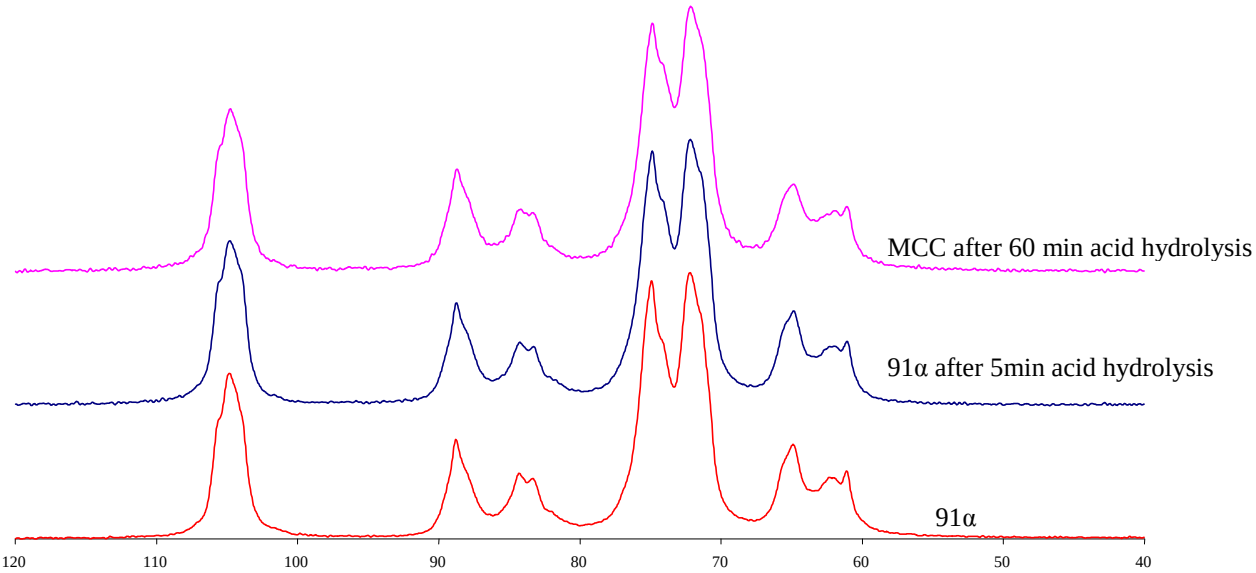

Figure 4.24: Spectra of 91α, 91α after 5 min acid hydrolysis and MCC after 60 min acid hydrolysis

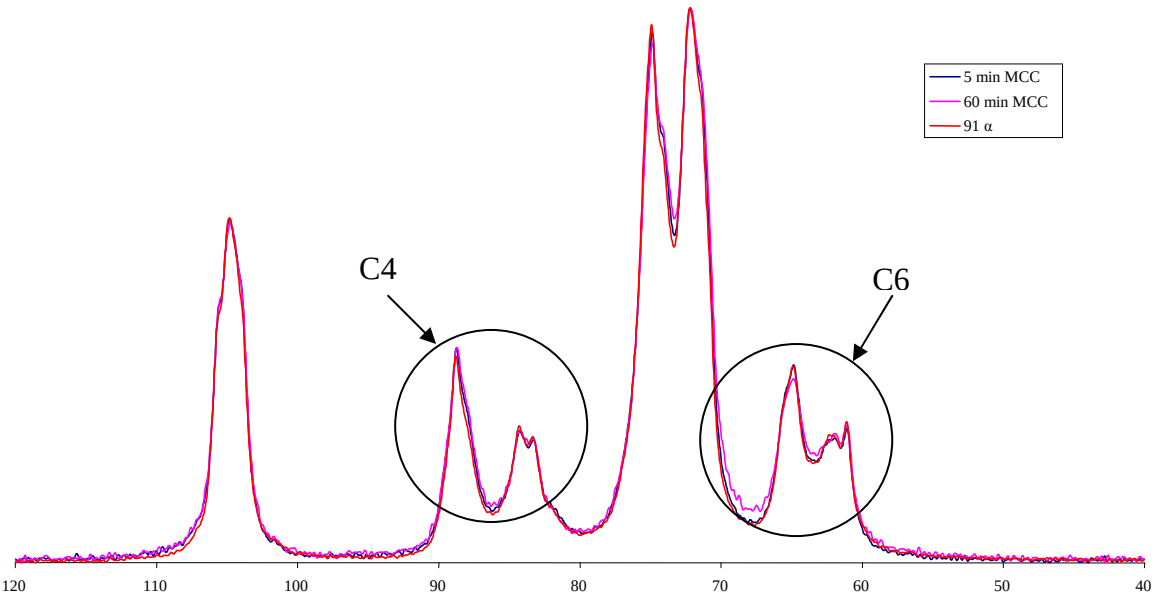

Figure 4.25: Overlaid spectra of 91α, 91α after 5 minutes acid hydrolysis and MCC after 60 minutes acid hydrolysis

Figure 4.24 and Figure 4.25 highlight that there is a marginal difference in spectra between the laboratory produced 91α, 91α after 5 minutes acid hydrolysis and MCC after 60 minutes acid hydrolysis at the C4 and C6 regions. The results are presented in Table 4.19, where LFD and LFAD measurements are presented for the three pulp samples.

Table 4.19: Solid state NMR on laboratory produced 91α, 91α after 5 minutes acid hydrolysis and MCC after 60 minutes acid hydrolysis

	LFD (nm)	**LFAD (nm)**
91α	3.73 ± 0.03	23.0 ± 0.6
91α after 5 minutes acid hydrolysis	3.97 ± 0.03	23.1 ± 0.7
MCC after 60 minutes acid hydrolysis	4.14 ± 0.06	22.7 ± 0.9

Spectral fitting for the 3 samples show that there is a significant increase in LFD with increasing hydrolysis time i.e. 3.73 ± 0.03 nm, 3.97 ± 0.03 nm and 4.14 ± 0.06 nm for the starting 91α, 91α after 5 minutes acid hydrolysis and MCC after 60 minutes acid hydrolysis respectively (Table 4.19). A decrease in the amount of accessible fibril surfaces would correspond to fibrils getting larger i.e. an increase in LFD. A study of the structure of cellulose and MCC by wide-angle X-ray scattering (WAXS) (Leppänen *et al*., 2009) revealed similar trends as noticed by solid state NMR. Leppänen *et al*. (2009) reported an increase in width of crystalline regions of cellulose fibrils when MCC was made. In contrast the LFAD measurements are similar within the analysis error. i.e. 23.0 ± 0.6 nm, 22.4 ± 0.7 nm and 22.7 ± 0.9 nm for the 91α, 91α after 5 minutes acid hydrolysis and MCC after 60 minutes acid hydrolysis respectively (Table 4.19). This could possibly be due to the fibrils (smaller in size) that suffer more from extensive hydrolysis rather than larger fibril aggregates. This experiment shows that apart from chain cleavage, prolonged hydrolysis may erode small fibrils while preserving LFAD i.e. the LFAD of the original starting material remains intact during the acid hydrolysis. There does not appear to be any relationship between LFAD, acid hydrolysis or MCC preparation. As discussed earlier the starting DP of the cellulose molecule govern the MCC LODP hence it is one of the important parameters to measure prior to acid hydrolysis. AFM is another technique that can be used to measure DP during acid hydrolysis and the MCC LODP (Kontturi and Vuorinen, 2009). This could possibly be used to track the changes in DP through the acid hydrolysis process.

Chapter 5

5. Summary and recommendations for future work

This study has demonstrated that solid state NMR can be used to investigate the supra-molecular structure of cellulose in hardwood acid bi-sulphite pulp, in-process and fully bleached 91α, 92α and 96α dissolving pulp samples, during their drying and subsequent conversion to microcrystalline cellulose, viscose and cellulose acetate respectively. Trends observed with LFAD measurements recorded using solid state NMR during bleaching and drying of dissolving pulp samples were supported by LFAD measurements recorded using AFM. Wet chemical properties for some of the pulp samples were shown to be intimately related to the LFAD upon bleaching, drying and for the formation of cellulose derivatives such as cellulose acetate, viscose and microcrystalline cellulose.

LFAD measurements recorded using solid state NMR during bleaching showed marginal changes in supra-molecular structure during 91α and 92α dissolving pulp production. The production of 96α dissolving pulp showed a change in LFAD at the alkali extraction (E) stage, a change which remained constant thereafter. These results pointed to the effect bleaching, using 91α, 92α and 96α conditions, has on LFAD. These bleaching effects were shown to be intimately related to the total hemicellulose content S_{18} (%) through the bleaching stages. This was highlighted in the alkali extraction stage, which is principally responsible for the extraction of hemicelluloses, where similar doses of sodium hydroxide, using the 91α and 92α conditions, showed no significant change in total extractable hemicellulose content S_{18} (%) and LFAD. Pulp bleached using the 96α conditions, with a higher dose of sodium hydroxide at the alkaline extraction stage, resulted in a decrease in total extractable hemicellulose content S_{18} (%) and an increase in LFAD. The reason behind the increase in LFAD was possibly due to the effect of ‘spacers’ on LFAD where the presence or lack thereof of hemicellulose either resulted in an increase in LFAD or not. This change in LFAD at the E stage for the pulp bleached using 96α conditions was however not evident in the measurements carried out using AFM. The LFAD, recorded using the

Atomic force microscope, was however distinguishable between the raw and final dissolving pulp samples.

Drying the pulp in different ways affected the LFAD measured suggesting that cellulose fibril aggregation can be controlled and manipulated during drying. Condition drying the pulp samples had a minimal effect on LFAD, possibly due to the rate at which water is removed from the pulp sample, whereas oven drying pulp produced a pronounced increase in LFAD. $LFAD_{NMR}$ and $LFAD_{AFM}$ results on never dried and oven dried pulp samples confirm that there is an irreversible increase in aggregate dimensions upon oven drying. The LFAD measured values correlated well with the total extractable material S_{10} (%) in pulp samples i.e. an increase in aggregate dimension during drying correlates with a decrease in total extractable material and vice versa. LFAD was thus shown to be related, in addition to the effect of total extractable material, to the manner in which water was removed from the pulp samples.

Solid state NMR and proton NMR proved valuable in relating specific surface area ratio to initial reaction rate constant ratio to acetylation for high purity pulp samples like cotton linters and commercially produced 96α. This application could prove vital commercially for predicting the pulp behaviour during cellulose acetate production. The use of SEC-MALLS to determine the reactivity of 92α pulp samples of low and high reactivity overcame the limitation of solid state NMR to differentiate between two 92α pulp samples. The solid state NMR can however differentiate between cellulose I and cellulose II which can prove valuable, in future, for cellulose II characterisation and as a qualitative measure of the rate of conversion of cellulose I into cellulose II. The solid state NMR could detect differences between 91α dissolving pulp samples and the hydrolysis products at different reaction times, pointing to the effect of prolonged hydrolysis on LFD. This work adds to the knowledge available on the supra-molecular structure of cellulose and highlights the need for the development of a fitting model for cellulose II in order to quantify the different regions within the spectrum.

This study focussed on the supra-molecular structure of cellulose and showed the influence of degraded cellulose and hemicellulose thereon. A structural

characterisation of the degraded cellulose and hemicellulose could provide further insight into the influence these components had on the structure of cellulose and may be a good starting point for further research. Future studies will also extend the current finding on a single clone from a single site to other clones grown on different site qualities. This will encompass the study of genetic and environmental effects on cellulose supra-molecular structure determined by solid state NMR and AFM. Nocanda *et al.* (2007) originally worked with a Eucalypt clone samples from extreme site qualities and explored the effect of drying on the cellulose supra-molecular structure using solid state NMR. Nocanda *et al.* (2007) showed similar trends in LFAD upon drying to those observed in the current study i.e. an increase in LFAD upon drying. The study explored the relationship between LFAD and total extractable material content S_{10} (%), LFAD and total hemicellulose content S_{18} (%) and showed that they are intimately related. The predictive LFAD models for condition and oven drying based on total extractable material S_{10} (%) can be expanded to include the other genotypes. Future studies can add to the current results such that a data base can be created for commercial application. This commercial application can be such that the prediction of the supramolecular structure of pulp samples at each stage in the bleaching process and also after drying is possible. The use of AFM can be explored further with determination of average pore and matrix (i.e. hemicellulose, degraded cellulose, lignin) distribution in the fibre wall. This can be related to yet another application of the proton NMR for the determination of pore size distribution in the fibre wall (Topgaard *et al*., 2001). This can be used in conjunction with LFAD where the distribution of pores within the fibre wall can be vital for determining the accessibility of chemicals for chemical reactions such as in cellulose acetate formation. Increased accessibility is often seen as the critical prerequisite for homogenous substitution of cellulose material and variation in pore size distribution results in inhomogeneous substituted cellulose derivatives.

This study is the first to relate (1) Structure, (2) Accessibility and (3) 'Reactivity' of *Eucalyptus* hardwood dissolving pulp samples, to LFAD measured using solid state NMR and AFM.

Other novel aspects of the study include:

- Measuring changes in the cellulose I supra-molecular structure upon drying, which can benefit the dissolving pulp industry, where the method in which the

pulp is dried can affect cellulose I structure, accessibility and ‘reactivity’ of the dissolving pulp samples

- Predicting LFAD using a wet chemical property such as total extractable material (S_{10}%).

The outputs from this study present a significant step forward for the dissolving pulp industry where a method of measuring dissolving pulp structure, understanding accessibility and predicting the ‘reactivity’ of dissolving pulp samples to further derivatisation is essential. Furthermore, these findings open up future research possibilities into developing process modifications to control cellulose I fibril aggregation for specific end use applications.

6. References

Acid insoluble lignin in wood and pulp, Tappi TM 222, Tappi Press, Atlanta.

Alexander, S., Hellemans, L., Marti, O., Schneir J, Elings V, Hansma P. K., An atomic resolution atomic force-microscope implemented using an optical lever, Journal of applied physics, 65, 1, 164-167, 1989.

Alkali solubility of pulp, Tappi T235 OM- 60, Tappi Press, Atlanta.

Andrews, D. H., Singh, R. P., Peroxide Bleaching. In 'The Bleaching of Pulp', 3rd Edition, Ed., R. P. Singh, Atlanta, GA: Tappi Press, 211-253, 1979.

Atalla, R. H., The structures of cellulose, Caulfield, D. F.; Passaretti, J. D.; Sobczynski, S. F. (editors), Materials interactions relevant to the pulp, paper, and wood industries: Proceedings, Materials Research Society symposium; April 18–20 1990; San Francisco, CA. Pittsburgh, PA: Materials Research Society, Vol. 197, 89-98, 1990.

Atalla, R. H., VanderHart, D. L., The role of solid state ^{13}C-NMR spectroscopy in studies of the nature of native celluloses, Solid State Nuclear Magnetic Resonance, 15, 1–19, 1999.

Atalla, R. H., VanderHart, D. L., Studies of microstructure in native celluloses using solid state ^{13}C-NMR, Macromolecules, 17, 1465-1472, 1984.

Atalla, R. H., Celluloses, Comprehensive natural products chemistry; Barton, D., Nakanishi, K., Meth-Cohn, M., editors, in Carbohydrates and their derivatives including tannins, cellulose, and related lignins, Pinto, B. M. editor, Elsevier Science, Oxford, 1999.

Bailey, J.W., Cell wall structure of higher plants, Ind. Eng. Chem. 30, 40–47, 1938.

Battista, O. A., Smith, P. A., Crystallite aggregates disintegrated in acid medium, United States Patent 3141875, 1964.

Béland, M. C., CLSM and AFM applied in Pulp and Paper research: A literature review, From the European conference on pulp and paper research - The present and the future: Proceedings: Stockholm, Sweden, 200-220, 1997.

Belfort M. A., Wortz, B. R., Colloidal oxycellulose by nitrogen dioxide treatment of level-off degree of polymerisation, I and EC product research and development, Vol 5, No. 1, 41-46, 1966.

Bhanu, P., Jena, J. K., Horber, H. (Editors), Methods in cell biology, Atomic Force Microscopy in cell biology, Vol. 68, 2002.

Blackwell, J., Gardner, K. H., The structure of native cellulose, Biopolymers, Vol. 13, 1975-2001, 1974.

Blackwell, J., Kolpak, F. J., Gardner, K. H., Structures of native and regenerated celluloses. Cellulose Chemistry and Technology, Arthur, J. C. (Editor), ACS-Symp. Series No. 48, Amer. Chem. Soc., Washington, 42-55, 1977.

Chen, S.-L.; Lucia, L. A., Fundamental Insight into the Mechanism of Oxygen Delignification of Kraft Pulps: Influence of a Novel Carbohydrate Protective System, Cell. Chem. Technol., 36, 339-351, 2002.

Christov, L. P., Akhtar, M., Prior, B. A., The potential of bi-sulfite pulping in dissolving pulp production, Enzyme and Microbial Technology, 23, 70-74, 1998.

Christoffersson, K. E., Dissolving Pulp – Multivariate Characterisation and Analysis of Reactivity and Spectroscopic Properties, KTH Doctoral thesis, 2005.

Chunilall, V., Wesley-Smith, J., Bush, T., Cellulose fibril aggregation studies of *eucalyptus* dissolving pulps using atomic force microscopy Proc. Microsc. Soc. South Afr., 36, 45, 2006.

Chunilall, V., Wesley-Smith, J., Bush, T., Cellulose Fibril aggregation studies of *Eucalyptus* dissolving pulps during drying using Atomic force microscopy, Proc. Microsc. Soc. South Afr., 38, 46, 2008.

Clarke, C. R. E., Are Eucalyptus clones more advantageous for the pulp mill? Southern African Forestry Journal, No. 190, 2001.

Clarke, C. R. E., Prospects for producing more pulp fibre per hectare in South Africa, Southern African Forestry Journal, No. 185, 1999.

Clarke, C. R. E., Clegg, P. A., Galloway, G. A., Measurement of productivity in trials of E. grandis hybrid clones at two sites. Proc IUFRO Conf. 'Silvicultura e Melhoramento de Eucaliptos', Salvador, Brazil Vol. 1, 259-263, 1997a.

Clarke, C. R. E., Garbutt, D. C. F., Pearce, J., Growth and wood properties of provenances and trees of nine Eucalypt species. Appita Journal, 50:121-130, 1997b.

Copper number of pulp, paper and paperboard, Tappi T430 OM 94, Tappi Press, Atlanta.

Copper number (Braidy's method), FFP 005, issue 2, May 2007.

Copper number (Braidy's method), Sappi/Saiccor laboratory test 023, revision 3, February 2004.

Côte, W.A., Jr., Wood Ultrastructure, University of Washington Press, Syracuse, NY, USA, 1967.

Daniel, G., Duchesne, I., Revealing the surface ultrastructure of spruce fibres using field emission-SEM. In Proc 7th Int Conf on Biotechnology in the Pulp and Paper Industry, June 16–19, Vancouver, Canada, pp. B81–84, 1998.

Davis, M. W. A rapid modified method for compositional carbohydrate analysis of lignocellulosics by high pH anion exchange chromatography with pulsed amperometric detection (HPAEC/PAD), J. of Wood Chem. Technol., 18(2), 235-252, 1998.

Dence, C. W., Reeve, W. (Editors), Pulp Bleaching - Principles and Practice, TAPPI press, Atlanta, Georgia, 1996.

Denison, N. P., Kietza, J. E., The development and utilization of vegetative propagation in Mondi for commercial afforestation programmes. South African Forestry Journal, 165, 47-54, 1993.

Desch, H. E., Dinwoodie, J. M., Timber, Structure, Properties, Conversion and use, 7th edition, Food Products Press, 1996.

Determination of the alkali solubility of pulp [S_{10} (%) and S_{18} (%)], FFP 004, May 2007.

Determination of the alkali solubility of pulp [S_{10} (%) and S_{18} (%)], Sappi/Saiccor Laboratory test 018, revision 3, December 2002.

De Souza, I. J., Bouchard, J., Methot, M., Berry, R., Argyropoulos, D. S., Changes in oxygen delignification. Part I: Changes in Celllulose crystallinity, Journal of Pulp and Paper Science: Vol. 28, No.5, 167-170, 2002.

Diniz Fernandes J. M. B., Gil, M. H., Castro, J. A. M. M., Hornification-its origin and interpretation in wood pulp samples, Wood Sci. Technology, 37, 489-494, 2004.

Duchesne, I., Daniel, G., Changes in surface ultrastructure of Norway spruce fibres during kraft pulping – visualisation by field emission-SEM. Nordic Pulp and Paper Research Journal, 15, 54-61, 2000.

Duchesne, I., Hult, E.-L., Molin, U., Daniel, G., Iversen, T., Lennholm, H., The influence of hemicellulose on fibril aggregation of kraft pulp fibres as revealed by FE-SEM and CP/MAS ^{13}C-NMR, Cellulose, 8, 2, 103-111, 2001.

Ekman, R., Holmbom, B., The chemistry of wood resin. In 'Pitch control, wood resin and deresination', Tappi Press, Atlanta, 37-76, 2000.

Engström, A. C., Ek, M., Henriksson, G., Improved Accessibility and Reactivity of Dissolving Pulp for the Viscose Process: Pretreatment with Monocomponent Endoglucanase, Biomacromolecules, 7, 6, 2027-2031, 2006.

Ek, M., Engstrom, A., Henriksson G., Vehvilainen M., Heikkila, E., Agnemo, R., Cellulose derivatives- improved accessibility and reactivity, Appita, 121-126, 2005.

Ek, M., Engström A-C. and Henriksson, G., Cellulose derivatives – improved accessibility and reactivity, 13th ISWFPC: International Symposium on Wood, Fibre and Pulping Chemistry, Auckland, New Zealand, 2005.

Fahlén, J., Salmén, L., On the lamellar structure of the tracheid cell wall. Plant Biol., 4, 3, 339-345, 2002.

Fahlén, J., Salmén, L., Cross-sectional structure of the secondary wall of fibres as affected by processing. J. Mater. Sci. 38, 119-126, 2003.

Fahlén, J., Salmén, L., Pore and matrix distribution in the fibre wall revealed by atomic force microscopy and image analysis. Biomacromolecules, 6, 433-438, 2005.

Fahlén, J., The cell wall ultra-structure of wood fibres – effects of the chemical pulp fibre line, Doctoral dissertation, Royal Institute of Technology (KTH), Sweden, 2005.

Fengel, D., Ultrastructural behaviour of cell wall polysaccharides, In: Page, D.H. (Ed.), The Physics and Chemistry of Wood Pulp Fibres. Tappi, 1970.

Fengel, D., Wegener, G. Wood. Chemistry, Ultrastructure, Reactions, Walter de Gruyter, Berlin, Germany, 613, 1984.

Fischer, K., Koch, R., Fischer, M., Schmidt, I., Characterization of cellulose and cellulose derivatives by SEC, Das Papier, 53, 12, 722-727, 1999.

Funaoka, M., Chang, V. L., Kolppo, K., Stokke, D. D., Comparison of condensation reactions at C_α positions in kraft and acid sulfite delignification of Western hemlock, Bull. Fac. Bioresources, Mie Univ., No. 5, 37-44, 1991.

Gardner, K. H., Blackwell, J., The structure of native cellulose, Biopolymers, 13, 1974.

Gierer, J., Chemistry of delignification Part 1: General concept and reactions during pulping, Wood Sci. Technol. 19, 289-312, 1985.

Gierer, J., Wännström, S., Formation of ether bonds between lignin and carbohydrates during alkaline pulping processes, Holzforschung, 40, 6, 347-352, 1986.

Goodlett, V.W., Dougherty, J.T., Patton, H.W., Characterisation of cellulose acetates by nuclear magnetic resonance, Journal of Polymer science: Part A-1, Vol. 9, 155 161, 1971.

Götzinger,G., Schrittwieser A. and Mühlbacher, R. Monosulfite splitting - an important part of the secondary recovery system of the magnesium base acid bi-sulfite cooking process, A-4860 Lenzing, AG, Austria.

Gubitz, G. M., Stebbing, D. W., Johansson, C. I., Lignin-hemicellulose complexes restrict enzymatic solubilisation of mannan and xylan from dissolving pulp, Appl. Microbiol. Biotechnol, 50: 390-395, 1998.

Gustafsson, J., Ciovica, L. & Peltonen, J. The ultrastructure of spruce kraft pulps studied by atomic force microscopy (AFM) and X-ray photoelectron spectroscopy (XPS). Polymer, 44, 661-670, 2002.

Hanley S. J., Gray D. G., Atomic Force Microscopy, In Surface analysis of paper, Conners, T. E., Banerjee, S., editors; Boca Raton, Florida: CRC press Inc, 301-324, 1995.

Haworth, W. N., The structure of carbohydrates. Helvetica Chimica Acta, 11, 534-548, 1928.

Heiner, A. P., Kuutti, L. And Teleman, O., Comparison of the interface between water and four surfaces of native crystalline cellulose by molecular dynamics simulations, carbohydrate Research, 306, 205-220, 1998.

Henriksson, G., Christiernin, M. and Agnemo, R., Monocomponent endoglucanase treatment increases the reactivity of softwood sulphite dissolving pulp, Journal of Industrial Microbiology & Biotechnology, 2005.

Holzer, W. F., In Cellulose and Cellulose Derivatives, Part II, Ott, E. and Spurlin, H. M., editors, New York: Wiley-Interscience,1954.

Hon, D. N.-S., Shiraishi N., Eds., Wood and cellulosic chemistry, 2nd Edition, CRC Press, 2000.

Horikawa, Y., Sugiyama, S., Accessibility and size of *Valonia* cellulose microfibril studied by combined deuteration/rehydrogenation and FTIR technique, Cellulose, 15, 419-424, 2008.

Hult, E-L., Larsson, P.T., Iversen, T., Cellulose Fibril aggregation-An inherent property of kraft pulps, Polymer, 42, 3309-3314, 2001.

Inari, G. N., Mounguengui, S., Dumarcay, S., Pétrissans, M., Gérardin, P., Evidence of char formation during wood heat treatment by mild pyrolysis, Polymer Degradation and Stability, 92, 997-1002, 2007.

Jayme, G., Mikro-Quellungsmessungen an Zellstoffen. Wochenbl Papierfabr., 6, 187-194, 1944.

Jayme, G., Koburg, E., 1959. Ueber den elektronisch bestimmten Durchmesser der MikroWbrillen von Laubholzzellelementen. Holzforschung 13, 37-43.

Jena, B. P., and H. J. K. Horber. Atomic force microscopy in cell biology. In Methods in Cell Biology, Vol 68, Jena, B. P. and Horber, H. J. K., editors, 2002.

Johnson, S. E., Optimal use of hydrogen peroxide, Tappi J., 77, 7, 262-264, 1994.

Karlsson, H., Fibre guide – Fibre analysis and process applications in the pulp and paper industry, AB Lorentzen & Wettre, Sweden, 2006.

Kataoka, Y., Saiki, H., Fujita, M., Arrangement and superimposition of cellulose microWbrils in the secondary walls of coniferous tracheids. Mokuzai Gakkaishi, 38, 4, 327-335, 1992.

Kerr, A.J., Goring, D.A.I., Ultrastructural arrangement of the wood cell wall. Cellulose Chem. Technol., 9, 563-573, 1975.

Klemm, D., Philipp, B., Heinze, T., Heinze, U. and Wagenknecht, W., Comprehensive cellulose chemistry, Wiley-VCH, Weinheim, Vol. 1/2, 1998.

Koch, F-T., Prieß, W., Witter, R., Sternberg, U., Calculation of solid state ^{13}C NMR spectra of cellulose Iα, Iβ and II using a semi-empirical approach and molecular dynamics, Macromol. Chem. Phys., No. 15, 201, 1930-1939, 2000.

Kontturi, E., Vuorinen, T., Indirect evidence of supramolecular changes within cellulose microfibrils of chemical pulp fibres upon drying, Cellulose, Vol 16, 1, 65-74, 2009.

Kordsachia, O., Roβkopf, S., Patt, R., Production of spruce dissolving pulp with the prehydrolysis-Alkaline sulphite process (PH-ASA), Lenzinger Berichte, 83, 24-34, 2004.

Krässig, H. A. Cellulose - Structure, Accessibility and Reactivity. Polymer Monographs M. B. Huglin. Amsterdam, Gordon and Breach science publishers, Vol. 11, 1996.

Laine, C., Structures of hemicelluloses and pectin in wood pulp, Doctoral thesis, Helsinki University of Technology, 2005.

Laka, M., Chernyavskaya, S., Treimanis, A., Faitelson, A., Preparation and properties of microcrystalline cellulose, Cellulose Chem. Tech., 34, 217-227, 2000.

Larsson, P.T., Westermark, U., Iversen, T., Determination of the cellulose Iα allomorph content in a tunicate cellulose by CP/MAS 13C-NMR spectroscopy. Carbohydr. Res. 278, 339-343, 1995.

Larsson, P.T., Wickholm, K., Iversen, T., A CP/MAS ^{13}C-NMR investigation of molecular ordering in celluloses, Carbohydrate Research, 302, 19-25, 1997.

Larsson, P.T., Hult, E., Wickholm, K., Pettersson, E., Iversen, T.,CP/MAS ^{13}C NMR spectroscopy applied to structure and interaction studies on cellulose I, Solid state NMR, 15, 31-40, 1999.

Larsson, P.T., Interaction between cellulose I and hemicelluloses studied by spectral fitting of CP/MAS ^{13}C NMR spectra, In Gatenholm, P. and Tenkanen, M., editors ACS Symposium Series No. 864/ Hemicelluloses: Science and Technology., Chapter 17, 2003.

Lennholm, H. and Iversen, T., Estimation of cellulose-I and cellulose-II in cellulosic samples by principal component analysis of CP/MAS ^{13}C-NMR-spectra. Holzforschung, 49, 2, 119-126, 1995.

Leppänen, K., Andersson, S., Torkkeli, M., Knaapila, M., Kotelnikova, N., Serimaa, R., Structure of cellulose and microcrystalline cellulose from various wood species, cotton and flax studied by X-ray scattering, Cellulose, 16, 999-1015, 2009.

Liang, C. Y., Marchessault, R. H., Infrared spectra of crystalline polysaccharides. I. Hydrogen bonds in native celluloses, Journal of polymer science, Vol. XXXVII, 385-395, 1959.

Lückhoff, H.A., The establishment and regeneration of Eucalyptus saligna plantations in the coastal belt of Zululand, Journal of the South African Forestry Association, 25, 1-20, 1955.

Mauna, S.L., NMR studies of wood and wood products, Progress in Nuclear Magnetic Resonance Spectroscopy, 40, 151-174, 2002.

Mark, R.E., Cell Wall Mechanics of Tracheids. Yale University Press, London, 1967.

McDonough, T. J., IPC Technical paper series, Number 132, Oxygen bleaching processes: An overview, January, 1983.

Meyer, K. H., Mark, H., Über den Bau des krystallisierten Anteils der Cellulose. Berichte der Deutschen Chemischen Gesesellschaft, 61: 593-614, 1928.

Meyer, G, Amer, N., Novel optical approach to atomic force microscopy, Applied physics letters, 53, 12, 1045-1047, 1988.

Meyer, E., Hug, H.J., Bennewitz, R., Scanning Probe Microscopy, The Lab on a Tip. Springer-Verlag, Berlin, Heidelberg, New York, 2004.

Miller, R. B., Wood handbook—Wood as an engineering material. Gen. Tech. Rep. FPL–GTR–113. Madison, WI: U.S. Department of Agriculture, Forest Service, Forest Products Laboratory, 1999.

Nagao, E. and Dvorak, J. A., Phase Imaging by Atomic Force Microscopy: Analysis of Living Homoiothermic Vertebrate Cells, Biophysical Journal, Vol. 76, 3289-3297, 1999.

Newman, R. H., Estimation of the lateral dimensions of cellulose crystallites using ^{13}C-NMR signal strengths, Solid state Nucl. Magn. Res., 15, 21-29, 1999.

Newman R. H., carbon 13 NMR evidence for the cocrystallization of cellulose as a mechanism for hornification of bleached kraft pulp, Cellulose, 11, 45-52, 2004.

Newman, R.H., Hemmingson, J.A., Suckling, I.D., Carbon-13 nuclear magnetic resonance studies of kraft pulping, Holzforschung, 47, 234, 1993.

Nicholson, H.B., The development of the market for Saligna gum in South Africa. Journal of the South African Forestry Association 37:10-15, 1961.

Niemi, H., Paulapuro, H., Application of scanning probe microscopy to wood, fibre and paper research, Paperi ja Puu, 84, 6: 389-406, 2002.

Nishikawa, S., Ono, S., Transmission of X-rays through fibrous, lamellar and granular substances. Proc. Tokyo Math. Phys. Soc. 7, p. 131, 1913.

Nishiyama, Y., Sugiyama, J., Chanzy, H., Crystal structure and hydrogen bonding system in cellulose Iβ, from synchrotron X-ray and neutron fibre diffraction. J. Am. Chem. Soc. 124, 9074-9082, 2002.

Nishiyama, Y., Sugiyama, J., Chanzy, H. and Langan, P., Crystal structure and hydrogen bonding system in cellulose Iα, from synchrotron X-ray and neutron fibre diffraction. J. Am. Chem. Soc. 125, 14300-14306, 2003.

Nocanda, X, Larsson, P.T., Spark, A, Bush, T, Olsson, A, Madikane, M., Bissessur, A., Iversen, T. Cross polarisation/ magic angle spinning ^{13}C-NMR spectroscopic studies of cellulose structural changes in hardwood dissolving pulp process. Holzforschung, 61, 6, 675-679, 2007.

Oksanen, T., Buchert, J. and Viikari, L., The role of hemicelluloses in the hornification of bleached kraft pulps, Holzforschung, 51, 4, 355-360, 1997.

Pallett RN, - Site Quality Classification based on Forest Land Types for Sappi Landholdings. Sappi Forests research Document 01/2001, 2001.

Park, S., Venditti, R. A., Abrecht, D. G., Jameel, H., Pawlak, J. J., Lee, J. M., Surface and pore structure modification of cellulose fibres through Cellulase treatment, Journal of Applied Polymer Science, Vol. 103, 3833-3839, 2007.

Pascoal Neto, C., Evtuguin, D., Pinto, P., Silvestre, A., Freire, C., Chemistry of plantation eucalypts: Specificities and influence on wood and fibre processing, Appita, 431-438, 2005.

Pereira, D. E. D., Meyer, E. and Guntherodt, H. J., The use of AFM to investigate the delignification process: part II – AFM performance in pulp pre-bleached with oxygen, Revue ATIP, 55, 6-9, 2001.

Poggi M. A., Mancosky, D. G., Bottomley L. A., Lucia, L. A., Atomic force microscopic analysis of hydrogen peroxide bleached kraft northern black spruce fibres, Journal of microscopy, Vol. 220, 2, 77-83, 2005.

Puttman, C. A. J., Van de Werf, K. O., De Grooth, B. G., Van Hulst, N. F., Greeve, J., Tapping Mode Atomic Force Microscopy in Liquid, Applied physics letters, 64, 18, 2454-2456, 1994.

Pinto, P.C., Evtuguin, D.V., Neto, C.P., Effect of structural features of wood biopolymer on hardwood pulping and bleaching performance, Ind. Eng. Chem. Res., 44, 9777-9784, 2005.

Permanganate number of pulp, Tappi T214 wd-76 (UM-251), Tappi Press, Atlanta.

Permanganate number, FFP 003, May 2007.

Permanganate number, Sappi/Saiccor Laboratory test 010, Revision 2, March 2004.

Preparation of cuprammonium solution, Sappi/Saiccor laboratory test 003, revision 3, November 2002.

Press, H. W., Flannery, P. B., Teukolsky, A. S., Vetterling, T. W. (editors), Numerical recipes, the art of scientific computing, Cambridge University Press, New York, 1986.

Rapson, H. W., Method of bleaching wood pulp, Patent 2587064, 1952.

Ragauskas, A. J., High selectivity oxygen delignification, Institute of Paper Science and Technology, Georgia Institute of Technology, Technical report DE-FC07-00ID13870, 2000.

Rebuzzi, F., Evtuguin, D. V, Effect of Glucuronoxylan on the hornification of *Eucalyptus globulus* bleached pulps, Macromol. Symp., 232, 121-128, 2006.

Reisch, M. S., Chem. Eng. News, 74, 15-16, 1995.

Röhrling, J., Potthast, A., Rosenau, T., Lange, T., Ebner, G., Sixta, H. and Kosma, P., A Novel Method for the Determination of Carbonyl Groups in Cellulosics by Fluorescence Labeling. 1. Method Development, Biomacromolecules, 3, 5, 959-968, 2002.

Rowland, S.P., Howley, P.S., Microstructural order in the developing cotton fiber based on availabilities of hydroxyl groups. J. Polym. Sci. Polym. Chem. Ed. 23, 183-192, 1985.

Rydholm, S. A., Pulp processing . Wiley Interscience, New York, 1133 – 1185, 1965.
Sanders, J. K. M., Hunter. B. K., Modern NMR Spectroscopy, Oxford University Press, U.S, 1987.

Sanders, K. M., Hunter, B. K., Modern NMR Spectroscopy, Oxford/New York/Toronto, Oxford University Press, 1987.

Sarkanen, K. V. ; Ludwig, C. H. , Lignins: occurrence, formation, structure and reactions, New York, Wiley-Interscience, 1971.

Sarko, A., Muggli, R., Packing analysis of carbohydrates and polysaccharides. 111. *Valonia* Cellulose and Cellulose II, Macromolecules, 7, 4, 1974.

Sarko, A., Cellulose - How much do we know about its structure. In Wood and Cellulosics: Industrial utilization, biotechnology, structure and properties (J. F. Kennedy, editor) Chichester, UK: Ellis Horwood, 55-70, 1987.

Schaefer, J. and Stejskal, E. O., Carbon-13 NMR of polymers spinning at the magic angle. J, Ant. Chem. Soc. 98, 1031-1033, 1976.

Schaefer, J., Stejskal, E. O. and Buchdahl, R., Magic-Angle ^{13}C NMR analysis of motion in solid glassy polymers. Macromolecules, 10, 384-405, 1977,

Schlotter, N. E., Rayon, in Mark, H. F., Encyclopaedia of polymer science and engineering, 14, 45-69, 1988.

Sell, J., Zimmermann, T., Das Gefüge der Zellwandschicht S2 - Untersuchungen mit dem Feldemissions-Rasterelektronenmikroskop an QuerbruchXächen von Fichten- und Tannenholz. Forschungs- und Arbeitsberichte Abteilung 115 (28), 1-27, 1993a.

Sell, J., Zimmermann, T., Radial Wbril agglomerations of the S2 on transverse-fracture surfaces of tracheids of tension-loaded spruce and white Wr. Holz als Roh- und Werkst. 51, 384, 1993b.

Sixta, H., Harms, H., Dapia, S., Parajo, J. C., Puls, J., Saake, B., Fink, H. P. and Roder, T., Evaluation of new organosolv dissolving pulps. Part I: Preparation, analytical characterization and viscose processability. Cellulose, 11, 1, 73-83, 2004.

Sixta, H., Promberger, A., Kock, G., Gradinger, C., Messner, K., Influence of beech wood quality on bisulphite dissolving pulp manufacture. Part 1: Influence of log storage on pulping and bleaching. Holzforschung, Vol.58, 14-21, 2004.

Sjöström, E., Wood Chemistry – Fundamentals and Applications, 2nd ed., Academic Press, San Diego, USA, 1993.

Sjöström, E., Wood Chemistry: Fundamentals and Applications. Academic Press, Orlando, 1981.

Solomon, K. R., Chlorine in the bleaching of pulp and paper, Pure & Appl. Chem., Vol. 68, No. 9, pp. 1721-1730, 1996.

Spurr, A. R., A low viscosity embedding medium for electron microscopy, J. Ultrastruct. Res., 26, 31-43, 1969.

Sugiyama, J., Vuong, R. and Chanzy, H., Electron diffraction studies on two crystalline phases occurring in native cellulose from an algal cell wall, Macromolecules, 24, 4168-4175, 1991.

Teeäär, R., Serimaa, R., Paalkkari, T., Crystallinity of cellulose, as determined by CP/MAS NMR and XRD methods, Polym. Bull., 17, 231-237, 1987.

Timell, T.E., Chemical composition of wood. In: Schniewind, A.P. (Ed.), Concise Encyclopedia of Wood and Wood-based Materials. Pergamon Press, Oxford, New York, Beijing, Frankfurt, Sâo Paulo, Sydney, Tokyo, Toronto, 319-324, 1989.

Toven, K., Ozone based ECF bleaching of oxygen delignified kraft pulp, Norwegian Pulp and Paper Research Institute (PFI), PO Box 24 Blindern N-0313, OSLO, 1998.

Topgaard, D., Soderman, O., Langmuir, Diffusion of water absorbed in cellulose fibres studied with ^{1}H-NMR, Vol. 17, 2694-2702, 2001.

Turnbull, J.W., Eucalypt plantations, New Forests, 17, 37-52, 1999.

Tsuboi, M., Infrared spectrum and crystal structure of cellulose, Journal of polymer science, Vol. XXV, 159-171, 1957

Uhlmann, T., Ullmann's encyclopedia of industrial chemistry, Vol. 18 A Paper and Pulp, completely rev.ed., ISBN 3-527-20118-1, 1991.

Valko, E. I., 'Bleaching', in Chemistry and Chemical Technology of Cotton (editor K. Ward) New York: Interscience Publishers, 117-215, 1955.

Verlhac, C., Dedier, J., Availability of surface hydroxyl groups in Valonia and Bacterial cellulose, Journal of Polymer science: Part A: Polymer crystallinity, Vol. 28, 1171-1177, 1990.

Virtanen, T., Maunu, S. L., Tamminen, T., Hortling, B., Liitia, T., Changes in fibre ultrastructure during various kraft pulping conditions evaluated by ^{13}C CP/MAS NMR spectroscopy, Carbohydrate Polymers 73, 156-163, 2008.

Viscosity of pulp, Tappi T230 om-94, Tappi Press, Atlanta.

Viscosity measurement of bleached pulp, Sappi Saiccor Laboratory test 003, 2002.

Wang, Y., Chen, X., Carbon nanotubes: A promising standard for quantitative evaluation of AFM tip apex geometry, Ultramicroscopy, 107, 293-298, 2007.

Wickholm, K., Larsson, P. T. and Iversen, T., Assignment of non-crystalline forms in cellulose I by CP/MAS ^{13}C NMR spectroscopy. Carbohydr. Res., 312, 123-129, 1998.

Wickholm, K., Structural Elements in Native Celluloses, Doctoral dissertation, Royal Institute of Technology (KTH), Sweden, 2001.

Wilder, H. D.; Daleski, E. J., Kraft Pulping Kinetics. I. Literature Review and Research Program, Tappi, 47, 5, 270-275, 1964.

Wingfield, M.J., Crous, P.W. and Coutinho, T.A., A serious canker disease of Eucalyptus in South Africa caused by a new species of Coniothyrium. Mycopathologia, 136, 139-145, 1997.

Yamada, H., AFM measurement in Liquid, in Roadmap of scanning probe microscopy, (Ed) Morita, S., Chapter 13, 2007.

Yamamoto, H. and Horii, F., CP MAS carbon-13 NMR analysis of the crystal transformation induced for Valonia cellulose by annealing at high temperatures Macromolecules, 26, 1313-1317, 1993.

Yang, R., Lucia, L., Ragauskas, A. J. and Jameel, H., Oxygen delignification chemistry and its impact on pulp fibres, Journal of Wood Chemistry and Technology, Vol. 23, No. 1, 13-29, 2003.

Yannoni, C. S. High-resolution NMR in Solids: The CP/MAS Experiment. Accounts of Chemical Research, 15, 201-208, 1982.

Zeronian, S. H., Inglesby M. K., Bleaching of cellulose by hydrogen peroxide. Cellulose 1995, 2, 265-272.

Zhao, H., Kwak, J. H., Zhang, Z. C., Brown, H. M., Arey, B. W., and Holladay, J. E., Studying cellulose fiber structure by SEM, XRD, NMR and acid hydrolysis, Carbohydrate Polymers Volume 68, Issue 2, 235-241, 2007.

Zhong Q, Kjoller D, Elings V B, Fractured polymer/silica fibre surface studied by tapping mode atomic force microscopy, Surface science, 290, 668-692, 1993.